Dynamic Stability of Piles under Earthquake with Fractional Damping Foundation

by
Mohammadmehdi Shahroudi

A thesis
submitted to Faculty of Graduate Studies
in partial fulfillment of the requirements for the
Degree of Master of Science
in
Civil Engineering

Supervisor
Dr. Jian Deng
Associate Professor - Dept. of Civil Engineering

Co-Supervisor
Dr. Yanglin Gong
Professor - Dept. of Civil Engineering

Lakehead University
Thunder Bay, ON
December 2022

Author Declaration

I hereby declare that I am the sole author of this thesis. This is a true copy of the thesis, including any required final revisions, as accepted by my examiners. I understand that my thesis may be made electronically available to the public.

Abstract

Pile foundation is an essential structural component in civil engineering. The failure of a pile foundation under an earthquake may result in significant economic consequences, such as interruption of transportation, property damage and failure, or even loss of lives. So, dynamic stability of piles is one of the emerging research topics for civil engineers.

Due to the excessive use of fractional models in research during recent years, which shows more compatibility of results with experimental models, and a lack of fractional models usage in the field of pile stability, this thesis investigates dynamic stability of piles under periodic earthquake loading, considering the Winkler mechanical model with fractional damping for the surrounding soil media.

During this research, an approximate theoretical and a numerical method are developed to study dynamic stability behavior and vibration responses of piles with fractional damping foundations under earthquake. Solving the equation of motion of a pile loaded by axial periodic load leads to fractional Mathieu differential equations. The approximate method is based on the Bolotin method and results in two matrices of coefficients. Putting determinants of matrices equal to zero results in different orders of approximation for finding instability regions' boundary. On the other hand, the numerical method is introduced by using block-pulse functions to calculate the vibration response of pile under the periodic load. Based on the numerical method, instability regions are generated, and results are used to validate different orders of approximation for each instability region.

Approximate method validation illustrates that for the first and second instability regions, third-order approximation should be used based on the matrices of coefficients. But, for finding an appropriate boundary for third and fourth instability regions, fourth-order approximation should be used. Also, higher instability regions should be found using higher orders of approximation.

This study also investigates the effects of various parameters such as foundation stiffness, damping coefficient, static load, and fractional order damping on pile instability. The

critical excitation load and critical dynamic load of each instability region increase with the soil foundation stiffness. Larger soil damping needs a more significant dynamic component load to produce instability. Increasing the static load parameter leads to a decrease of the critical excitation frequency of parametric resonance. It is also found that damping with fractional order has significant effects on the stability diagrams at the lower dynamic load parameter.

Finally, using an actual earthquake wave, it is explained how the stability behavior of a pile should be examined under a specific earthquake wave.

Acknowledgment

First, I would like to express my deep and sincere gratitude to my supervisor, Dr. Jian Deng, for providing me the opportunity to continue my education and supporting me with his patience, motivation, and suggestions for completing the thesis. I also appreciate Dr. Yanglin Gong, my co-supervisor, for his companionship and sincere help during this academic program. In addition, a special thanks to my thesis examiners, Dr. Kefu Liu and Dr. Ahmed Elshaer, for their time and consideration of my work. The suggestions and insight provided by you were precious and greatly improved the quality of my research.

I should also express my sincere thanks to my dear friend, Dr. Mohammad Mahdi Share Pasand, for his active cooperation, kind, and helpful guidance during the thesis.

Moreover, my deepest gratitude goes to my supportive and caring wife, Shahrbanoo. It was greatly appreciated that she encouraged me during rough times, also other family members and friends who motivated me with love during these two years.

This thesis is dedicated to my wife, ***Shahrbanoo***, and my children, ***Nikan*** and ***Nora***,

for their endless love, support, and encouragement.

Table of Contents

Table of Figures

Nomenclature

Symbol	Description
A	Cross-section area
c_s	Viscous damping coefficient
D	Flexural rigidity per unit width
D^α	Fractional order derivative operator
E	Elastic modulus
G	Shear rigidity per unit width
I	Moment of inertia
I^α	Fractional order integral operator
k	Soil stiffness
k_s	Linear foundation stiffness
L	Length of pile
L_e	Effective length of pile
M	Moment
n	Mode number
P	Static axial load
$P(x,t)$	Subgrade reaction
$P(t)$	Dynamic axial load
P_{cr}	The critical Euler buckling load
P_d	Dynamic component of dynamic axial load
P_n	Euler load for n^{th} mode of deformation
P_s	Static component of dynamic axial load
q (or q_n)	State function for the first mode of deformation (q_n for n^{th} mode)
T	Period frequency of dynamic load
t	Time
v	Lateral displacement
y	Deflection
β	Damping coefficient
Γ	Gamma function
δ	Logarithmic decrement of damping
$\delta(x)$	Dirac's delta function
ϵ	Dimensionless dynamic load parameter
η	Dimensionless foundation stiffness parameter
θ	Angular frequency of dynamic load
λ	Dimensionless static load parameter
ρ	Density
$\Phi(t)$	Axial loading periodic function
$\phi_i(x)$	Modal function
Ω (or Ω_n)	Natural frequency of a simply supported pile for the first mode (Ω_n for n^{th} mode)
ω (or ω_n)	frequency of free vibrations of the pile loaded by force P_s and constrained by soil foundation for the first mode (ω_n for n^{th} mode)

C H A P T E R   1

Introduction

The use of piles in structures can extend across a wide range, from bridges and high-rise buildings built on loose soil to piers [1]. Loads from superstructures can be transferred from loose soil to deeper, more stable layers with pile foundations. Combined longitudinal frictional resistance and pile tip resistance are responsible for transferring loads to high-strength layers. In areas where soft or loose soil deposits occupy a substantial part of the near-surface soil profile, such as port structures and bridge piers, piles are an excellent solution. Furthermore, piles are a valuable form of structural support on man-made fills, historical floodplains, or swamps, where loose soil conditions exist near the ground surface [2]. Due to the widespread use of piles in various structures, their study of the effect of lateral and axial loads produced by earthquakes is of particular importance.

A literature review, as well as a description of the thesis outline, is presented in this chapter.

1.1. Literature review

To conduct the literature review relating to dynamic stability of piles under earthquake with fractional damping foundation, the first is to explain the behaviour of pile foundation under earthquakes and modes of fractures. Then, the concept of buckling instability of a compressive element is reviewed. We will see how other researchers use a beam to model a pile and review some mechanical models which can be used to model the surrounding soil of

the pile. At the end of this section, we introduce fractional calculus and review some previous research on fractional damping.

1.1.1.   Pile foundations under earthquakes

There are multiple failure modes of pile foundations during earthquakes, but soil displacement and liquefaction of sandy soil are the most frequent ones[3]. Failure patterns of pile foundations without liquefaction-induced failure are as follows:

- A result of inertial forces acting on the superstructure. The most common places for damage to occur are at the joints between the pile head and the pile cap or the pile's top.
- Failure at the interface between soft and hard soil layers as the result of excessive bending moment and shear force.
- An insufficient vertical bearing capacity causing the pile to settle.

Pile foundations are most likely to be distressed because of the liquefaction of the soil. There are two types of pile damage caused by liquefaction-induced phenomena: pile damage without soil lateral spread and pile damage with soil lateral spread. Structures are damaged due to large lateral displacement of the ground during earthquakes caused by liquefaction.

Various phenomena can be observed if the soil is liquefiable but does not spread laterally during an earthquake, such as sand erupting, water oozing, pile cap detachment from the soil, etc. Also, pile foundations often experience quite large settlements due to non-uniform conditions of load distribution, liquefied soil quality, and soil thickness [4].

The failure mechanisms of the pile under soil lateral spreading have been discussed in detail by Xiao Wei in his summary on seismic damage to liquefiable pile foundations under soil lateral spreading conditions. There are several mechanisms that cause piles to be damaged when soil spreads laterally [3]:

- Due to shear and bending failure caused by lateral compression of piles induced by soil movement, piles in the middle and bottom of liquefied layers fail (Figure 1.1).
- During pile head fixation, a flexure-shear failure occurs (Figure 1.2).

- When the superstructure settles unevenly, the tall structure becomes unstable and the horizontal displacement and bending moment greatly increase. In this situation, the interior side pile experiences additional compressive stress and the failure mechanism occurs with two plastic hinges. The exterior side pile is subjected to tensile stress, so earthquake damage on the pile can be reduced, and often only one plastic hinge is present on the exterior side pile (Figure 1.3).
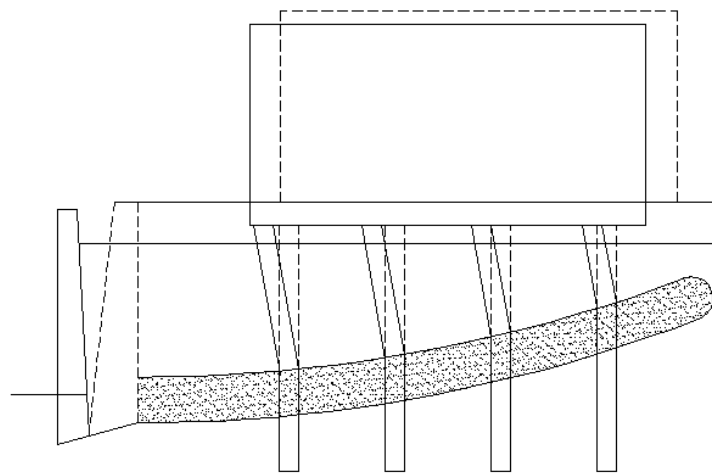
Figure 1.1 Shear and bending failure [3]
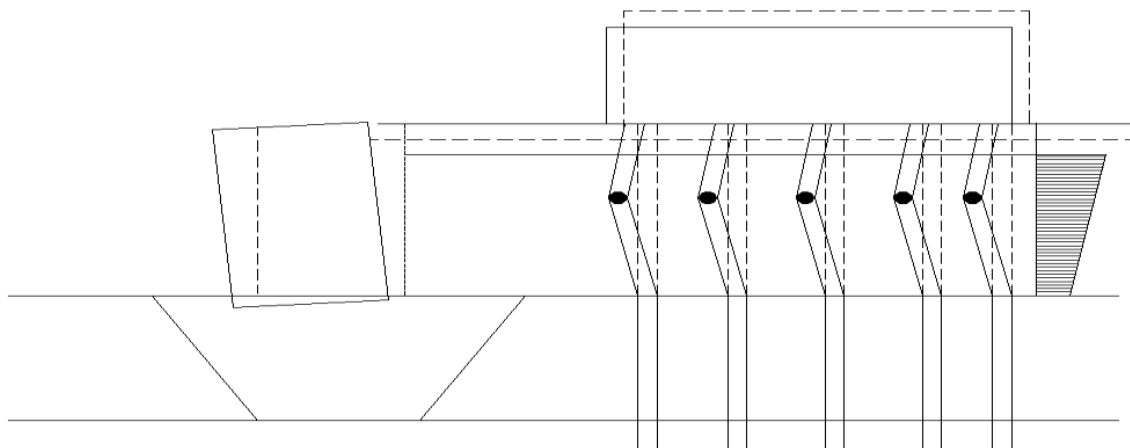
Figure 1.2 Flexure-shear failure [3]
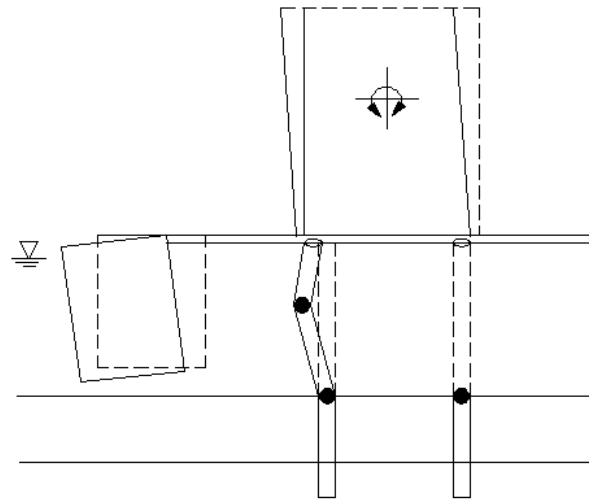
Figure 1.3 Pile failure due to the superstructure overturning [3]

Two types of pile shaft forces can be identified under earthquake loading:

- Additional dynamic stress is brought about by the interaction between the soil, piles, and the structure.

- Extra static stress due to lateral deformation of pile shafts.

The soil will exhibit lateral movement under earthquake loading, which will cause the pile to deform because of the lateral thrust of the soil. Among piles that are not subject to lateral movement during earthquakes, additional dynamic stress is created by soil-pile-superstructure interaction. However, piles suffer from additional dynamic and static stresses because of soil lateral movement caused by earthquake loading. The pile cap connects the pile to the superstructure and its movement must be coordinated with soil displacement causing dynamic stress. Additionally, the pile cap acts as a conduit for seismic inertial forces generated by the superstructure resulting in dynamic stresses in the pile. Thus, the pile is exposed to the two components mentioned above when it is under earthquake loading.

Under earthquake loading, the failure mechanism is dependent on the forces acting on the pile and is therefore subcategorized into three groups [3]:

1- The failure mode which results from additional dynamic stresses that are induced by vibration. In general, weak piles in weak soil layers may experience this mode of failure

during a strong earthquake vibration. As a result, the reaction forces from surrounding soil tend to be relatively small, pile deformation is relatively high, and the pile shafts experience relatively large additional dynamic stresses.

2- The failure mode caused by additional static stress generated by soil movement which typically occurs on slopes. This situation usually occurs in the weak layer of soil by the shear stress which occurs during an earthquake in the same direction as slop. Lateral movement will therefore be generated in the direction of stress.

3- Due to liquefaction of sandy soil under earthquake loading, pile foundations can easily lose bearing capacity when their length penetrating into the steady soil layer is not enough, or the pile tip doesn't reach the steady soil layer.

Based on the first mode of failure (explained above), piles may experience more axial loads due to earthquakes. In this case, the pile may be subjected to axial instability, like a slender column. Additionally, to increase the axial load, a reduction in lateral supporting force caused by an earthquake may also lead to axial instability. Eventually, this instability will result in buckling deformation and a plastic joint will be formed. Since the piles buckle suddenly and without clear signs of danger, it is necessary to study the piles' buckling stability and calculate their critical buckling load [5].

An example of pile failure was Showa Bridge during 1964 Niigata earthquake in Japan. Figure 1.4 and Figure 1.5 show photos of the bridge after the earthquake and a longitudinal view of the bridge which indicate the damaged pile foundations during the earthquake. Many researchers, such as Hamada and O'Rourke [6] and Ishihara [7], have explained that the collapse of the bridge was due to the lateral spreading of soil layers surrounding the piles.

On the other hand, Bhattacharya (2003) focused on the fact that pile P5 had been deformed to the left, while the pile P6 had been deformed to the right. If the cause of the failure of the piles was lateral spreading, the piles should have deformed in the same direction of the slope. In addition, no damage was observed near the riverbank, while lateral expansion was very severe in this area. Also, due to lateral spreading, a plastic joint should be created on the surface between the liquefied and non-liquefied layers, but as can be seen in the three piles,

these joints are created above the piles. Consequently, he concluded that the piles failed because of buckling instability, not because they spread laterally.

This thesis will investigate the dynamic instability of piles (buckling) under dynamic loads caused by earthquakes. In the continuation of this chapter, we will discuss how to model the piles under earthquakes.

Figure 1.4 Showa Bridge after Niigata earthquake [8]
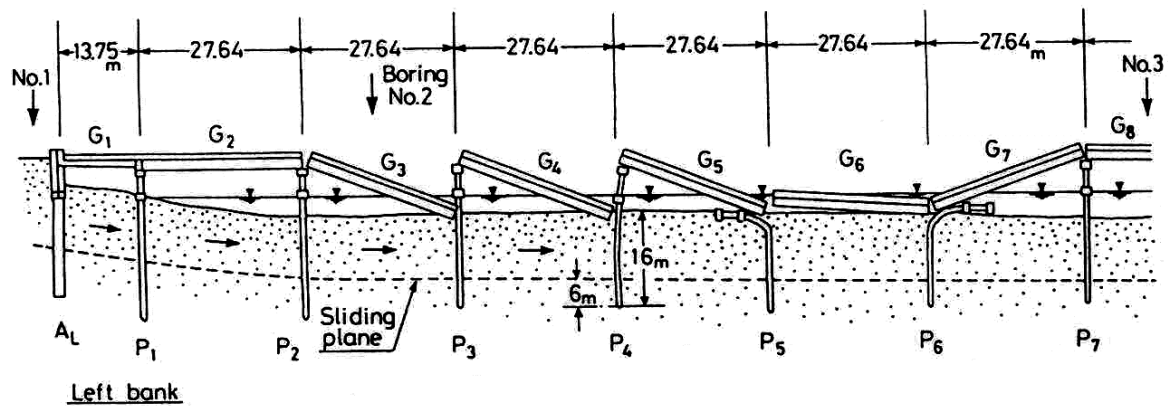
Figure 1.5 Schematic diagram of the fall-off of the girders in Showa bridge [8]

1.1.2.   Buckling instability of piles

An axial load that can be supported by a column just prior to its buckling is known as the critical load, P_{cr}. To understand the nature of this instability, we can look at the two-bar mechanism made up of weightless rigid bars that are connected to each other by pins and a spring which provide lateral support against instability (Figure 1.6).

Solving the equilibrium equations for the static load P leads to

$$P_{cr} = \frac{kL}{4},$$ (1.1)

where k and L is the stiffness of spring and column length, respectively.
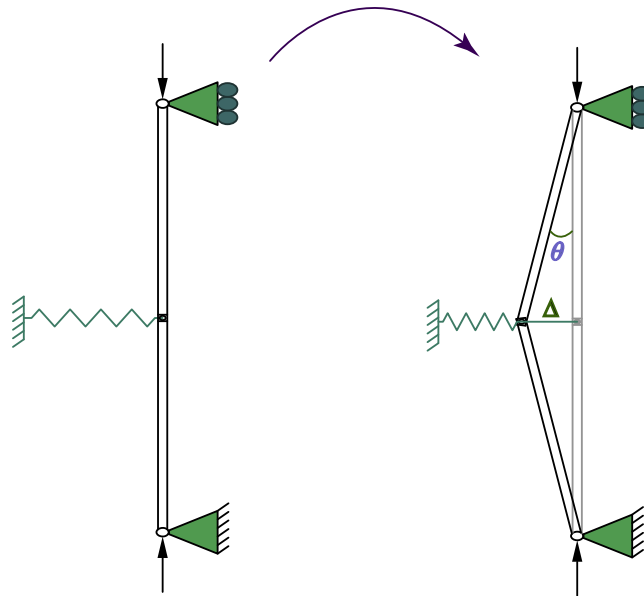
Figure 1.6 The buckling model of a column

Provided that there is an ideal column (straight column consisting of homogeneous linear elastic material) with pin-pin supports, by using [9]

$$EI\frac{d^2v}{dx^2} = M,$$ (1.2)

as a relation between the internal moment of the column and its deflection, the critical load for the first mode of deformation, 'Euler load', is known as

$$P_1 = \frac{EI\pi^2}{L^2},$$ (1.3)

where L is the length of the column and EI is the flexural properties of the column [9].

Generally, Euler load will be found from

$$P_n = EI \left(\frac{n\pi}{L_e}\right)^2 , \tag{1.4}$$

where L_e is the effective length of the column (based on both supports' restrictions), and n is the mode number of deformation.

It is not always easy to analyze stability as above. The loads placed on this type of element are usually both static and dynamic. Dynamic loads change in amplitude and direction over time, unlike static loads which are usually specific. Dynamic stability problems are generally modeled by differential equations of second-order with periodic coefficients [10]. For these kinds of problems, researchers have explored different approximate methods, which cannot provide an exact solution. The main goal is to develop a method to determine the response of the system and to assess the stability that goes along with it.

Beliaev first studied the stability of uniform bars under varying axial forces, followed by Timoshenko, Bolotin and others [11]. In 1964, Bolotin [10] examined the transverse vibrations of a straight rod loaded by a periodic longitudinal force. On the one hand, it is assumed the rod is simply supported on one end, and its cross section is uniform along its length. To arrive at the equation for the transverse vibrations of a rod loaded by the periodic longitudinal force $P(t) = P_s + P_d \cos \theta t$, where P_s and P_d are static and dynamic force respectively, and θ is the angular frequency of the dynamic load. Thus, Bolotin, wrote the differential equation in the form of

$$\ddot{q}_n + \omega_n^2(1 - 2\mu_n \cos \theta t)q_n = 0, \tag{1.5}$$

where

$$\omega_n^2 = \Omega_n^2 \left(1 - \frac{P_s}{P_n}\right) \quad , \quad 2\mu_n = \frac{P_d}{P_n - P_s}, \quad \Omega_n = \left(\frac{n\pi}{L}\right)^2 \sqrt{\frac{EI}{\rho A}} ,$$

where Ω_n is the nth natural frequency of a simply supported column when $P(t) = 0$. Also, ω_n is the frequency of free vibrations of the pile loaded by a constant longitudinal compressive force P_s and constrained by a lateral foundation stiffness. Eq. (1.5) is the well-known Mathieu

equation. In general, if the axial load is $P(t) = P_s + P_d \Phi(t)$ which $\Phi(t)$ is a periodic function, i.e. $\Phi(t + T) = \Phi(t)$, the result will be in form of

$$\ddot{q}_n + \omega_n^2(1 - 2\mu_n\Phi(t))q_n = 0, \tag{1.6}$$

which is called the Mathieu-Hill equation. Bolotin suggested parametric solution to find the relation between parameters which leads to the stable or unstable response region of the systems.

Bolotin's book also includes discussions on how damping affects the dynamic stability region of a beam. The study of the Mathieu-Hill equation has generated a tremendous amount of literature by finding a stability region diagram under different conditions. In 1970, Burney [11] used a numerical method to determine the areas of dynamic instability in a column subject to different boundary conditions. As an idealized system, a column consisted of massless springs and lumped masses. It is possible to solve non-uniform columns quickly with this method by applying an appropriate subdivision. In 1972, Iwatsubo [12] studied problems associated with cantilevered columns exposed to periodic axial (Euler-type problem) and tangential load (Beck-type problem) conditions at their free ends.

In 2020, Zhang also investigated how soil liquefaction impacts critical buckling loads of pile foundations. A finite element method was used in this study and centrifuge test results validated the results. Moreover, using the parametric analytical method, the effects of soil relative density, the initial geometric imperfections of the pile, the flexural rigidity of the pile, and the pier height on buckling load were investigated [13].

A study was conducted in 2021 by Rui Zhang on the buckling stability of piles in slope foundations. The study examines slope angle, landslide thrust distribution behind the pile, pile-embedded ratio, pile support condition, pile-body friction, and pile-side soil resistance [14].

Deng in 2019 and 2021 examined the mechanism behind pillar rockburst under the influence of triangular stress waves induced by underground blasting. The failure may damage equipment, cause a worker to be injured, or even result in tunnels and mines being abandoned. An analytical method was employed to investigate the effects of various factors on the mechanism of pillar rockburst, such as the amplitude of static and dynamic component loads,

frequency, slope, duration, multimode, peakedness, and the time gap between two dynamic loads [15], [16].
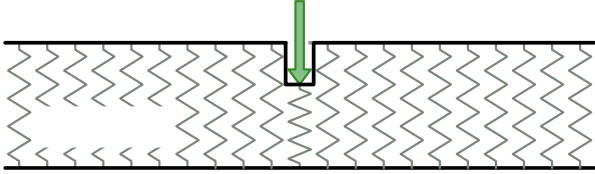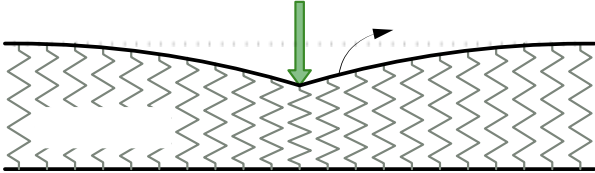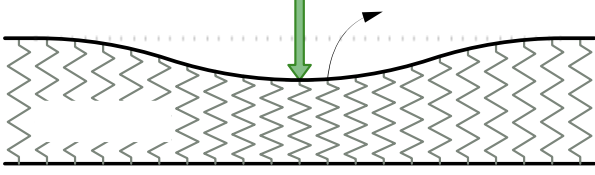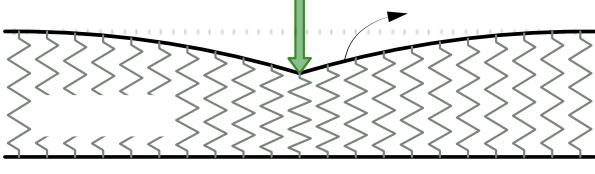
1.1.3.   Modeling piles by a beam on an elastic foundation

The interaction between a beam and a foundation is driven primarily by foundation types. Analyses of railroad tracks were conducted first using beams on elastic foundations in the nineteenth century. Since then, a wide variety of mechanical models have been proposed for analyzing static soil-structure interactions. Tanahashi [17] summarized the mechanical models of soil and described their applications. The governing equation and model figure for each mechanical model is given in Table 1.1. The origin is the loading point of the soil, x represents the distance, y shows the deflection. Depending on their parameters, they can be divided into two types: one-parameter and two-parameter models.

The simplest and only one-parameter model for continuous systems, the Winkler model, states that a continuum is a set of discrete, independent linear springs whose reaction forces are proportional to their displacements. Some other models are the Filonenko-Borodich Model (with tensile component), Hetenyi Model (with flexural component), and Pasternak Model (with shear member) [17]. These models try to address the discontinuity shortcoming of the Winkler Model by adding a member above the springs.

It is essential to understand the static behaviour of these types of foundations in order to understand their dynamic behavior. As well, the study of the impact of the surrounding medium on dynamic stability is crucial to understanding how these media will behave under different types of time-varying loads.

Table 1.1 Mechanical soil models [17]

Model of soil		Deflection Curve of the Surface	Equations
One-Parameter model	Winkler		$p = ky$ $y = \dfrac{P}{k}\delta(x)$
Two-Parameter model	Filonenko -Borodich		$p = ky - Ty''$ $y = \dfrac{P\gamma}{2k}e^{-\gamma|x|}, \gamma = \sqrt{k/T}$
Two-Parameter model	Hetenyi		$p = ky + Dy^{(4)}$ $y = \dfrac{P\beta}{2k}e^{-\beta x}(\cos\beta|x|$ $+ \sin\beta|x|)$ $\beta = \sqrt[4]{k/4D}$
Two-Parameter model	Pasternak		$p = ky - Gy''$ $y = \dfrac{P\gamma}{2k}e^{-\gamma|x|}$ $\gamma = \sqrt{k/G}$

In 1973, Sugiyama [18] indicated that it is possible to approximate a continuous system with a discrete system if finite differences are applied to the equation of motion. Ahuja [19], in 1974, studied both theoretically and experimentally the parametric response of a beam with a variable cross-section that lay on an elastic foundation and was subjected to the dynamic axial load. He used the Winkler-type foundation and indicated that both theoretical and experimental results show the exact boundaries for the region of instability. In 1987, Yokoyama [20] analyzed the behavior of a Timoshenko beam rested on an elastic foundation modeled by Winkler by using finite element methods. Timoshenko beams with different end conditions were investigated for their natural frequencies, their static buckling loads, and their dynamic instabilities influenced by elastic foundations. As a result of the subgrade reaction theory, Gabr [21] developed a model in 1997 to evaluate the critical buckling capacity of long slender

friction piles that features lateral soil support. Within the model, a general power distribution is used to determine the coefficient of the subgrade reaction (k_h). The study was related stability of a slender pile with different tip and top supports (pinned, fixed, or free end).

Engel [22] used a beam rested on visco-elastic supports. Viscous damping of the supporting medium has been incorporated into the Winkler, Hetenyi, and Pastemak foundation models by Engel. By mean of Floquet theory, he determined the critical dynamic loads and the regions of instability. He illustrated the influence of the viscous damping of the foundation properties on the stability behavior. He also compared the instability boundary during the different modes of buckling deformation as well as the effect of the different soil pile interaction models.

1.1.4.   Fractional calculus

The concept of fractional derivatives goes back as far as calculus. A question asked by L'Hopital in 1695 was: What is the meaning of $\frac{d^n f}{dx^n}$ if $n = 1/2$? Researchers have been trying to derive a definition of a fractional derivative ever since.

The purpose of this section is to give a quick overview of fractional calculus definitions and theorems in a brief manner. With respect to the variable t and starting point $t = a$, the Riemann–Liouville fractional derivative is [23]

$$_aD_t^\alpha f(t) = \begin{cases} \frac{1}{\Gamma(n-\alpha)} \frac{d^n}{dt^n} \int_a^t \frac{f(\tau)}{(t-\tau)^{\alpha-n+1}} d\tau; & 0 \le n-1 \le \alpha < n, \\ \frac{d^n}{dt^n}; & \alpha = n \text{ and } \alpha \in N, \end{cases} \tag{1.7}$$

where

$$\Gamma(n-\alpha) = \int_0^\infty x^{n-\alpha-1}e^{-x}dx.$$

Based on Riemann-Liouville principles, the fractional order integrals are defined as

$$I^\alpha(f(t)) = \quad _aD_t^{-\alpha}f(t) = \frac{1}{\Gamma(\alpha)}\int_a^t (t-\tau)^{\alpha-1}f(\tau)d\tau; \quad \alpha > 0. \tag{1.8}$$

Also, the fractional derivatives of Caputo are defined as

$$D^\alpha f(t) = \begin{cases} I^{n-\alpha} D_t^n f(t); & n-1 < \alpha \leq n, n \in N, t > 0, \\ \frac{d^n}{dt^n} f(t); & \alpha = n. \end{cases} \tag{1.9}$$

The former definition was introduced first and is now well established. However, it is challenging to apply to real problems. The latter concept, the Caputo type derivative, is thus introduced to address these challenges [24]. By using Caputo, the derivative of a constant value is zero, and we get

$$D_t^\alpha t^n = \begin{cases} 0; & n \in N, n < \lceil \alpha \rceil, \\ \frac{\Gamma(n+1)}{\Gamma(n+1-\alpha)} t^{n-\alpha}; & n \in N, n > \lceil \alpha \rceil, \end{cases} \tag{1.10}$$

where $\lceil \alpha \rceil$ is the smallest integer greater than α. Also, there is a relationship between the Caputo operator and the Riemann-Liouville definition according to

$$_a D_t^\alpha I^\alpha f(t) = f(t),$$
$$I^\alpha \quad _a D_t^\alpha f(t) = f(t) - \sum_{k=0}^{n-1} f(k)(a^+) \frac{(t-a)^k}{k!}, t > 0. \tag{1.11}$$

There are several lemmas related to fractional calculus which are useful for fractional calculation. There are

$$I^\alpha I^\beta f(t) = I^\beta I^\alpha f(t), \tag{1.12}$$

$$I^\alpha I^\beta f(t) = I^{\alpha+\beta} f(t), \text{ and} \tag{1.13}$$

$$D^\alpha(c_1 f(t) + c_2 g(t)) = c_1 D^\alpha f(t) + c_2 D^\alpha g(t), \tag{1.14}$$

where $\alpha, \beta \geq 0, c_1, c_2 \in \mathbb{R}$ and $f(t), g(t) \in L_1[0, b]$.

1.1.5. Fractional Damping

In the past three decades, fractional calculus has become more widely used. Several dynamic systems have been successfully modeled and controlled using this mathematical tool [25]. Fractional models provide an easy way to demonstrate the vibrational properties of elements with complex formulations, such as the multielement model, by rendering the damping mechanisms correctly using a low number of parameters [26]. Considering soil modeling, when $\alpha=0$, soil behaves like completely elastic material, while a Kelvin viscoelastic model can be obtained when $\alpha=1$. According to recent studies, a fractional order between 0 and

1 better describes the stress-strain relationship of viscoelastic soil, and the results show more compatibility with the experimental studies [27] [28] [29].

Shokooh [30] used two numerical methods to solve SDOF and MDOF systems with fractional damping. He considered both the central difference method and the average acceleration method for calculation and compared the result with the analytical solution in some cases. He indicated that the results of two numerical solutions were the same in the case of zero initial conditions but different when considering the non-zero initial value and significant damping coefficients.

In 2012, Yan studied the free vibration of an elastic Timoshenko beam on a fractional derivative Winkler viscoelastic foundation. Using numerical examples, he demonstrated how fractional derivative order and shear shape factor influenced elastic Timoshenko beam free vibration [31].

Cai studied the fractional modeling of Pasternak-type viscoelastic foundations. The new governing equation was determined by analyzing the viscoelastic reaction on a four-edged simply supported thin rectangular plate. As part of the research, a comparison was made between fractional Pasternak-type and Winkler foundation models [32].

In 2016, Germoso [33] developed an extended version of visco-elasto dynamics that incorporated frequency-dependent damping, investigating the impact of taking fractional derivatives for the representation of viscous contributions in the models. Also, by considering the fractional form of one degree of freedom (1 DOF) systems, he compared the evolution of phase angles with respect to frequency and damping power.

The dynamic response of beams resting on a foundation with fractional damping subjected to a moving load was investigated by Ouzizi in 2019. Using finite difference methods, he illustrated the influences of different variables like foundation stiffness, fractional damping order as well as moving load speed on the beam response [34]. In the same year, Zarraga studied the dynamical behaviour of systems with fractional damping. He analyzed SDOF system with fractional damping as well as the dynamics of a machine shaft supported by two bearings presenting fractional damping [35].

1.2. Thesis outline

In this research, Chapter 1 reviews some of the related literature and explains some introductory concepts. Chapter 2 considers pile as a beam on an elastic foundation with fractional damping and generates the pile's equation of motion during buckling instability. In Chapter 3, approximate and numerical solutions are introduced to solve equations of motion and to explain how these methods obtain instability regions. Chapter 4 includes an example of a pile and illustrates the results and comparisons from numerical and approximate methods and the influences of various parameters on buckling instability. Finally, Chapter 5 gives the conclusion and some ideas for further research.

C H A P T E R 2

Beams on elastic foundations with fractional damping

Piles with surrounding soil can be considered as a beam supported by an elastic or a viscoelastic foundation for investigating buckling instability. Many researchers have investigated the beams' static deflections and dynamic responses resting on different elastic and viscoelastic foundations. While the Winkler model has discontinuity between loaded and unloaded, many researchers prefer to use this model in their dynamic studies because of its simplicity in solving the problem. The Winkler model is considered a soil media around the pile foundation in this study.

2.1. Problem formulation

To study the stability of a pile, we consider an infinitesimal vertical element among the pile and write the equation of motion for that element. This equation is written based on the different properties of the vertical element and surrounding media. The equation of motion can often be derived from the force balance or energy balance equations and we will utilize the former in this study.

As indicated in Figure 2.1, a pile with a uniform cross-section, length of L, and the flexural rigidity of EI. The pile is simply supported at both ends (pin-pin condition) and is restricted by soil media against lateral deformations. In Figure 2.1, $p(x,t)$ is the subgrade

reaction per length of the pile, which includes the effects of springs and dampers. Also, force (ma) is the inertia force (D'alembert's force) that acts against particle movement and is equal to $(\rho A \Delta x \ddot{v})$. In which ρ is the pile's mass density per unit volume, and A is the cross-sectional area. In addition, v is a function of x and t due to the dynamic axial load.
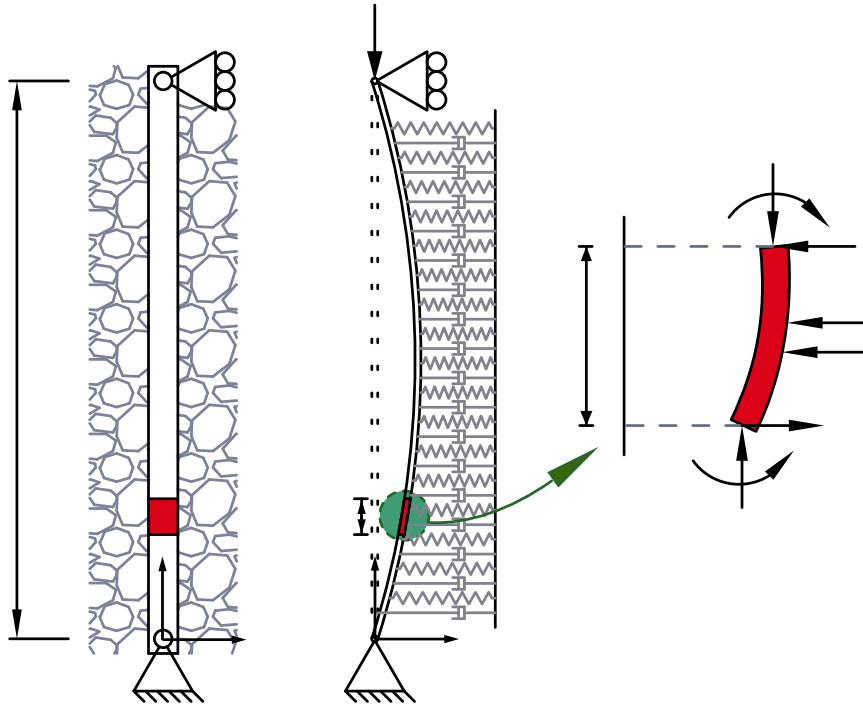
Figure 2.1 Pile foundation surrounded by the soil under axial load

Consider the equilibrium equations for the infinitesimal length of the pile. When the forces are summed in the vertical direction x, the result is $\Delta P = 0$. By adding up the forces in the horizontal direction v, we get

$$(S + \Delta S) + (\rho A \Delta x)\ddot{v} - S + p(x, t) \times \Delta x = 0 \quad \Rightarrow \quad \frac{\Delta S}{\Delta x} = -\rho A \ddot{v} - p(x, t). \tag{2.1}$$

Summarizing the moment of the midpoint of the pile segment results in

$$(M + \Delta M) + P(t) \times [(v + \Delta v) - v] - M - (S + \Delta S) \times \Delta x - (\rho A \Delta x)\ddot{v} \times \frac{\Delta x}{2} - p(x, t)\Delta x \times \frac{\Delta x}{2} = 0$$

$$\Rightarrow \quad \Delta M + P(t) \times \Delta v - (S + \Delta S) \times \Delta x - (\rho A \Delta x)\ddot{v} \times \frac{\Delta x}{2} - p(x, t)\Delta x \times \frac{\Delta x}{2} = 0. \tag{2.2}$$

Substituting Eq. (2.1) into Eq. (2.2) leads to

$$\frac{\Delta M}{\Delta x} + P(t) \times \frac{\Delta v}{\Delta x} = (S + \Delta S) - \frac{\Delta S}{2}. \tag{2.3}$$

Provided that $\Delta x \to 0$, Eq. (2.1) into Eq. (2.3) are changed into the forms of

$$\frac{\partial S}{\partial x} = -\rho A \ddot{v} - p(x, t), \text{ and} \tag{2.4}$$

$$\frac{\partial M}{\partial x} + P(t) \times \frac{\partial v}{\partial x} = S, \tag{2.5}$$

respectively. By differentiating from Eq. (2.5) with respect to x, we get

$$\frac{\partial^2 M}{\partial x^2} = \frac{\partial S}{\partial x} - P(t) \times \frac{\partial^2 v}{\partial x^2}. \tag{2.6}$$

Replacing (2.4) into Eq. (2.6) results in

$$\frac{\partial^2 M}{\partial x^2} = -\rho A \ddot{v} - p(x, t) - P(t) \times \frac{\partial^2 v}{\partial x^2}. \tag{2.7}$$

On the other hand, the Moment-Curvature relationship of an elastic beam is

$$M = EI \frac{\partial^2 v}{\partial x^2}, \tag{2.8}$$

and by substituting Eq. (2.8) into Eq. (2.7), the motion equation of the pile can be written as

$$EI \frac{\partial^4 v}{\partial x^4} + P(t) \frac{\partial^2 v}{\partial x^2} + \rho A \frac{\partial^2 v}{\partial t^2} + p(x, t) = 0. \tag{2.9}$$

In addition to axial static loads, piles are often subjected to axial dynamic loads as well. Various dynamic loads may occur, including earthquakes, vibrations from machines, and engineering blasts [36]. Consider the dynamic axial load with the period of $T = \frac{2\pi}{\theta}$ equal to

$$P(t) = P_s + P_d \cos \theta t, \tag{2.10}$$

where P_s and P_d are the static and dynamic parts of the axial force imposed to the pile. Then, Eq. (2.9) is equal to

$$EI \frac{\partial^4 v}{\partial x^4} + (P_s + P_d \cos \theta t) \frac{\partial^2 v}{\partial x^2} + \rho A \frac{\partial^2 v}{\partial t^2} + p(x, t) = 0. \tag{2.11}$$

Considering the fractional damping for the soil which surrounds the pile, the soil reaction force along the length of the pile is

$$p(x, t) = k_s v + c_s D_t^\alpha v, \tag{2.12}$$

where k_s is the linear foundation stiffness, and c_s is the viscous damping coefficient of the soil foundation. Also, $c_s D_t^\alpha v$ shows the fractional damping force of the soil. Based on Eq. (2.12) and Figure (2.1), when the pile is deflected to the right (positive direction of v), the spring force

is directed to the left (because of the soil at the right-hand side of the pile) and when pile is deflected to the left (negative direction of v) the spring force is directed to the right (because of the soil at the left-hand side of the pile). So, the mechanical model of soil shown in Figure (2.1) considers the reaction of soil media on both sides of the pile together.

Substituting Eq. (2.12) into Eq. (2.11) yields

$$EI \frac{\partial^4 v}{\partial x^4} + (P_s + P_d \cos \theta t) \frac{\partial^2 v}{\partial x^2} + \rho A \frac{\partial^2 v}{\partial t^2} + (k_s v + c_s D_t^\alpha v \ ) = 0. \tag{2.13}$$

For simply supported piles, the boundary conditions are given by

$$\begin{cases} at \ x = 0: & v(0,t) = 0, \frac{\partial^2 v(0,t)}{\partial x^2} = 0, \\ at \ x = L: & v(L,t) = 0, \frac{\partial^2 v(L,t)}{\partial x^2} = 0. \end{cases} \tag{2.14}$$

Eq. (2.13) is a partial differential equation (PDE), which needs to be converted to an ordinary differential equation (ODE) in the study of dynamic stability. For this purpose, $v(x,t)$ is considered as

$$v(x,t) = \sum_{i=1}^{\infty} q_i(t) \phi_i(x), \phi_i(x) = \sin \frac{i\pi x}{L} \qquad (i = 1,2, \dots), \tag{2.15}$$

where $\phi_i(x)$ are the modal functions of a simply supported column satisfying the boundary conditions Eq. (2.14), which possess the orthogonality property

$$\int_0^L \phi_i(x) \phi_j(x) dx = \begin{cases} 0, & i \neq j, \\ \frac{1}{2} L, & i = j, \end{cases} \tag{2.16}$$

which results in the following

$$\frac{\partial^2 v}{\partial x^2} = \sum_{i=1}^{\infty} q_i(t) \frac{\partial^2 \Phi_i(x)}{\partial x^2} = -\sum_{i=1}^{\infty} q_i(t) \left(\frac{i\pi}{L}\right)^2 \sin\left(\frac{i\pi x}{L}\right), \tag{2.17}$$

$$\frac{\partial^4 v}{\partial x^4} = \sum_{i=1}^{\infty} q_i(t) \frac{\partial^4 \Phi_i(x)}{\partial x^4} = \sum_{i=1}^{\infty} q_i(t) \left(\frac{i\pi}{L}\right)^4 \sin\left(\frac{i\pi x}{L}\right), \tag{2.18}$$

$$\frac{\partial^2 v}{\partial t^2} = \sum_{i=1}^{\infty} \ddot{q}_i(t) \Phi_i(x) = \sum_{i=1}^{\infty} \ddot{q}_i(t) \sin\left(\frac{i\pi x}{L}\right), \tag{2.19}$$

$$\frac{\partial^\alpha v}{\partial t^\alpha} = \sum_{i=1}^{\infty} \frac{\partial^\alpha q_i(t)}{\partial t^\alpha} \phi_i(x) = \sum_{i=1}^{\infty} \frac{\partial^\alpha q_i(t)}{\partial t^\alpha} \sin\left(\frac{i\pi x}{L}\right). \tag{2.20}$$

Substituting Eqs. (2.17) to (2.20) into Eq. (2.13) results in

$$EI \sum_{i=1}^{\infty} q_i(t) \left(\frac{i\pi}{L}\right)^4 \sin\left(\frac{i\pi x}{L}\right) - (P_s + P_d \cos \theta t) \times \sum_{i=1}^{\infty} q_i(t) \left(\frac{i\pi}{L}\right)^2 \sin\left(\frac{i\pi x}{L}\right) +$$

$$\rho A \sum_{i=1}^{\infty} \ddot{q}_i(t) \sin\left(\frac{i\pi x}{L}\right) + \left(k_s \sum_{i=1}^{\infty} q_i(t) \sin\left(\frac{i\pi x}{L}\right) + c_s \sum_{i=1}^{\infty} D_t^\alpha q_i(t) \ \sin\left(\frac{i\pi x}{L}\right)\right) = 0. \tag{2.21}$$

Multiplying both sides of Eq. (2.21) by $\Phi_n(x) = \sin\left(\frac{n\pi x}{L}\right)$, integrating with respect to

x from 0 to L and using orthogonality property, Eq. (2.16), leads to

$$EI q_n(t)\left(\frac{n\pi}{L}\right)^4 - (P_s + P_d \cos\theta t) \times q_n(t)\left(\frac{n\pi}{L}\right)^2 + \rho A \ddot{q}_n(t) + \left(k_s q_n(t) + c_s D_t^\alpha q_n(t)\right) = 0,$$

$$\rho A \ddot{q}_n(t) + c_s D_t^\alpha q_n(t) + \left[EI\left(\frac{n\pi}{L}\right)^4 - (P_s + P_d \cos\theta t) \times \left(\frac{n\pi}{L}\right)^2 + k_s\right] q_n(t) = 0. \qquad (2.22)$$

Considering

$$\lambda = \frac{P_s}{P_{cr}} = \frac{P_s L^2}{\pi^2 EI}, \quad \epsilon = \frac{P_d}{P_{cr}} = \frac{P_d L^2}{\pi^2 EI}, \quad \eta = \frac{k_s L^4}{\pi^2 EI}, \quad \beta = \frac{c_s}{2\rho A} = \frac{\delta \cdot \omega}{2\pi} = \frac{\delta \Omega \sqrt{n^4 - \lambda n^2 + \eta}}{2\pi}, \qquad (2.23)$$

where λ is the dimensionless static load parameter, ϵ is the dimensionless dynamic load

parameter, η dimensionless foundation stiffness parameter, β is the damping coefficient, and

δ is the logarithmic decrement of damping. Also, P_{cr} and Ω are the critical Euler buckling load

and natural frequency of a simply supported pile for the first mode, where

$$P_{cr} = \frac{EI\pi^2}{L^2}, \qquad \Omega = \frac{\pi^2}{L^2}\sqrt{\frac{EI}{\rho A}}. \qquad (2.24)$$

Using the introduced dimensionless coefficients in Eq. (2.23) and simplifying, results in

$$\ddot{q}_n(t) + 2\beta D_t^\alpha q_n(t) + \omega^2(1 - 2\mu \cos\theta t)q_n(t) = 0, \qquad (2.25)$$

where

$$\omega^2 = \Omega^2(n^4 - \lambda n^2 + \eta), \qquad 2\mu = \frac{\Omega^2 \epsilon n^2}{\omega^2} = \frac{\epsilon n^2}{n^4 - \lambda n^2 + \eta}. \qquad (2.26)$$

The first mode is the most critical mode of deformation; then, by considering $n = 1$

and eliminating the subscript, Eq. (2.25) can be written as

$$\ddot{q}(t) + 2\beta D_t^\alpha q(t) + \omega^2(1 - 2\mu \cos\theta t)q(t) = 0, \qquad (2.27)$$

where

$$\omega^2 = \Omega^2(1 - \lambda + \eta), \qquad \beta = \frac{\delta \cdot \omega}{2\pi}. \qquad (2.28)$$

Provided that $\alpha = 1$, Eq. (2.27) is transformed into

$$\ddot{q}(t) + 2\beta \dot{q}(t) + \omega^2(1 - 2\mu \cos\theta t)q(t) = 0. \qquad (2.29)$$

Eq. (2.29) demonstrates the famous damped Mathieu equation. It has been suggested

by Xie [37] that the variable change can eliminate the damping term. If $q(t) = e^{(-\beta t)}u(t)$ then

the first and second derivative of the $q(t)$ is

$$\dot{q} = -\beta e^{(-\beta t)} u + e^{(-\beta t)} \dot{u}, \quad \ddot{q} = \beta^2 e^{(-\beta t)} u - 2\beta e^{(-\beta t)} \dot{u} + e^{(-\beta t)} \ddot{u}. \tag{2.30}$$

Substituting Eq. (2.30) into Eq. (2.29) results in

$$\beta^2 e^{(-\beta t)} u - 2\beta e^{(-\beta t)} \dot{u} + e^{(-\beta t)} \ddot{u} + 2\beta\left(-\beta e^{(-\beta t)} u + e^{(-\beta t)} \dot{u}\right) + \omega^2(1 - $$

$$2\mu \cos\theta t)e^{(-\beta t)} u = 0,$$

$$\ddot{u} + \omega^2 \left[\left(1 - \frac{\beta^2}{\omega^2}\right) - 2\mu \cos\theta t\right] u = 0. \tag{2.31}$$

Eq. (2.31) is the typical form of an undamped Mathieu equation.

2.2. Summary

In this chapter, we introduce the model consisting of a beam supported by the Winkler foundation with fractional-order damping. The equation of motion is found, using the equilibrium equations, in the form of a partial differential equation shown in Eq. (2.13). Next, the Galerkin method converts the partial differential equation into the ordinary differential equation shown in Eq. (2.22). In the final step, introducing some dimensionless parameters, the equation is reduced into the fractional Mathieu differential equation, Eq. (2.27).

The next chapter introduces approximate and numerical methods to solve the fractional Mathieu differential equation. It also explains how instability diagrams should be found using the vibration responses.

CHAPTER 3

Theoretical and numerical studies of dynamic stability

It was illustrated in Chapter 2 that the motion equation of a pile, considering Winkler foundation with damping from the surrounding lateral supporting soil, under dynamic axial loading, results in the conventional Mathieu equation. While fractional damping of soil results in the fractional Mathieu equation.

The first section of this chapter explains the Bolotin method based on the Floquet theory. It illustrates the matrices of coefficients and how it is possible to find the instability regions using the matrices.

Next, an approximate method is introduced based on the Bolotin method to solve the fractional Mathieu equation. For this purpose, the fractional derivative is expanded based on Caputo's definition.

Finally, a numerical method based on block-pulse functions is explained to solve the fractional Mathieu equation to find vibration responses. It is also indicated how instability diagrams of a pile under dynamic axial load should be found by using the vibration responses.

3.1. Bolotin method

Consider a typical damped Mathieu equation [37] such as

$$\ddot{q} + 2\beta\dot{q} + \omega^2(1 - 2\mu\cos\theta t)q = 0, \qquad T = \frac{2\pi}{\theta} \ . \tag{3.1}$$

Mathieu's equation corresponds to periodic solutions at its stability boundaries. Based on the classical Floquet theory, periodic solutions of $q(t)$ (periods $2T$ and T) can be written in the form of the Fourier series.

For finding the solutions with period $2T$, we consider the odd numbered terms of the Fourier series, thus

$$q(t) = \sum_{k=1\ (odd)}^{\infty} \left(a_k \sin\frac{k\pi t}{T} + b_k \cos\frac{k\pi t}{T} \right) = \sum_{k=1\ (odd)}^{\infty} \left(a_k \sin\frac{k\theta t}{2} + b_k \cos\frac{k\theta t}{2} \right). \qquad (3.2)$$

Substitute Eq. (3.2) into Eq. (3.1) and use the trigonometric identities conversions

$$\cos(\alpha)\sin(\beta) = \frac{1}{2}(\sin(\alpha+\beta) - \sin(\alpha-\beta)),$$
$$\cos(\alpha)\cos(\beta) = \frac{1}{2}(\cos(\alpha-\beta) + \cos(\alpha+\beta)), \qquad (3.3)$$

to simplify the required terms. Also, we know that the functions $\sin\frac{k\theta t}{2}, \cos\frac{k\theta t}{2}$ are independent, so by setting the coefficients of $\sin\frac{\theta t}{2}, \cos\frac{\theta t}{2}, \sin\frac{3\theta t}{2}, \cos\frac{3\theta t}{2}, \dots$ equal to zero the system of equations becomes equal to

$$k = 1: \quad \begin{cases} (1+\mu-r^2)a_1 - \mu a_3 - (2\beta r/\omega)b_1 = 0, \\ (1-\mu-r^2)b_1 - \mu b_3 + (2\beta r/\omega)a_1 = 0, \end{cases}$$

$$k = 3,5,\dots: \quad \begin{cases} (1-k^2 r^2)a_k - \mu(a_{k-2} + a_{k+2}) - (2k\beta r/\omega)b_k = 0, \\ (1-k^2 r^2)b_k - \mu(b_{k-2} + b_{k+2}) + (2k\beta r/\omega)a_k = 0, \end{cases} \qquad (3.4)$$

where $r = \theta/2\omega$. The above system of equations can be simplified in form of

$$|C|_{2T} \times [\dots, a_5, a_3, a_1, b_1, b_3, b_5, \dots]^T = 0, \qquad (3.5)$$

where $|C|_{2T}$ is the matrix of coefficients and the determinant of the matrix should be equal to zero to find the boundary of regions of instability, which results in

$$|C|_{2T} = \begin{vmatrix} \cdots & \cdots & \cdots & \cdots & \cdots & \cdots & \cdots & \cdots \\ \cdots & 1-25r^2 & -\mu & 0 & 0 & 0 & -10\beta r/\omega & \cdots \\ \cdots & -\mu & 1-9r^2 & -\mu & 0 & -6\beta r/\omega & 0 & \cdots \\ \cdots & 0 & -\mu & 1+\mu-r^2 & -2\beta r/\omega & 0 & 0 & \cdots \\ \cdots & 0 & 0 & 2\beta r/\omega & 1-\mu-r^2 & -\mu & 0 & \cdots \\ \cdots & 0 & 6\beta r/\omega & 0 & -\mu & 1-9r^2 & -\mu & \cdots \\ \cdots & 10\beta r/\omega & 0 & 0 & 0 & -\mu & 1-25r^2 & \cdots \\ \cdots & \cdots & \cdots & \cdots & \cdots & \cdots & \cdots & \cdots \end{vmatrix} = 0 \ .$$

$$(3.6)$$

The determinant in Eq. (3.6) corresponds to the periodic solutions of period $2T$. Since the determinant has an infinite order, it is impossible to solve it directly, but it allows us to estimate the approximate borders of the region of instability based on the order. For instance, the first and second order approximations of the boundary of the first stability region are found by plotting the relations between r and μ from the following determinants.

$$\begin{vmatrix} 1 + \mu - r^2 & -2\beta r/\omega \\ 2\beta r/\omega & 1 - \mu - r^2 \end{vmatrix} = 0 \qquad \text{(First approximation),} \tag{3.7}$$

$$\begin{vmatrix} 1 - 9r^2 & -\mu & 0 & -6\beta r/\omega \\ -\mu & 1 + \mu - r^2 & -2\beta r/\omega & 0 \\ 0 & 2\beta r/\omega & 1 - \mu - r^2 & -\mu \\ 6\beta r/\omega & 0 & -\mu & 1 - 9r^2 \end{vmatrix} = 0 \qquad \text{(Second approximation).} \tag{3.8}$$

On the other hand, to find solutions with period T, we consider the even numbered terms of the Fourier series, thus

$$q(t) = b_0 + \sum_{k=2 \text{ (even)}}^{\infty} \left(a_k \sin \frac{k\pi t}{T} + b_k \cos \frac{k\pi t}{T} \right) = b_0 + \sum_{k=2 \text{ (even)}}^{\infty} \left(a_k \sin \frac{k\theta t}{2} + \right.$$

$$\left. b_k \cos \frac{k\theta t}{2} \right). \tag{3.9}$$

Simplifying, using the trigonometric identity conversions in Eq. (3.3) when required, and setting the coefficients of $\sin \theta t$, $\cos \theta t$, $\sin 2\theta t$, $\cos 2\theta t$, ... equal to zero, leads to the system of equations

$$\begin{array}{ll} 1: & b_0 - \mu b_2 = 0, \\ \cos vt: & (4\beta r/\omega)a_2 - 2\mu b_0 + (1 - 4r^2)b_2 - \mu b_4 = 0, \\ \sin (k\theta t/2), k = 2,4, \dots: & -\mu a_{k+2} + (1 - k^2 r^2)a_k - \mu a_{k-2} - (2k\beta r/\omega)b_k = 0, \\ \cos (k\theta t/2), k = 4,6, \dots: & (2k\beta r/\omega)a_k - \mu b_{k-2} + (1 - k^2 r^2)b_k - \mu b_{k+2} = 0, \end{array} \tag{3.10}$$

where $r = {\theta}/{2\omega}$. Writing the above system of equations in matrix form results in

$$|C|_T \times [\dots, a_4, a_2, b_0, b_2, b_4, \dots]^T = 0 \tag{3.11}$$

where $|C|_T$ is the matrix of coefficients and the determinant of the matrix should be equal to zero, thus

$$|C|_T = \begin{vmatrix} \cdots & \cdots & \cdots & \cdots & \cdots & \cdots & \cdots & \cdots & \cdots \\ \cdots & 1-36r^2 & -\mu & 0 & 0 & 0 & 0 & -12\beta r/\omega & \cdots \\ \cdots & -\mu & 1-16r^2 & -\mu & 0 & 0 & -8\beta r/\omega & 0 & \cdots \\ \cdots & 0 & -\mu & 1-4r^2 & 0 & -4\beta r/\omega & 0 & 0 & \cdots \\ \cdots & 0 & 0 & 0 & 1 & -\mu & 0 & 0 & \cdots \\ \cdots & 0 & 0 & 4\beta r/\omega & -2\mu & 1-4r^2 & -\mu & 0 & \cdots \\ \cdots & 0 & 8\beta r/\omega & 0 & 0 & -\mu & 1-16r^2 & -\mu & \cdots \\ \cdots & 12\beta r/\omega & 0 & 0 & 0 & 0 & -\mu & 1-36r^2 & \cdots \\ \cdots & \cdots & \cdots & \cdots & \cdots & \cdots & \cdots & \cdots & \cdots \end{vmatrix} = 0 \quad .$$

(3.12)

The determinant shown in Eq. (3.12) corresponds to the periodic solutions of period T. Since the determinant has an infinite order, it is impossible to solve directly, but it allows us to estimate the approximate borders of the region of instability based on the order. For instance, the first and second order approximations of the boundary of the second stability region are found by plotting the relations between r and μ from the following determinants.

$$\begin{vmatrix} 1-4r^2 & 0 & -4\beta r/\omega \\ 0 & 1 & -\mu \\ 4\beta r/\omega & -2\mu & 1-4r^2 \end{vmatrix} = 0 \qquad \text{(First approximation)}, \tag{3.13}$$

$$\begin{vmatrix} 1-16r^2 & -\mu & 0 & 0 & -8\beta r/\omega \\ -\mu & 1-4r^2 & 0 & -4\beta r/\omega & 0 \\ 0 & 0 & 1 & -\mu & 0 \\ 0 & 4\beta r/\omega & -2\mu & 1-4r^2 & -\mu \\ 8\beta r/\omega & 0 & 0 & -\mu & 1-16r^2 \end{vmatrix} = 0 \text{ (Second approximation)}. \tag{3.14}$$

The flow chart of the Bolotin method for solving ordinary Mathieu equations is shown in Figure 3.1.

$$\ddot{q} + 2\beta\dot{q} + \omega^2(1 - 2\mu\cos\theta t)q = 0$$

| 2T period solutions | T period solutions |

Using **odd** terms of the Fourier series to substitute $q, \dot{q}$ and $\ddot{q}$

Using **even** terms of the Fourier series to substitute $q, \dot{q}$ and $\ddot{q}$

Using the trigonometric identity conversions in Eq. (3.3) to simplify

Using the trigonometric identity conversions in Eq. (3.3) to simplify

Setting the coefficients of $\sin\frac{\theta t}{2}, \cos\frac{\theta t}{2}$, $\sin\frac{3\theta t}{2}, \cos\frac{3\theta t}{2}, \ldots$ equal to zero to find the system of equations (Eq. (3.4))

Setting the coefficients of $\sin\theta t, \cos\theta t$, $\sin 2\theta t, \cos 2\theta t, \ldots$ equal to zero to find the system of equations (Eq. (3.10))

Writing the system of equations in the matrix and putting the determinant of the coefficients equal to zero (Eq. (3.6)) to find the instability regions.

Writing the system of equations in the matrix and putting the determinant of the coefficients equal to zero (Eq. (3.12)) to find the instability regions.
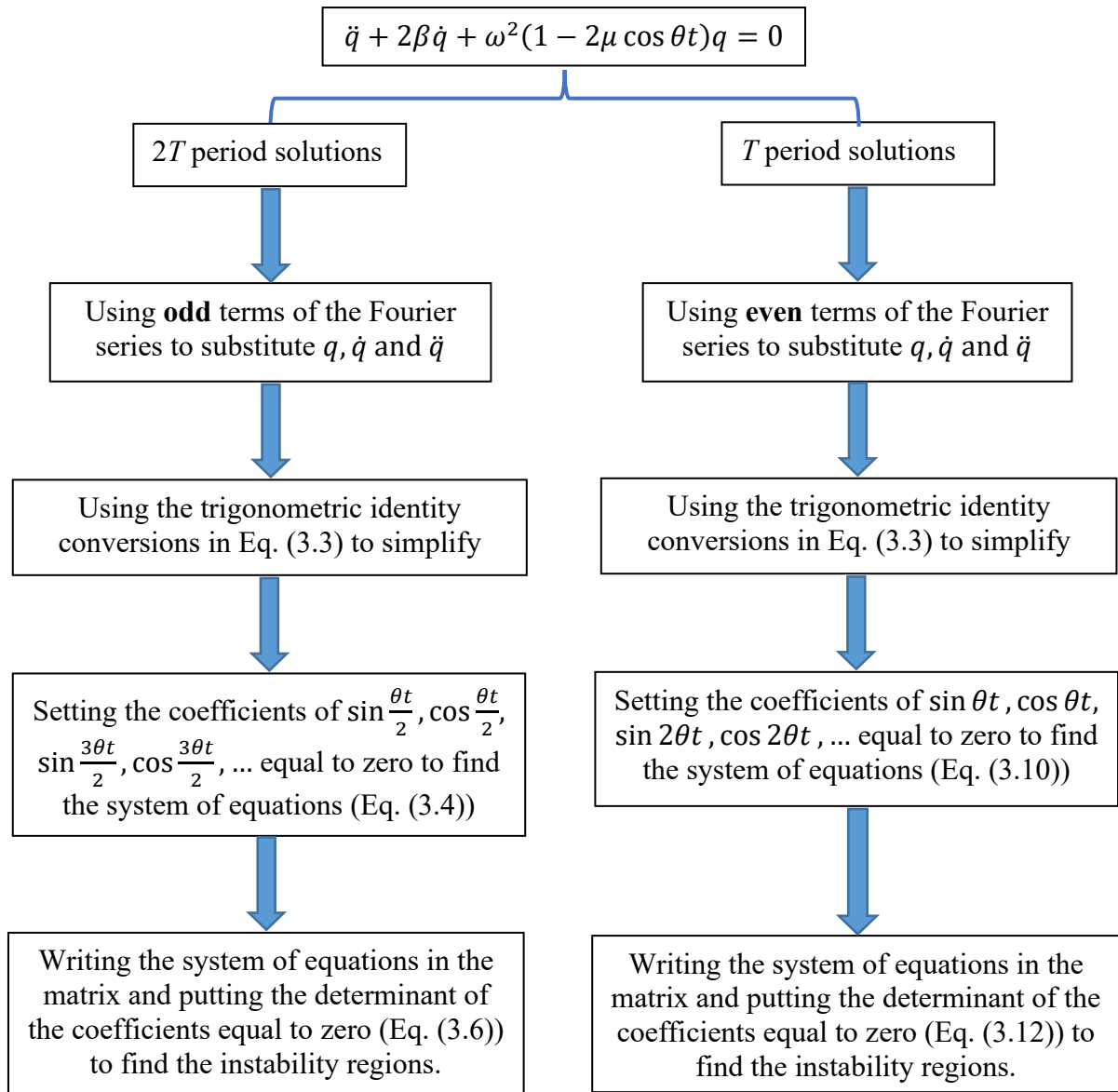
Figure 3.1 Bolotin method for solving ordinary Mathieu equations

3.2. Approximate solution for solving fractional Mathieu equation

Consider a fractional Mathieu equation [38]

$$\ddot{q} + 2\beta D^\alpha q + \omega^2(1 - 2\mu \cos \theta t)q = 0, \qquad T = \frac{2\pi}{\theta}, \tag{3.15}$$

where $\ddot{q}$ is the second derivative and $D^\alpha q$ is the fractional derivative order of α $(0 < \alpha < 1)$ of q with respect to t. From the Floquet theory, it is known that on the boundary, there exists periodic solutions to q with period $2T$ or T. The same idea is used as the ordinary Mathieu equation. To find the solution with period $2T$, one can take $q(t)$ equal to the sum of the odd numbered terms of the Fourier series,

$$q(t) = \sum_{k=1 \text{ (odd)}}^{\infty} \left(a_k \sin \frac{k\pi t}{T} + b_k \cos \frac{k\pi t}{T} \right) = \sum_{k=1 \text{ (odd)}}^{\infty} \left(a_k \sin \frac{k\theta t}{2} + b_k \cos \frac{k\theta t}{2} \right).$$

In general, using more terms of the Fourier series results in a larger matrix of coefficients. In the following, the relationship between the amount of k in the Fourier series and the degree of approximation of the instability regions will be discussed. But at this step, to indicate the calculation process, we consider $k = 1,3,5$ so

$$q(t) = a_1 \sin \frac{\theta t}{2} + b_1 \cos \frac{\theta t}{2} + a_3 \sin \frac{3\theta t}{2} + b_3 \cos \frac{3\theta t}{2} + a_5 \sin \frac{5\theta t}{2} + b_5 \cos \frac{5\theta t}{2}. \tag{3.16}$$

Based on Caputo's definition [23], when $0 < \alpha < 1$, the fractional derivative from order α is

$$D^\alpha q = \frac{1}{\Gamma(1-\alpha)} \int_0^t v^{-\alpha} q'(t - v)dv, \tag{3.17}$$

where

$$\Gamma(z) = \int_0^\infty x^{z-1} e^{-x} dx.$$

Substituting Eq. (3.16) into Eq. (3.17) results in

$$D^\alpha q = \frac{1}{\Gamma(1-\alpha)} \int_0^t v^{-\alpha} q'(t - v)dv = \frac{\theta}{2\Gamma(1-\alpha)} \int_0^t v^{-\alpha} \left[a_1 \cos \frac{\theta(t-v)}{2} - b_1 \sin \frac{\theta(t-v)}{2} + \right.$$

$$3a_3 \cos \frac{3\theta(t-v)}{2} - 3b_3 \sin \frac{3\theta(t-v)}{2} + 5a_5 \cos \frac{5\theta(t-v)}{2} - 5b_5 \sin \frac{5\theta(t-v)}{2} \right] dv, \tag{3.18}$$

then, using trigonometric identities

$$\sin(\alpha - \beta) = \sin \alpha \cos \beta - \cos \alpha \sin \beta,$$
$$\cos(\alpha - \beta) = \cos \alpha \cos \beta + \sin \alpha \sin \beta,$$

(3.19)

Eq. (3.18) is transformed into the form of

$$D^\alpha q = \frac{\theta}{2\Gamma(1-\alpha)} \int_0^t v^{-\alpha} \left[a_1 \left(\cos \frac{\theta t}{2} \cos \frac{\theta v}{2} + \sin \frac{\theta t}{2} \sin \frac{\theta v}{2} \right) - b_1 \left(\sin \frac{\theta t}{2} \cos \frac{\theta v}{2} - \cos \frac{\theta t}{2} \sin \frac{\theta v}{2} \right) + \right.$$

$$3a_3 \left(\cos \frac{3\theta t}{2} \cos \frac{3\theta v}{2} + \sin \frac{3\theta t}{2} \sin \frac{3\theta v}{2} \right) - 3b_3 \left(\sin \frac{3\theta t}{2} \cos \frac{3\theta v}{2} - \cos \frac{3\theta t}{2} \sin \frac{3\theta v}{2} \right) +$$

$$5a_5 \left(\cos \frac{5\theta t}{2} \cos \frac{5\theta v}{2} + \sin \frac{5\theta t}{2} \sin \frac{5\theta v}{2} \right) - 5b_5 \left(\sin \frac{5\theta t}{2} \cos \frac{5\theta v}{2} - \cos \frac{5\theta t}{2} \sin \frac{5\theta v}{2} \right) \right] dv,$$

$$D^\alpha q = \frac{\theta}{2\Gamma(1-\alpha)} \left[\sin \frac{\theta t}{2} \int_0^t v^{-\alpha} \left(a_1 \sin \frac{\theta v}{2} - b_1 \cos \frac{\theta v}{2} \right) dv + \cos \frac{\theta t}{2} \int_0^t v^{-\alpha} \left(b_1 \sin \frac{\theta v}{2} + \right. \right.$$

$$a_1 \cos \frac{\theta v}{2} \right) dv + 3 \sin \frac{3\theta t}{2} \int_0^t v^{-\alpha} \left(a_3 \sin \frac{3\theta v}{2} - b_3 \cos \frac{3\theta v}{2} \right) dv + 3 \cos \frac{3\theta t}{2} \int_0^t v^{-\alpha} \left(b_3 \sin \frac{3\theta v}{2} + \right.$$

$$a_3 \cos \frac{3\theta v}{2} \right) dv + 5 \sin \frac{5\theta t}{2} \int_0^t v^{-\alpha} \left(a_5 \sin \frac{5\theta v}{2} - b_5 \cos \frac{5\theta v}{2} \right) dv +$$

$$5 \cos \frac{5\theta t}{2} \int_0^t v^{-\alpha} \left(b_5 \sin \frac{5\theta v}{2} + a_5 \cos \frac{5\theta v}{2} \right) dv \right].$$

(3.20)

By using the variable change, $w = \frac{\theta v}{2}$, Eq. (3.20) can be written in form of

$$D^\alpha q = \frac{1}{\Gamma(1-\alpha)} \left[\left(\frac{\theta}{2} \right)^\alpha \sin \frac{\theta t}{2} \int_0^{\frac{\theta t}{2}} w^{-\alpha} (a_1 \sin w - b_1 \cos w) dw + \right.$$

$$\left(\frac{\theta}{2} \right)^\alpha \cos \frac{\theta t}{2} \int_0^{\frac{\theta t}{2}} w^{-\alpha} (b_1 \sin w + a_1 \cos w) dw + 3 \left(\frac{\theta}{2} \right)^\alpha \sin \frac{3\theta t}{2} \int_0^{\frac{\theta t}{2}} w^{-\alpha} (a_3 \sin 3w -$$

$$b_3 \cos 3w) dw + 3 \left(\frac{\theta}{2} \right)^\alpha \cos \frac{3\theta t}{2} \int_0^{\frac{\theta t}{2}} w^{-\alpha} (b_3 \sin 3w + a_3 \cos 3w) dw +$$

$$5 \left(\frac{\theta}{2} \right)^\alpha \sin \frac{5\theta t}{2} \int_0^{\frac{\theta t}{2}} w^{-\alpha} (a_5 \sin 5w - b_5 \cos 5w) dw + 5 \left(\frac{\theta}{2} \right)^\alpha \cos \frac{5\theta t}{2} \int_0^{\frac{\theta t}{2}} w^{-\alpha} (b_5 \sin 5w +$$

$$a_5 \cos 5w) dw \right],$$

(3.21)

or

$$D^\alpha q = \frac{1}{\Gamma(1-\alpha)} \left(\frac{\theta}{2} \right)^\alpha \left[\sin \frac{\theta t}{2} (a_1 I_{s1} - b_1 I_{c1}) + \cos \frac{\theta t}{2} (b_1 I_{s1} + a_1 I_{c1}) + 3 \sin \frac{3\theta t}{2} (a_3 I_{s3} - \right.$$

$$b_3 I_{c3}) + 3 \cos \frac{3\theta t}{2} (b_3 I_{s3} + a_3 I_{c3}) + 5 \sin \frac{5\theta t}{2} (a_5 I_{s5} - b_5 I_{c5}) + 5 \cos \frac{5\theta t}{2} (b_5 I_{s5} + a_5 I_{c5}) \right],$$

(3.22)

where

$$I_{s1} = \int_0^{\frac{\theta t}{2}} w^{-\alpha} \sin w \, dw \quad , \quad I_{c1} = \int_0^{\frac{\theta t}{2}} w^{-\alpha} \cos w \, dw \, ,$$

$$I_{s3} = \int_0^{\frac{\theta t}{2}} w^{-\alpha} \sin 3w \, dw \quad , \quad I_{c3} = \int_0^{\frac{\theta t}{2}} w^{-\alpha} \cos 3w \, dw \, , \quad (3.23)$$

$$I_{s5} = \int_0^{\frac{\theta t}{2}} w^{-\alpha} \sin 5w \, dw \quad , \quad I_{c5} = \int_0^{\frac{\theta t}{2}} w^{-\alpha} \cos 5w \, dw \, .$$

It is known that the integrals in Eq. (3.23) cannot be solved for general values t in the

close form solution, but Rand [38] illustrated that in the limit $t \to \infty$

$$I_{s1} = \int_0^{\infty} w^{-\alpha} \sin w \, dw = \Gamma(1 - \alpha) \cos \frac{\alpha \pi}{2} \, ,$$

$$I_{c1} = \int_0^{\infty} w^{-\alpha} \cos w \, dw = \Gamma(1 - \alpha) \sin \frac{\alpha \pi}{2} \, . \quad (3.24)$$

Also, using the variable change $v = 3w$ to solve integrals I_{s3}, I_{c3} and the variable change $v = 5w$ to solve integrals I_{s5}, I_{c5} results in

$$I_{s3} = \int_0^{\infty} w^{-\alpha} \sin 3w \, dw = \frac{\Gamma(1-\alpha)}{3^{(1-\alpha)}} \cos \frac{\alpha \pi}{2} \, ,$$

$$I_{c3} = \int_0^{\infty} w^{-\alpha} \cos 3w \, dw = \frac{\Gamma(1-\alpha)}{3^{(1-\alpha)}} \sin \frac{\alpha \pi}{2} \, , \quad (3.25)$$

$$I_{s5} = \int_0^{\infty} w^{-\alpha} \sin 5w \, dw = \frac{\Gamma(1-\alpha)}{5^{(1-\alpha)}} \cos \frac{\alpha \pi}{2} \, ,$$

$$I_{c5} = \int_0^{\infty} w^{-\alpha} \cos 5w \, dw = \frac{\Gamma(1-\alpha)}{5^{(1-\alpha)}} \sin \frac{\alpha \pi}{2} \, . \quad (3.26)$$

Replacing Eqs. (3.24) and (3.25) into Eq. (3.22) leads to

$$D^\alpha q = \left(\frac{\theta}{2}\right)^\alpha \left[\sin \frac{\theta t}{2} \left(a_1 \cos \frac{\alpha \pi}{2} - b_1 \sin \frac{\alpha \pi}{2} \right) + \cos \frac{\theta t}{2} \left(b_1 \cos \frac{\alpha \pi}{2} + a_1 \sin \frac{\alpha \pi}{2} \right) + \right.$$

$$3^\alpha \sin \frac{3\theta t}{2} \left(a_3 \cos \frac{\alpha \pi}{2} - b_3 \sin \frac{\alpha \pi}{2} \right) + 3^\alpha \cos \frac{3\theta t}{2} \left(b_3 \cos \frac{\alpha \pi}{2} + a_3 \sin \frac{\alpha \pi}{2} \right) +$$

$$\left. 5^\alpha \sin \frac{5\theta t}{2} \left(a_5 \cos \frac{\alpha \pi}{2} - b_5 \sin \frac{\alpha \pi}{2} \right) + 5^\alpha \cos \frac{5\theta t}{2} \left(b_5 \cos \frac{\alpha \pi}{2} + a_5 \sin \frac{\alpha \pi}{2} \right) \right]. \quad (3.27)$$

On the other hand, using Eq. (3.16) results in

$$\dot{q}(t) = \frac{\theta}{2} \left(a_1 \cos \frac{\theta t}{2} - b_1 \sin \frac{\theta t}{2} + 3a_3 \cos \frac{3\theta t}{2} - 3b_3 \sin \frac{3\theta t}{2} + 5a_5 \cos \frac{5\theta t}{2} - 5b_5 \sin \frac{5\theta t}{2} \right),$$

$$(3.28)$$

$$\ddot{q}(t) = -\frac{\theta^2}{4} \left(a_1 \sin \frac{\theta t}{2} + b_1 \cos \frac{\theta t}{2} + 9a_3 \sin \frac{3\theta t}{2} + 9b_3 \cos \frac{3\theta t}{2} + 25a_5 \sin \frac{5\theta t}{2} + \right.$$

$$\left. 25b_5 \cos \frac{5\theta t}{2} \right). \quad (3.29)$$

Inserting Eq. (3.16) and Eqs. (3.27) to (3.29) into Eq. (3.15) leads to

$$-\frac{\theta^2}{4}\left(a_1 \sin\frac{\theta t}{2} + b_1 \cos\frac{\theta t}{2} + 9a_3 \sin\frac{3\theta t}{2} + 9b_3 \cos\frac{3\theta t}{2} + 25a_5 \sin\frac{5\theta t}{2} + 25b_5 \cos\frac{5\theta t}{2}\right) +$$

$$2^{1-\alpha}\theta^\alpha\beta\left[\sin\frac{\theta t}{2}\left(a_1 \cos\frac{\alpha\pi}{2} - b_1 \sin\frac{\alpha\pi}{2}\right) + \cos\frac{\theta t}{2}\left(b_1 \cos\frac{\alpha\pi}{2} + a_1 \sin\frac{\alpha\pi}{2}\right) +$$

$$3^\alpha \sin\frac{3\theta t}{2}\left(a_3 \cos\frac{\alpha\pi}{2} - b_3 \sin\frac{\alpha\pi}{2}\right) + 3^\alpha \cos\frac{3\theta t}{2}\left(b_3 \cos\frac{\alpha\pi}{2} + a_3 \sin\frac{\alpha\pi}{2}\right) +$$

$$5^\alpha \sin\frac{5\theta t}{2}\left(a_5 \cos\frac{\alpha\pi}{2} - b_5 \sin\frac{\alpha\pi}{2}\right) + 5^\alpha \cos\frac{5\theta t}{2}\left(b_5 \cos\frac{\alpha\pi}{2} + a_5 \sin\frac{\alpha\pi}{2}\right)\right] + \omega^2\left(a_1 \sin\frac{\theta t}{2} +\right.$$

$$\left. b_1 \cos\frac{\theta t}{2} + a_3 \sin\frac{3\theta t}{2} + b_3 \cos\frac{3\theta t}{2} + a_5 \sin\frac{5\theta t}{2} + b_5 \cos\frac{5\theta t}{2}\right) - 2\mu\omega^2 \cos\theta t\left(a_1 \sin\frac{\theta t}{2} +\right.$$

$$\left. b_1 \cos\frac{\theta t}{2} + a_3 \sin\frac{3\theta t}{2} + b_3 \cos\frac{3\theta t}{2} + a_5 \sin\frac{5\theta t}{2} + b_5 \cos\frac{5\theta t}{2}\right) = 0. \tag{3.30}$$

Using trigonometric identities

$$\begin{aligned}\cos(\alpha)\sin(\beta) &= \frac{1}{2}(\sin(\alpha+\beta) - \sin(\alpha-\beta)), \\ \cos(\alpha)\cos(\beta) &= \frac{1}{2}(\cos(\alpha-\beta) + \cos(\alpha+\beta)),\end{aligned} \tag{3.31}$$

Eq. (3.30) can be simplified as

$$-\frac{\theta^2}{4}\left(a_1 \sin\frac{\theta t}{2} + b_1 \cos\frac{\theta t}{2} + 9a_3 \sin\frac{3\theta t}{2} + 9b_3 \cos\frac{3\theta t}{2} + 25a_5 \sin\frac{5\theta t}{2} + 25b_5 \cos\frac{5\theta t}{2}\right) +$$

$$2^{1-\alpha}\theta^\alpha\beta\left[\sin\frac{\theta t}{2}\left(a_1 \cos\frac{\alpha\pi}{2} - b_1 \sin\frac{\alpha\pi}{2}\right) + \cos\frac{\theta t}{2}\left(b_1 \cos\frac{\alpha\pi}{2} + a_1 \sin\frac{\alpha\pi}{2}\right) + 3^\alpha \sin\frac{3\theta t}{2}\left(a_3 \cos\frac{\alpha\pi}{2} -\right.\right.$$

$$\left. b_3 \sin\frac{\alpha\pi}{2}\right) + 3^\alpha \cos\frac{3\theta t}{2}\left(b_3 \cos\frac{\alpha\pi}{2} + a_3 \sin\frac{\alpha\pi}{2}\right) + 5^\alpha \sin\frac{5\theta t}{2}\left(a_5 \cos\frac{\alpha\pi}{2} - b_5 \sin\frac{\alpha\pi}{2}\right) +$$

$$5^\alpha \cos\frac{5\theta t}{2}\left(b_5 \cos\frac{\alpha\pi}{2} + a_5 \sin\frac{\alpha\pi}{2}\right)\right] + \omega^2\left(a_1 \sin\frac{\theta t}{2} + b_1 \cos\frac{\theta t}{2} + a_3 \sin\frac{3\theta t}{2} + b_3 \cos\frac{3\theta t}{2} +\right.$$

$$\left. a_5 \sin\frac{5\theta t}{2} + b_5 \cos\frac{5\theta t}{2}\right) - \mu\omega^2\left[a_1\left(\sin\frac{3\theta t}{2} - \sin\frac{\theta t}{2}\right) + b_1\left(\cos\frac{\theta t}{2} + \cos\frac{3\theta t}{2}\right) + a_3\left(\sin\frac{5\theta t}{2} +\right.\right.$$

$$\left.\left. \sin\frac{\theta t}{2}\right) + b_3\left(\cos\frac{\theta t}{2} + \cos\frac{5\theta t}{2}\right) + a_5\left(\sin\frac{7\theta t}{2} + \sin\frac{3\theta t}{2}\right) + b_5\left(\cos\frac{3\theta t}{2} + \cos\frac{7\theta t}{2}\right)\right] = 0 \quad \Rightarrow$$

$$\left[-\frac{\theta^2}{4}a_1 + 2^{1-\alpha}\theta^\alpha\beta\left(a_1 \cos\frac{\alpha\pi}{2} - b_1 \sin\frac{\alpha\pi}{2}\right) + \omega^2 a_1 + \mu\omega^2 a_1 - \mu\omega^2 a_3\right]\sin\frac{\theta t}{2} + \left[-\frac{\theta^2}{4}b_1 +\right.$$

$$\left. 2^{1-\alpha}\theta^\alpha\beta\left(b_1 \cos\frac{\alpha\pi}{2} + a_1 \sin\frac{\alpha\pi}{2}\right) + \omega^2 b_1 - \mu\omega^2 b_1 - \mu\omega^2 b_3\right]\cos\frac{\theta t}{2} + \left[-\frac{\theta^2}{4}9a_3 + 3^\alpha \times\right.$$

$$\left. 2^{1-\alpha}\theta^\alpha\beta\left(a_3 \cos\frac{\alpha\pi}{2} - b_3 \sin\frac{\alpha\pi}{2}\right) + \omega^2 a_3 - \mu\omega^2 a_1 - \mu\omega^2 a_5\right]\sin\frac{3\theta t}{2} + \left[-\frac{\theta^2}{4}9b_3 + 3^\alpha \times\right.$$

$$\left. 2^{1-\alpha}\theta^\alpha\beta\left(b_3 \cos\frac{\alpha\pi}{2} + a_3 \sin\frac{\alpha\pi}{2}\right) + \omega^2 b_3 - \mu\omega^2 b_1 - \mu\omega^2 b_5\right]\cos\frac{3\theta t}{2} + \left[-\frac{\theta^2}{4}25a_5 + 5^\alpha \times\right.$$

$$\left. 2^{1-\alpha}\theta^\alpha\beta\left(a_5 \cos\frac{\alpha\pi}{2} - b_5 \sin\frac{\alpha\pi}{2}\right) + \omega^2 a_5 - \mu\omega^2 a_3\right]\sin\frac{5\theta t}{2} + \left[-\frac{\theta^2}{4}25b_5 + 5^\alpha \times\right.$$

$$2^{1-\alpha}\theta^{\alpha}\beta\left(b_5\cos\frac{\alpha\pi}{2}+a_5\sin\frac{\alpha\pi}{2}\right)+\omega^2 b_5-\mu\omega^2 b_3\Big]\cos\frac{5\theta t}{2}+[-\mu\omega^2 a_5]\sin\frac{7\theta t}{2}+$$

$$[-\mu\omega^2 b_5]\cos\frac{7\theta t}{2}=0. \tag{3.32}$$

Knowing that the functions $\sin\frac{\theta t}{2}, \cos\frac{\theta t}{2}, \sin\frac{3\theta t}{2}, \cos\frac{3\theta t}{2}, \sin\frac{5\theta t}{2}, \cos\frac{5\theta t}{2}, \dots$ in Eq. (3.32) are independents, results a system of equations equal to

$$-\frac{\theta^2}{4}a_1+2^{1-\alpha}\theta^{\alpha}\beta\left(a_1\cos\frac{\alpha\pi}{2}-b_1\sin\frac{\alpha\pi}{2}\right)+\omega^2 a_1+\mu\omega^2 a_1-\mu\omega^2 a_3=0,$$

$$-\frac{\theta^2}{4}b_1+2^{1-\alpha}\theta^{\alpha}\beta\left(b_1\cos\frac{\alpha\pi}{2}+a_1\sin\frac{\alpha\pi}{2}\right)+\omega^2 b_1-\mu\omega^2 b_1-\mu\omega^2 b_3=0,$$

$$-\frac{\theta^2}{4}9a_3+3^{\alpha}\times 2^{1-\alpha}\theta^{\alpha}\beta\left(a_3\cos\frac{\alpha\pi}{2}-b_3\sin\frac{\alpha\pi}{2}\right)+\omega^2 a_3-\mu\omega^2 a_1-\mu\omega^2 a_5=0,$$

$$-\frac{\theta^2}{4}9b_3+3^{\alpha}\times 2^{1-\alpha}\theta^{\alpha}\beta\left(b_3\cos\frac{\alpha\pi}{2}+a_3\sin\frac{\alpha\pi}{2}\right)+\omega^2 b_3-\mu\omega^2 b_1-\mu\omega^2 b_5=0,$$

$$-\frac{\theta^2}{4}25a_5+5^{\alpha}\times 2^{1-\alpha}\theta^{\alpha}\beta\left(a_5\cos\frac{\alpha\pi}{2}-b_5\sin\frac{\alpha\pi}{2}\right)+\omega^2 a_5-\mu\omega^2 a_3=0,$$

$$-\frac{\theta^2}{4}25b_5+5^{\alpha}\times 2^{1-\alpha}\theta^{\alpha}\beta\left(b_5\cos\frac{\alpha\pi}{2}+a_5\sin\frac{\alpha\pi}{2}\right)+\omega^2 b_5-\mu\omega^2 b_3=0. \tag{3.33}$$

Considering the use of infinite terms of the Fourier series ($k=1,3,5,\dots$), the system of equations becomes

$$k=1:\begin{cases}(1+\mu-r^2)a_1-\mu a_3+\frac{2\beta r^{\alpha}}{\omega^{2-\alpha}}\left(a_1\cos\frac{\alpha\pi}{2}-b_1\sin\frac{\alpha\pi}{2}\right)=0,\\[2mm](1-\mu-r^2)b_1-\mu b_3+\frac{2\beta r^{\alpha}}{\omega^{2-\alpha}}\left(b_1\cos\frac{\alpha\pi}{2}+a_1\sin\frac{\alpha\pi}{2}\right)=0,\end{cases}$$

$$k=3,5,\dots:\begin{cases}(1-k^2 r^2)a_k-\mu(a_{k-2}+a_{k+2})+k^{\alpha}\frac{2\beta r^{\alpha}}{\omega^{2-\alpha}}\left(a_k\cos\frac{\alpha\pi}{2}-b_k\sin\frac{\alpha\pi}{2}\right)=0,\\[2mm](1-k^2 r^2)b_k-\mu(b_{k-2}+b_{k+2})+k^{\alpha}\frac{2\beta r^{\alpha}}{\omega^{2-\alpha}}\left(b_k\cos\frac{\alpha\pi}{2}+a_k\sin\frac{\alpha\pi}{2}\right)=0,\end{cases}$$

$$\tag{3.34}$$

where $r=\theta/2\omega$. The above system of equations can be written in matrix form

$$[\boldsymbol{C}]_{2T}\times[\dots,a_5,a_3,a_1,b_1,b_3,b_5,\dots]^T=0, \tag{3.35}$$

where $[\boldsymbol{C}]_{2T}$ is the matrix of coefficients for the solutions with $2T$ periods.

To find solutions with period T, the even numbered terms of the Fourier series should be considered

$$q(t)=\sum_{k=0 \text{ (even)}}^{\infty}\left(a_k\sin\frac{k\pi t}{T}+b_k\cos\frac{k\pi t}{T}\right)=\sum_{k=0 \text{ (even)}}^{\infty}\left(a_k\sin\frac{k\theta t}{2}+b_k\cos\frac{k\theta t}{2}\right).$$

In general, using more terms of the Fourier series result in a larger matrix of coefficients. In the following chapter, the relationship between the amount of k in the Fourier series and the degree of approximation of the instability regions will be discussed but at this step, to indicate the calculation process, we consider $k = 0,2,4,6$ so

$$q(t) = b_0 + a_2 \sin \theta t + b_2 \cos \theta t + a_4 \sin 2\theta t + b_4 \cos 2\theta t + a_6 \sin 3\theta t + b_6 \cos 3\theta t.$$

$$(3.36)$$

Inserting Eq. (3.36) in the Caputo fractional derivative definition (Eq. (3.17)) results in

$$D^\alpha q = \frac{\theta}{\Gamma(1-\alpha)} \int_0^t v^{-\alpha} [a_2 \cos \theta(t-v) - b_2 \sin \theta(t-v) + 2a_4 \cos 2\theta(t-v) -$$

$$2b_4 \sin 2\theta(t-v) + 3a_6 \cos 3\theta(t-v) - 3b_6 \sin 3\theta(t-v)] dv. \qquad (3.37)$$

Using the trigonometric identities shown in Eq. (3.19), Eq. (3.37) can be written in the form of

$$D^\alpha q = \frac{\theta}{\Gamma(1-\alpha)} \int_0^t v^{-\alpha} [a_2 (\cos \theta t \cos \theta v + \sin \theta t \sin \theta v) - b_2 (\sin \theta t \cos \theta v -$$

$$\cos \theta t \sin \theta v) + 2a_4 (\cos 2\theta t \cos 2\theta v + \sin 2\theta t \sin 2\theta v) - 2b_4 (\sin 2\theta t \cos 2\theta v -$$

$$\cos 2\theta t \sin 2\theta v) + 3a_6 (\cos 3\theta t \cos 3\theta v + \sin 3\theta t \sin 3\theta v) - 3b_6 (\sin 3\theta t \cos 3\theta v -$$

$$\cos 3\theta t \sin 3\theta v)] dv \quad \Rightarrow$$

$$D^\alpha q = \frac{\theta}{\Gamma(1-\alpha)} \Big[\sin \theta t \int_0^t v^{-\alpha} (a_2 \sin \theta v - b_2 \cos \theta v) dv + \cos \theta t \int_0^t v^{-\alpha} (b_2 \sin \theta v +$$

$$a_2 \cos \theta v) dv + 2 \sin 2\theta t \int_0^t v^{-\alpha} (a_4 \sin 2\theta v - b_4 \cos 2\theta v) dv +$$

$$2 \cos 2\theta t \int_0^t v^{-\alpha} (b_4 \sin 2\theta v + a_4 \cos 2\theta v) dv + 3 \sin 3\theta t \int_0^t v^{-\alpha} (a_6 \sin 3\theta v -$$

$$b_6 \cos 3\theta v) dv + 3 \cos 3\theta t \int_0^t v^{-\alpha} (b_6 \sin 3\theta v + a_6 \cos 3\theta v) dv \Big]. \qquad (3.38)$$

By using the variable change $w = \frac{\theta v}{2}$, Eq. (3.38) can be written in the form of

$$D^\alpha q = \frac{1}{\Gamma(1-\alpha)} \Big[2 \left(\frac{\theta}{2}\right)^\alpha \sin \theta t \int_0^{\frac{\theta t}{2}} w^{-\alpha} (a_2 \sin 2w - b_2 \cos 2w) dw +$$

$$2 \left(\frac{\theta}{2}\right)^\alpha \cos \theta t \int_0^{\frac{\theta t}{2}} w^{-\alpha} (b_2 \sin 2w + a_2 \cos 2w) dw + 4 \left(\frac{\theta}{2}\right)^\alpha \sin 2\theta t \int_0^{\frac{\theta t}{2}} w^{-\alpha} (a_4 \sin 4w -$$

$$b_4 \cos 4w) dw + 4 \left(\frac{\theta}{2}\right)^\alpha \cos 2\theta t \int_0^{\frac{\theta t}{2}} w^{-\alpha} (b_4 \sin 4w + a_4 \cos 4w) dw +$$

$$6 \left(\frac{\theta}{2}\right)^\alpha \sin 3\theta t \int_0^{\frac{\theta t}{2}} w^{-\alpha}(a_6 \sin 6w - b_6 \cos 6w)dw + 6 \left(\frac{\theta}{2}\right)^\alpha \cos 3\theta t \int_0^{\frac{\theta t}{2}} w^{-\alpha}(b_6 \sin 6w +$$

$$\left. a_6 \cos 6w)dw \right] , \tag{3.39}$$

or

$$D^\alpha q = \frac{1}{\Gamma(1-\alpha)} \left(\frac{\theta}{2}\right)^\alpha [2 \sin \theta t \, (a_2 I_{s2} - b_2 I_{c2}) + 2\cos \theta t \, (b_2 I_{s2} + a_2 I_{c2}) + 4 \sin 2\theta t \, (a_4 I_{s4} -$$

$$b_4 I_{c4}) + 4 \cos 2\theta t \, (b_4 I_{s4} + a_4 I_{c4}) + 6 \sin 3\theta t \, (a_6 I_{s6} - b_6 I_{c6}) + 6 \cos 3\theta t \, (b_6 I_{s6} + a_6 I_{c6})] ,$$

$$\tag{3.40}$$

where

$$I_{s2} = \int_0^{\frac{\theta t}{2}} w^{-\alpha} \sin 2w \, dw \quad , \quad I_{c2} = \int_0^{\frac{\theta t}{2}} w^{-\alpha} \cos 2w \, dw \ ,$$

$$I_{s4} = \int_0^{\frac{\theta t}{2}} w^{-\alpha} \sin 4w \, dw \quad , \quad I_{c4} = \int_0^{\frac{\theta t}{2}} w^{-\alpha} \cos 4w \, dw \ , \tag{3.41}$$

$$I_{s6} = \int_0^{\frac{\theta t}{2}} w^{-\alpha} \sin 6w \, dw \quad , \quad I_{c6} = \int_0^{\frac{\theta t}{2}} w^{-\alpha} \cos 6w \, dw \ .$$

It is known that the integrals in Eq. (3.41) cannot be solved for general values t in the close

form solution, but Rand [38] illustrated that in the limit $t \to \infty$

$$I_{s1} = \int_0^\infty w^{-\alpha} \sin w \, dw = \Gamma(1 - \alpha) \cos \frac{\alpha \pi}{2} \ ,$$

$$I_{c1} = \int_0^\infty w^{-\alpha} \cos w \, dw = \Gamma(1 - \alpha) \sin \frac{\alpha \pi}{2} \ . \tag{3.42}$$

Using the variable change $v = 2w$ to solve integrals I_{s2}, I_{c2} , the variable change $v = 4w$ to

solve integrals I_{s4}, I_{c4} , and the variable change $v = 6w$ to solve integrals I_{s6}, I_{c6} results in

$$I_{s2} = \int_0^\infty w^{-\alpha} \sin 2w \, dw = \frac{\Gamma(1-\alpha)}{2^{(1-\alpha)}} \cos \frac{\alpha \pi}{2},$$

$$I_{c2} = \int_0^\infty w^{-\alpha} \cos 2w \, dw = \frac{\Gamma(1-\alpha)}{2^{(1-\alpha)}} \sin \frac{\alpha \pi}{2}, \tag{3.43}$$

$$I_{s4} = \int_0^\infty w^{-\alpha} \sin 4w \, dw = \frac{\Gamma(1-\alpha)}{4^{(1-\alpha)}} \cos \frac{\alpha \pi}{2},$$

$$I_{c4} = \int_0^\infty w^{-\alpha} \cos 4w \, dw = \frac{\Gamma(1-\alpha)}{4^{(1-\alpha)}} \sin \frac{\alpha \pi}{2}, \tag{3.44}$$

$$I_{s6} = \int_0^\infty w^{-\alpha} \sin 6w \, dw = \frac{\Gamma(1-\alpha)}{6^{(1-\alpha)}} \cos \frac{\alpha \pi}{2},$$

$$I_{c6} = \int_0^\infty w^{-\alpha} \cos 6w \, dw = \frac{\Gamma(1-\alpha)}{6^{(1-\alpha)}} \sin \frac{\alpha \pi}{2}. \tag{3.45}$$

Inserting Eqs. (3.43) to (3.45) into Eq. (3.40) leads to

$$D^\alpha q = \left(\frac{\theta}{2}\right)^\alpha \left[2^\alpha \sin\theta t \left(a_2 \cos\frac{\alpha\pi}{2} - b_2 \sin\frac{\alpha\pi}{2}\right) + 2^\alpha \cos\theta t \left(b_2 \cos\frac{\alpha\pi}{2} + a_2 \sin\frac{\alpha\pi}{2}\right) + \right.$$

$$4^\alpha \sin 2\theta t \left(a_4 \cos\frac{\alpha\pi}{2} - b_4 \sin\frac{\alpha\pi}{2}\right) + 4^\alpha \cos 2\theta t \left(b_4 \cos\frac{\alpha\pi}{2} + a_4 \sin\frac{\alpha\pi}{2}\right) +$$

$$\left. 6^\alpha \sin 3\theta t \left(a_6 \cos\frac{\alpha\pi}{2} - b_6 \sin\frac{\alpha\pi}{2}\right) + 6^\alpha \cos 3\theta t \left(b_6 \cos\frac{\alpha\pi}{2} + a_6 \sin\frac{\alpha\pi}{2}\right)\right]. \tag{3.46}$$

Also, the first and second derivatives of $q(t)$ based on Eq. (3.36) are

$$\dot{q}(t) = \theta(a_2 \cos\theta t - b_2 \sin\theta t + 2a_4 \cos 2\theta t - 2b_4 \sin 2\theta t + 3a_6 \cos 3\theta t - 3b_6\sin 3\theta t), \tag{3.47}$$

$$\ddot{q}(t) = -\theta^2(a_2 \sin\theta t + b_2 \cos\theta t + 4a_4 \sin 2\theta t + 4b_4 \cos 2\theta t + 9a_6 \sin 3\theta t +$$

$$9b_6 \cos 3\theta t), \tag{3.48}$$

and inserting Eqs. (3.46) to Eq. (3.48) into Eq. (3.15) results in

$$-\theta^2(a_2 \sin\theta t + b_2 \cos\theta t + 4a_4 \sin 2\theta t + 4b_4 \cos 2\theta t + 9a_6 \sin 3\theta t + 9b_6\cos 3\theta t) +$$

$$2\beta \left(\frac{\theta}{2}\right)^\alpha \left[2^\alpha \sin\theta t \left(a_2 \cos\frac{\alpha\pi}{2} - b_2 \sin\frac{\alpha\pi}{2}\right) + 2^\alpha \cos\theta t \left(b_2 \cos\frac{\alpha\pi}{2} + a_2 \sin\frac{\alpha\pi}{2}\right) + \right.$$

$$4^\alpha \sin 2\theta t \left(a_4 \cos\frac{\alpha\pi}{2} - b_4 \sin\frac{\alpha\pi}{2}\right) + 4^\alpha \cos 2\theta t \left(b_4 \cos\frac{\alpha\pi}{2} + a_4 \sin\frac{\alpha\pi}{2}\right) +$$

$$\left. 6^\alpha \sin 3\theta t \left(a_6 \cos\frac{\alpha\pi}{2} - b_6 \sin\frac{\alpha\pi}{2}\right) + 6^\alpha \cos 3\theta t \left(b_6 \cos\frac{\alpha\pi}{2} + a_6 \sin\frac{\alpha\pi}{2}\right)\right] + \omega^2(b_0 +$$

$$a_2 \sin\theta t + b_2 \cos\theta t + a_4 \sin 2\theta t + b_4 \cos 2\theta t + a_6 \sin 3\theta t + b_6 \cos 3\theta t) -$$

$$2\mu\omega^2 \cos\theta t (b_0 + a_2 \sin\theta t + b_2 \cos\theta t + a_4 \sin 2\theta t + b_4 \cos 2\theta t + a_6 \sin 3\theta t +$$

$$b_6 \cos 3\theta t) = 0. \tag{3.49}$$

Using trigonometric identities in Eq. (3.31) to simplify Eq. (3.49) leads to

$$-\theta^2(a_2 \sin\theta t + b_2 \cos\theta t + 4a_4 \sin 2\theta t + 4b_4 \cos 2\theta t + 9a_6 \sin 3\theta t + 9b_6 \cos 3\theta t) +$$

$$2\beta \left(\frac{\theta}{2}\right)^\alpha \left[2^\alpha \sin\theta t \left(a_2 \cos\frac{\alpha\pi}{2} - b_2 \sin\frac{\alpha\pi}{2}\right) + 2^\alpha \cos\theta t \left(b_2 \cos\frac{\alpha\pi}{2} + a_2 \sin\frac{\alpha\pi}{2}\right) + \right.$$

$$4^\alpha \sin 2\theta t \left(a_4 \cos\frac{\alpha\pi}{2} - b_4 \sin\frac{\alpha\pi}{2}\right) + 4^\alpha \cos 2\theta t \left(b_4 \cos\frac{\alpha\pi}{2} + a_4 \sin\frac{\alpha\pi}{2}\right) +$$

$$\left. 6^\alpha \sin 3\theta t \left(a_6 \cos\frac{\alpha\pi}{2} - b_6 \sin\frac{\alpha\pi}{2}\right) + 6^\alpha \cos 3\theta t \left(b_6 \cos\frac{\alpha\pi}{2} + a_6 \sin\frac{\alpha\pi}{2}\right)\right] + \omega^2(b_0 \cos 0 +$$

$$a_2 \sin\theta t + b_2 \cos\theta t + a_4 \sin 2\theta t + b_4 \cos 2\theta t + a_6 \sin 3\theta t + b_6 \cos 3\theta t) -$$

$$\mu\omega^2[2b_0 \cos\theta t + a_2(\sin 2\theta t) + b_2(\cos 0 + \cos 2\theta t) + a_4(\sin 3\theta t + \sin\theta t) + b_4(\cos\theta t +$$

$$\cos 3\theta t) + a_6(\sin 4\theta t + \sin 2\theta t) + b_6(\cos 2\theta t + \cos 4\theta t)] = 0 \quad \Rightarrow$$

$$[\omega^2 b_0 - \mu\omega^2 b_2]\cos 0 + \left[-\theta^2 a_2 + 2\beta\left(\frac{\theta}{2}\right)^\alpha 2^\alpha\left(a_2\cos\frac{\alpha\pi}{2} - b_2\sin\frac{\alpha\pi}{2}\right) + \omega^2 a_2 - \right.$$

$$\left.\mu\omega^2 a_4\right]\sin\theta t + \left[-\theta^2 b_2 + 2\beta\left(\frac{\theta}{2}\right)^\alpha 2^\alpha\left(b_2\cos\frac{\alpha\pi}{2} + a_2\sin\frac{\alpha\pi}{2}\right) + \omega^2 b_2 - \mu\omega^2(2b_0 + \right.$$

$$\left.b_4)\right]\cos\theta t + \left[-4\theta^2 a_4 + 2\beta\left(\frac{\theta}{2}\right)^\alpha 4^\alpha\left(a_4\cos\frac{\alpha\pi}{2} - b_4\sin\frac{\alpha\pi}{2}\right) + \omega^2 a_4 - \mu\omega^2(a_2 + \right.$$

$$\left.a_6)\right]\sin 2\theta t + \left[-4\theta^2 b_4 + 2\beta\left(\frac{\theta}{2}\right)^\alpha 4^\alpha\left(b_4\cos\frac{\alpha\pi}{2} + a_4\sin\frac{\alpha\pi}{2}\right) + \omega^2 b_4 - \mu\omega^2(b_2 + \right.$$

$$\left.b_6)\right]\cos 2\theta t + \left[-9\theta^2 a_6 + 2\beta\left(\frac{\theta}{2}\right)^\alpha 6^\alpha\left(a_6\cos\frac{\alpha\pi}{2} - b_6\sin\frac{\alpha\pi}{2}\right) + \omega^2 a_6 - \mu\omega^2 a_4\right]\sin 3\theta t + $$

$$\left[-9\theta^2 b_6 + 2\beta\left(\frac{\theta}{2}\right)^\alpha 6^\alpha\left(b_6\cos\frac{\alpha\pi}{2} + a_6\sin\frac{\alpha\pi}{2}\right) + \omega^2 b_6 - \mu\omega^2 b_4\right]\cos 3\theta t - $$

$$\mu\omega^2 a_6\sin 4\theta t - \mu\omega^2 b_6\cos 4\theta t = 0. \tag{3.50}$$

Knowing that the functions $\cos 0$, $\sin\theta t$, $\cos\theta t$, $\sin 2\theta t$, $\cos 2\theta t$, ... in Eq. (3.50) are independents results a system of equations equal to

$$\omega^2 b_0 - \mu\omega^2 b_2 = 0,$$

$$-\theta^2 a_2 + 2\beta\left(\frac{\theta}{2}\right)^\alpha 2^\alpha\left(a_2\cos\frac{\alpha\pi}{2} - b_2\sin\frac{\alpha\pi}{2}\right) + \omega^2 a_2 - \mu\omega^2 a_4 = 0,$$

$$-\theta^2 b_2 + 2\beta\left(\frac{\theta}{2}\right)^\alpha 2^\alpha\left(b_2\cos\frac{\alpha\pi}{2} + a_2\sin\frac{\alpha\pi}{2}\right) + \omega^2 b_2 - \mu\omega^2(2b_0 + b_4) = 0,$$

$$-4\theta^2 a_4 + 2\beta\left(\frac{\theta}{2}\right)^\alpha 4^\alpha\left(a_4\cos\frac{\alpha\pi}{2} - b_4\sin\frac{\alpha\pi}{2}\right) + \omega^2 a_4 - \mu\omega^2(a_2 + a_6) = 0,$$

$$-4\theta^2 b_4 + 2\beta\left(\frac{\theta}{2}\right)^\alpha 4^\alpha\left(b_4\cos\frac{\alpha\pi}{2} + a_4\sin\frac{\alpha\pi}{2}\right) + \omega^2 b_4 - \mu\omega^2(b_2 + b_6) = 0,$$

$$-9\theta^2 a_6 + 2\beta\left(\frac{\theta}{2}\right)^\alpha 6^\alpha\left(a_6\cos\frac{\alpha\pi}{2} - b_6\sin\frac{\alpha\pi}{2}\right) + \omega^2 a_6 - \mu\omega^2 a_4 = 0,$$

$$-9\theta^2 b_6 + 2\beta\left(\frac{\theta}{2}\right)^\alpha 6^\alpha\left(b_6\cos\frac{\alpha\pi}{2} + a_6\sin\frac{\alpha\pi}{2}\right) + \omega^2 b_6 - \mu\omega^2 b_4 = 0. \tag{3.51}$$

Considering the use of infinite terms of the Fourier series ($k = 0,2,4,...$), the system of equations becomes

$$k = 0: \ b_0 - \mu b_2 = 0,$$

$$k = 2: \begin{cases} -4r^2 a_2 + \frac{2\beta(2r)^\alpha}{\omega^{2-\alpha}}\left(a_2\cos\frac{\alpha\pi}{2} - b_2\sin\frac{\alpha\pi}{2}\right) + a_2 - \mu a_4 = 0, \\ -4r^2 b_2 + \frac{2\beta(2r)^\alpha}{\omega^{2-\alpha}}\left(b_2\cos\frac{\alpha\pi}{2} + a_2\sin\frac{\alpha\pi}{2}\right) + b_2 - \mu(2b_0 + b_4) = 0, \end{cases}$$

$$k = 4,6,...: \begin{cases} -k^2 r^2 a_k + \frac{2\beta(kr)^\alpha}{\omega^{2-\alpha}}\left(a_k\cos\frac{\alpha\pi}{2} - b_k\sin\frac{\alpha\pi}{2}\right) + a_k - \mu(a_{k-2} + a_{k+2}) = 0, \\ -k^2 r^2 b_k + \frac{2\beta(kr)^\alpha}{\omega^{2-\alpha}}\left(b_k\cos\frac{\alpha\pi}{2} + a_k\sin\frac{\alpha\pi}{2}\right) + b_k - \mu(b_{k-2} + b_{k+2}) = 0, \end{cases}$$

$$\tag{3.52}$$

where $r = {\theta}/{2\omega}$. The above system of equations can be written in matrix form, then

$$[C]_T \times [\dots, a_6, a_4, a_2, b_0, b_2, b_4, b_6, \dots]^T = 0 , \tag{3.53}$$

where $[C]_T$ is the matrix of coefficients for the solutions with period T.

The matrix of coefficients of the solutions with the period of $2T$ and T, $[C]_{2T}$ and $[C]_T$, are shown in Eqs. (3.54) and (3.55) respectively. Provided that $\alpha = 1$, these matrices become equal to the matrices shown in Eqs. (3.6) and (3.12). The flow chart of the approximate method of solving fractional Mathieu equations is shown in Figure 3.2.

The matrices shown in Eqs. (3.54) and (3.55) are infinite, so it is impossible to solve their determinants directly, but they allow us to estimate the approximate borders of the region of instability based on the order. For instance, the first and second order approximations of the boundary of the first stability region are found by plotting the relations between r and μ from Eqs. (3.56) and (3.57) respectively. Also, the first and second order approximations of the boundary of the second stability region are found by using Eqs. (3.58) and (3.59) respectively.
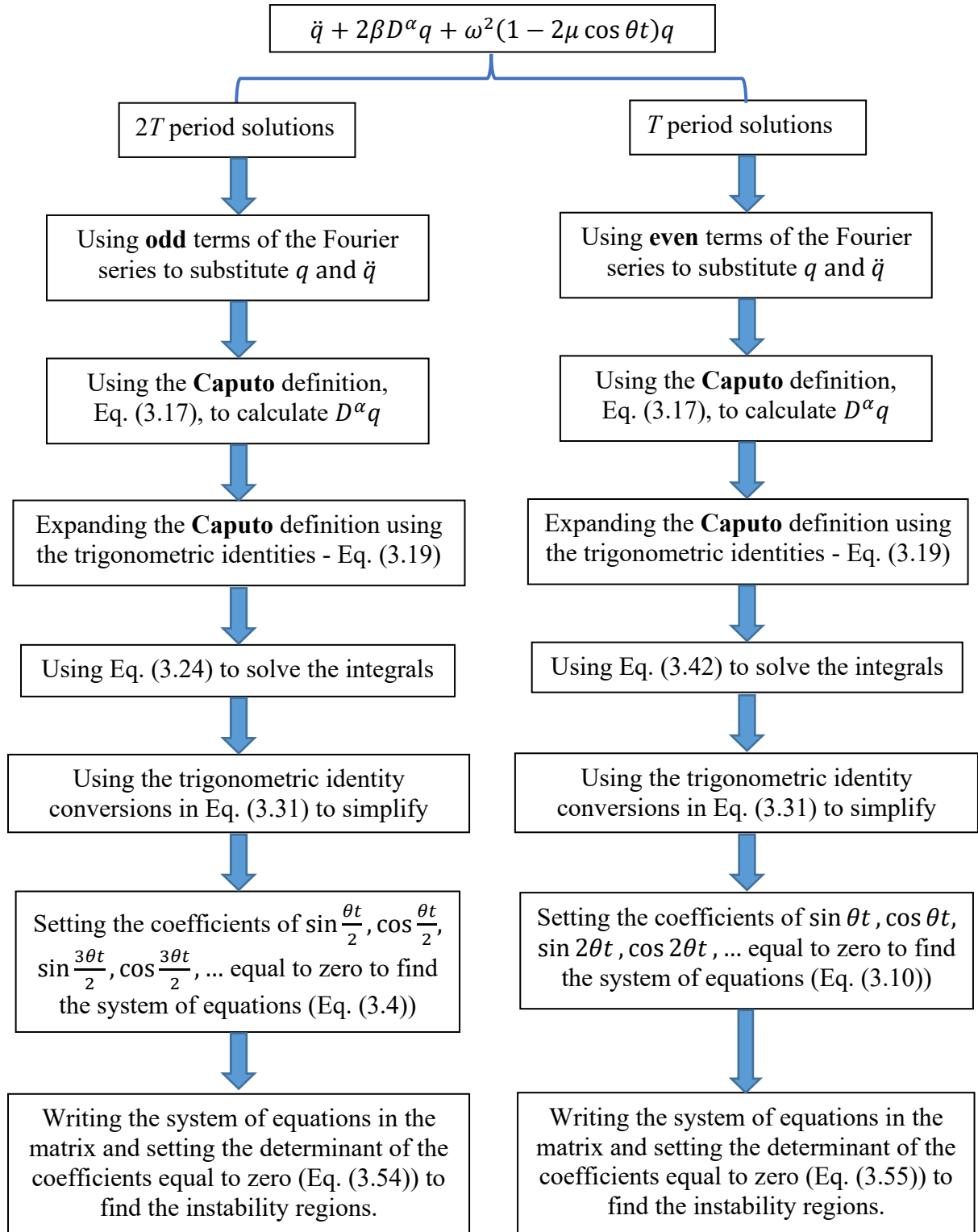
$$\ddot{q} + 2\beta D^\alpha q + \omega^2(1 - 2\mu\cos\theta t)q$$

2*T* period solutions	*T* period solutions
Using **odd** terms of the Fourier series to substitute q and $\ddot{q}$	Using **even** terms of the Fourier series to substitute q and $\ddot{q}$
Using the **Caputo** definition, Eq. (3.17), to calculate $D^\alpha q$	Using the **Caputo** definition, Eq. (3.17), to calculate $D^\alpha q$
Expanding the **Caputo** definition using the trigonometric identities - Eq. (3.19)	Expanding the **Caputo** definition using the trigonometric identities - Eq. (3.19)
Using Eq. (3.24) to solve the integrals	Using Eq. (3.42) to solve the integrals
Using the trigonometric identity conversions in Eq. (3.31) to simplify	Using the trigonometric identity conversions in Eq. (3.31) to simplify
Setting the coefficients of $\sin\frac{\theta t}{2}$, $\cos\frac{\theta t}{2}$, $\sin\frac{3\theta t}{2}$, $\cos\frac{3\theta t}{2}$, ... equal to zero to find the system of equations (Eq. (3.4))	Setting the coefficients of $\sin\theta t$, $\cos\theta t$, $\sin 2\theta t$, $\cos 2\theta t$, ... equal to zero to find the system of equations (Eq. (3.10))
Writing the system of equations in the matrix and setting the determinant of the coefficients equal to zero (Eq. (3.54)) to find the instability regions.	Writing the system of equations in the matrix and setting the determinant of the coefficients equal to zero (Eq. (3.55)) to find the instability regions.

Figure 3.2 Approximate method for solving fractional Mathieu equations

$$[C]_{2T} = \begin{bmatrix} \cdots & \cdots & \cdots & \cdots & \cdots & \cdots \\ \cdots & -\mu & 0 & 0 & 0 & \cdots \\ \cdots & 1-9r^2+\frac{2\beta(3r)^\alpha}{\omega^{2-\alpha}}\cos\frac{\alpha\pi}{2} & -\mu & 0 & -\frac{2\beta(3r)^\alpha}{\omega^{2-\alpha}}\sin\frac{\alpha\pi}{2} & \cdots \\ \cdots & -\mu & 1+\mu-r^2+\frac{2\beta r^\alpha}{\omega^{2-\alpha}}\cos\frac{\alpha\pi}{2} & -\frac{2\beta r^\alpha}{\omega^{2-\alpha}}\sin\frac{\alpha\pi}{2} & 0 & \cdots \\ \cdots & 0 & \frac{2\beta r^\alpha}{\omega^{2-\alpha}}\sin\frac{\alpha\pi}{2} & 1-\mu-r^2+\frac{2\beta r^\alpha}{\omega^{2-\alpha}}\cos\frac{\alpha\pi}{2} & -\mu & \cdots \\ \cdots & \frac{2\beta(3r)^\alpha}{\omega^{2-\alpha}}\sin\frac{\alpha\pi}{2} & 0 & -\mu & 1-9r^2+\frac{2\beta(3r)^\alpha}{\omega^{2-\alpha}}\cos\frac{\alpha\pi}{2} & \cdots \\ \cdots & 0 & 0 & 0 & -\mu & \cdots \\ \cdots & \cdots & \cdots & \cdots & \cdots & \cdots \end{bmatrix}$$

(3.54)

$$[C]_{T} = \begin{bmatrix} \cdots & \cdots & \cdots & \cdots & \cdots & \cdots & \cdots \\ \cdots & -\mu & 0 & 0 & 0 & 0 & \cdots \\ \cdots & 1-16r^2+\frac{2\beta(4r)^\alpha}{\omega^{2-\alpha}}\cos\frac{\alpha\pi}{2} & -\mu & 0 & 0 & -\frac{2\beta(4r)^\alpha}{\omega^{2-\alpha}}\sin\frac{\alpha\pi}{2} & \cdots \\ \cdots & -\mu & 1-4r^2+\frac{2\beta(2r)^\alpha}{\omega^{2-\alpha}}\cos\frac{\alpha\pi}{2} & 0 & -\frac{2\beta(2r)^\alpha}{\omega^{2-\alpha}}\sin\frac{\alpha\pi}{2} & 0 & \cdots \\ \cdots & 0 & 0 & 1 & -\mu & 0 & \cdots \\ \cdots & 0 & \frac{2\beta(2r)^\alpha}{\omega^{2-\alpha}}\sin\frac{\alpha\pi}{2} & -2\mu & 1-4r^2+\frac{2\beta(2r)^\alpha}{\omega^{2-\alpha}}\cos\frac{\alpha\pi}{2} & -\mu & \cdots \\ \cdots & \frac{2\beta(4r)^\alpha}{\omega^{2-\alpha}}\sin\frac{\alpha\pi}{2} & 0 & 0 & 0 & 1-16r^2+\frac{2\beta(4r)^\alpha}{\omega^{2-\alpha}}\cos\frac{\alpha\pi}{2} & \cdots \\ \cdots & 0 & 0 & 0 & 0 & -\mu & \cdots \\ \cdots & \cdots & \cdots & \cdots & \cdots & \cdots & \cdots \end{bmatrix}$$

(3.55)

$$
\begin{vmatrix}
1 + \mu - r^2 + \frac{2\beta r^\alpha}{\omega^{2-\alpha}}\cos\frac{\alpha\pi}{2} & -\frac{2\beta r^\alpha}{\omega^{2-\alpha}}\sin\frac{\alpha\pi}{2} \\
\frac{2\beta r^\alpha}{\omega^{2-\alpha}}\sin\frac{\alpha\pi}{2} & 1 - \mu - r^2 + \frac{2\beta r^\alpha}{\omega^{2-\alpha}}\cos\frac{\alpha\pi}{2}
\end{vmatrix} = 0
\tag{3.56}
$$

$$
\begin{vmatrix}
1 - 9r^2 + \frac{2\beta(3r)^\alpha}{\omega^{2-\alpha}}\cos\frac{\alpha\pi}{2} & -\mu & 0 & -\frac{2\beta(3r)^\alpha}{\omega^{2-\alpha}}\sin\frac{\alpha\pi}{2} \\
-\mu & 1 + \mu - r^2 + \frac{2\beta r^\alpha}{\omega^{2-\alpha}}\cos\frac{\alpha\pi}{2} & -\frac{2\beta r^\alpha}{\omega^{2-\alpha}}\sin\frac{\alpha\pi}{2} & 0 \\
0 & \frac{2\beta r^\alpha}{\omega^{2-\alpha}}\sin\frac{\alpha\pi}{2} & 1 - \mu - r^2 + \frac{2\beta r^\alpha}{\omega^{2-\alpha}}\cos\frac{\alpha\pi}{2} & -\mu \\
\frac{2\beta(3r)^\alpha}{\omega^{2-\alpha}}\sin\frac{\alpha\pi}{2} & 0 & -\mu & 1 - 9r^2 + \frac{2\beta(3r)^\alpha}{\omega^{2-\alpha}}\cos\frac{\alpha\pi}{2}
\end{vmatrix} = 0
\tag{3.57}
$$

$$
\begin{vmatrix}
1 - 4r^2 + \frac{2\beta(2r)^\alpha}{\omega^{2-\alpha}}\cos\frac{\alpha\pi}{2} & 0 & -\frac{2\beta(2r)^\alpha}{\omega^{2-\alpha}}\sin\frac{\alpha\pi}{2} \\
0 & 1 & -\mu \\
\frac{2\beta(2r)^\alpha}{\omega^{2-\alpha}}\sin\frac{\alpha\pi}{2} & -2\mu & 1 - 4r^2 + \frac{2\beta(2r)^\alpha}{\omega^{2-\alpha}}\cos\frac{\alpha\pi}{2}
\end{vmatrix} = 0
\tag{3.58}
$$

$$
\begin{vmatrix}
1 - 16r^2 + \frac{2\beta(4r)^\alpha}{\omega^{2-\alpha}}\cos\frac{\alpha\pi}{2} & -\mu & 0 & 0 & -\frac{2\beta(4r)^\alpha}{\omega^{2-\alpha}}\sin\frac{\alpha\pi}{2} \\
-\mu & 1 - 4r^2 + \frac{2\beta(2r)^\alpha}{\omega^{2-\alpha}}\cos\frac{\alpha\pi}{2} & 0 & -\frac{2\beta(2r)^\alpha}{\omega^{2-\alpha}}\sin\frac{\alpha\pi}{2} & 0 \\
0 & 0 & 1 & -\mu & 0 \\
0 & \frac{2\beta(2r)^\alpha}{\omega^{2-\alpha}}\sin\frac{\alpha\pi}{2} & -2\mu & 1 - 4r^2 + \frac{2\beta(2r)^\alpha}{\omega^{2-\alpha}}\cos\frac{\alpha\pi}{2} & -\mu \\
\frac{2\beta(4r)^\alpha}{\omega^{2-\alpha}}\sin\frac{\alpha\pi}{2} & 0 & 0 & -\mu & 1 - 16r^2 + \frac{2\beta(4r)^\alpha}{\omega^{2-\alpha}}\cos\frac{\alpha\pi}{2}
\end{vmatrix} = 0
\tag{3.59}
$$

3.3. Numerical solution to fractional Mathieu equations

In this section, a numerical method using block pulse functions (BPFs) to solve fractional Mathieu differential equations will be introduced. Initially, BPFs will be briefly explained, followed using BPFs in fractional calculus, and finally, a numerical solution to solve fractional Mathieu equations.

3.3.1.   Block pulse functions

Consider a set of block pulse functions (BPFs), $\boldsymbol{\Phi_m}(t)$, containing m components in the semi-open interval $[0, T)$

$$\boldsymbol{\Phi_m}(t) = [\varphi_0(t)\ \varphi_1(t) \cdots \varphi_i(t) \cdots \varphi_{m-1}(t)]^T, \tag{3.60}$$

where T indicates transpose. The ith function of the BPF vector, $\varphi_i(t)$, is

$$\varphi_i(t) = \begin{cases} 1 & ih \leq t < (i+1)h, \\ 0 & \text{otherwise,} \end{cases} \tag{3.61}$$

where $i = 0, 1, 2, \ldots, (m-1)$. m is a positive integer value and each component's BPF length along the time scale is $h = T/m$.

One of the properties of BPFs is that they are disjointed from one another [39], which means

$$\phi_i(t)\phi_j(t) = \begin{cases} \phi_i(t), & i = j, \\ 0, & i \neq j. \end{cases} \tag{3.62}$$

Another of their characteristics is that they are orthogonal with each other, that is

$$\int_0^T \phi_i(t)\phi_j(t)dt = \begin{cases} h, & i = j, \\ 0, & \text{otherwise,} \end{cases} \tag{3.63}$$
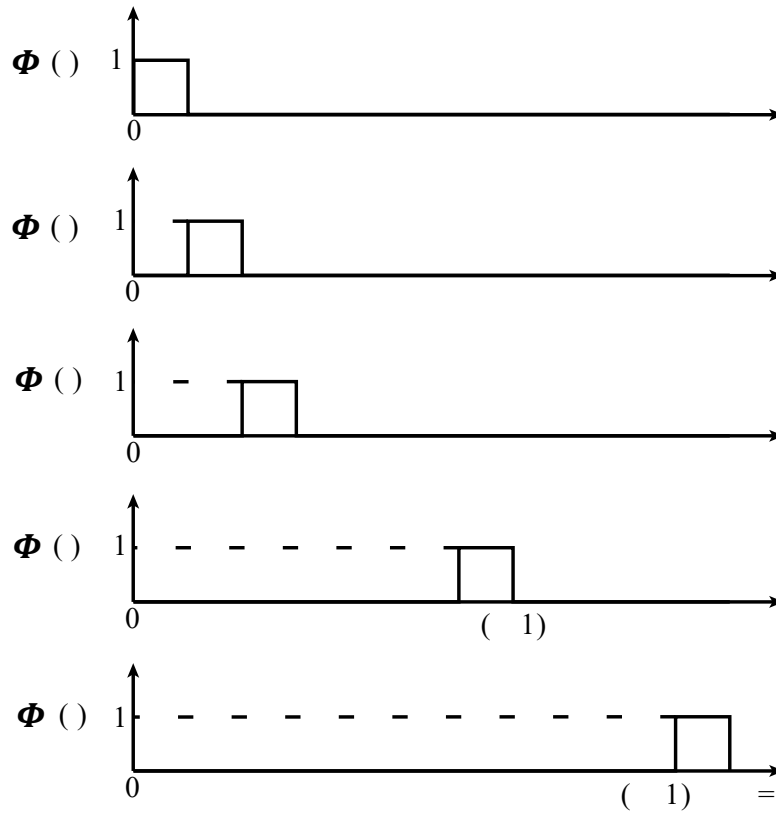
where $i, j = 0, \ldots, m-1$.

Figure 3.3 A set of block pulse functions

Provided that $f(t)$ is an integrable function with respect to time, it can be expanded over the period $[0, T)$ by using an m-term BPFs series

$$f(t) \cong \sum_{i=0}^{m-1} c_i \phi_i(t) = \boldsymbol{C}^T \boldsymbol{\Phi_m}(t) = \boldsymbol{\Phi}_m^T(t)\boldsymbol{C}, \tag{3.64}$$

where

$$\boldsymbol{C}^T = [c_0 \quad c_1 \cdots c_i \cdots c_{(m-1)}], \tag{3.65}$$

$$\boldsymbol{\Phi_m}(t) = [\varphi_0(t) \ \varphi_1(t) \cdots \varphi_i(t) \cdots \varphi_{m-1}(t)]^T, \tag{3.66}$$

and the constant coefficients (c_i's) in Eq. (3.65) are equal to

$$c_i = \left(\frac{1}{h}\right) \int_{ih}^{(i+1)h} f(t)\mathrm{d}t. \tag{3.67}$$

3.3.2.   Block pulse operational matrices

Below, we introduce the block-pulse functions operational matrix of fractional integration. Consider

$$f(t) \simeq \boldsymbol{C}^T \boldsymbol{\Phi}_m(t), \tag{3.68}$$

where $\boldsymbol{C}^T$ and $\boldsymbol{\Phi}_m(t)$ are equal to Eqs. (3.65) and (3.66). Therefore, the fractional integration of the block-pulse vector is

$$I^\alpha(\boldsymbol{C}^T \boldsymbol{\Phi}_m(t)) = \boldsymbol{C}^T \boldsymbol{F}_\alpha \boldsymbol{\Phi}_m(t), \tag{3.69}$$

where I^α is the fractional integration operator from the order of α, $\boldsymbol{F}_\alpha$ is the block pulse operational matrix of fractional order integration, and

$$\boldsymbol{F}_\alpha = \frac{h^\alpha}{\Gamma(\alpha+2)} \begin{bmatrix} 1 & \xi_1 & \xi_2 & \cdots & \xi_{m-1} \\ 0 & 1 & \xi_1 & \cdots & \xi_{m-2} \\ 0 & 0 & 1 & \cdots & \xi_{m-3} \\ 0 & 0 & 0 & \ddots & \vdots \\ 0 & 0 & 0 & 0 & 1 \end{bmatrix}, \tag{3.70}$$

where

$$\xi_k = (k+1)^{\alpha+1} - 2k^{\alpha+1} + (k-1)^{\alpha+1} \quad , \quad (k = 1,2,\dots,m-1). \tag{3.71}$$

Additionally, $\boldsymbol{D}_\alpha$ represents the operational matrix for fractional differentiation [40]. Based on the fractional calculus property

$$\boldsymbol{D}_\alpha \cdot \boldsymbol{F}_\alpha = \boldsymbol{I}_m, \tag{3.72}$$

where $\boldsymbol{I}_m$ is the identity matrix of the order $m \times m$. That is

$$\begin{bmatrix} 1 & \xi_1 & \xi_2 & \cdots & \xi_{m-1} \\ 0 & 1 & \xi_1 & \cdots & \xi_{m-2} \\ 0 & 0 & 1 & \cdots & \xi_{m-3} \\ 0 & 0 & 0 & \ddots & \vdots \\ 0 & 0 & 0 & 0 & 1 \end{bmatrix} \cdot \begin{bmatrix} d_0 & d_1 & d_2 & \cdots & d_{m-1} \\ 0 & d_0 & d_1 & \cdots & d_{m-2} \\ 0 & 0 & d_0 & \cdots & d_{m-3} \\ 0 & 0 & 0 & \ddots & \vdots \\ 0 & 0 & 0 & 0 & d_0 \end{bmatrix} = \boldsymbol{I}_m, \tag{3.73}$$

or

$$\boldsymbol{D}_\alpha = \begin{bmatrix} d_0 & d_1 & d_2 & \cdots & d_{m-1} \\ 0 & d_0 & d_1 & \cdots & d_{m-2} \\ 0 & 0 & d_0 & \cdots & d_{m-3} \\ 0 & 0 & 0 & \ddots & \vdots \\ 0 & 0 & 0 & 0 & d_0 \end{bmatrix} = \begin{bmatrix} 1 & \xi_1 & \xi_2 & \cdots & \xi_{m-1} \\ 0 & 1 & \xi_1 & \cdots & \xi_{m-2} \\ 0 & 0 & 1 & \cdots & \xi_{m-3} \\ 0 & 0 & 0 & \ddots & \vdots \\ 0 & 0 & 0 & 0 & 1 \end{bmatrix}^{-1}. \tag{3.74}$$

For example, considering $T = 1$ and $m = 8$, the fractional integration and differentiation operational matrices from the order 0.5, $\boldsymbol{F}_{0.5}$ and $\boldsymbol{D}_{0.5}$, are

$$F_{0.5} = \begin{bmatrix} 0.2660 & 0.2203 & 0.1434 & 0.1160 & 0.1001 & 0.0894 & 0.0816 & 0.0755 \\ 0 & 0.2660 & 0.2203 & 0.1434 & 0.1160 & 0.1001 & 0.0894 & 0.0816 \\ 0 & 0 & 0.2660 & 0.2203 & 0.1434 & 0.1160 & 0.1001 & 0.0894 \\ 0 & 0 & 0 & 0.2660 & 0.2203 & 0.1434 & 0.1160 & 0.1001 \\ 0 & 0 & 0 & 0 & 0.2660 & 0.2203 & 0.1434 & 0.1160 \\ 0 & 0 & 0 & 0 & 0 & 0.2660 & 0.2203 & 0.1434 \\ 0 & 0 & 0 & 0 & 0 & 0 & 0.2660 & 0.2203 \\ 0 & 0 & 0 & 0 & 0 & 0 & 0 & 0.2660 \end{bmatrix}$$

and

$$D_{0.5} = \begin{bmatrix} 3.7599 & -3.1148 & 0.5527 & -0.4178 & -0.0091 & -0.0998 & -0.0442 & -0.0460 \\ 0 & 3.7599 & -3.1148 & 0.5527 & -0.4178 & -0.0091 & -0.0998 & -0.0442 \\ 0 & 0 & 3.7599 & -3.1148 & 0.5527 & -0.4178 & -0.0091 & -0.0998 \\ 0 & 0 & 0 & 3.7599 & -3.1148 & 0.5527 & -0.4178 & -0.0091 \\ 0 & 0 & 0 & 0 & 3.7599 & -3.1148 & 0.5527 & -0.4178 \\ 0 & 0 & 0 & 0 & 0 & 3.7599 & -3.1148 & 0.5527 \\ 0 & 0 & 0 & 0 & 0 & 0 & 3.7599 & -3.1148 \\ 0 & 0 & 0 & 0 & 0 & 0 & 0 & 3.7599 \end{bmatrix}.$$

3.3.3.   Numerical solution

Consider the fractional damped Mathieu differential equation

$$D^2 q(t) = -2\beta D^\alpha q(t) - \omega^2(1 - 2\mu \cos \theta t)q(t), \quad 0 < \alpha \leq 1, \tag{3.75}$$

where D^2 and D^α are the second derivative and the Caputo fractional derivative operator of order α respectively. Also, the initial conditions of the function $q(t)$ are

$$q(0) = q_0 \text{ and } D^1 q(0) = q_1, \tag{3.76}$$

where D^1 is the first derivative operator.

In general, fractional differential equations can be numerically solved in two steps. The first step in solving a problem with an initial value is converting it to a problem with zero initial conditions. This stage involves obtaining a modified equation, which incorporates the initial values instead of the given equation.

An algebraic equation is generated from the fractional differential equation using the block pulse operational matrix of fractional integration.

The solution of the fractional damped Mathieu differential equation, Eq. (3.75), can be written in the form

$$q(t) = q_*(t) + z(t), \tag{3.77}$$

where $q_*(t)$ is a function that satisfies the initial conditions in Eq. (3.76) and $z(t)$ is the new

unknown function with zero initial conditions. Inserting Eq. (3.77) into Eq. (3.75) results in

$$D^2 z(t) = -2\beta D^\alpha z(t) - \omega^2(1 - 2\mu \cos \theta t)z(t) + g(t). \tag{3.78}$$

In Eq. (3.78), $g(t)$ is a known and $z(t)$ is an unknown function with the initial conditions

$$z(0) = 0 \text{ and } D^1 z(0) = 0. \tag{3.79}$$

Considering block pulse functions, functions $g(t)$ and $D^2 z(t)$ can be expanded into

$$g(t) \cong \boldsymbol{G}^T \boldsymbol{\Phi}_m(t), \tag{3.80}$$

and

$$D^2 z(t) \cong \boldsymbol{C}^T \boldsymbol{\Phi}_m(t), \tag{3.81}$$

where $\boldsymbol{G}^T = [g_0 \quad g_1 \cdots g_i \cdots g_{(m-1)}]$ is a known but $\boldsymbol{C}^T = [c_0 \quad c_1 \cdots c_i \cdots c_{(m-1)}]$ is an

unknown $m \times 1$ column vector. Similarly,

$$-\omega^2(1 - 2\mu \cos \theta t) \cong \boldsymbol{A}^T \boldsymbol{\Phi}_m(t), \tag{3.82}$$

and

$$-2\beta \cong \boldsymbol{B}^T \boldsymbol{\Phi}_m(t), \tag{3.83}$$

where $\boldsymbol{A}^T = [a_0 \quad a_1 \cdots a_i \cdots a_{(m-1)}]$ and $\boldsymbol{B}^T = [-2\beta \quad -2\beta \cdots -2\beta \cdots -2\beta]$ are both

known $m \times 1$ column vectors.

Considering the fractional calculus properties explained in chapter one

$$D^\alpha z(t) = I^{2-\alpha}[D^2 z(t)] = I^{2-\alpha}[\boldsymbol{C}^T \boldsymbol{\Phi}_m(t)] = \boldsymbol{C}^T \boldsymbol{F}_{2-\alpha} \boldsymbol{\Phi}_m(t) = [\boldsymbol{\Phi}_m(t)]^T [\boldsymbol{F}_{2-\alpha}]^T \boldsymbol{C}, \tag{3.84}$$

and

$$z(t) = I^2[D^2 z(t)] = I^2[\boldsymbol{C}^T \boldsymbol{\Phi}_m(t)] = \boldsymbol{C}^T \boldsymbol{F}_2 \boldsymbol{\Phi}_m(t) = [\boldsymbol{\Phi}_m(t)]^T [\boldsymbol{F}_2]^T \boldsymbol{C}, \tag{3.85}$$

where I^2 and $I^{2-\alpha}$ are the integration operator of order 2 and the fractional integral of order

$2 - \alpha$, respectively. Also, $\boldsymbol{F}_{2-\alpha}$ and $\boldsymbol{F}_2$ are the fractional integration operational matrices of

order $2 - \alpha$ and 2 which should be calculated based on Eq. (3.70).

Inserting Eqs. (3.80) to (3.85) into Eq. (3.78) leads to

$$\boldsymbol{C}^T \boldsymbol{\Phi}_m(t) = \boldsymbol{B}^T \boldsymbol{\Phi}_m(t)[\boldsymbol{\Phi}_m(t)]^T [\boldsymbol{F}_{2-\alpha}]^T \boldsymbol{C} + \boldsymbol{A}^T \boldsymbol{\Phi}_m(t)[\boldsymbol{\Phi}_m(t)]^T [\boldsymbol{F}_2]^T \boldsymbol{C} + \boldsymbol{G}^T \boldsymbol{\Phi}_m(t). \tag{3.86}$$

Using this method, we can find the unknown vector $\boldsymbol{C}$ by solving a system of algebraic

equations. Based on the BPF's properties, the below can be found

$$\boldsymbol{\Phi_m}(t)[\boldsymbol{\Phi_m}(t)]^T = \begin{bmatrix} \varphi_1(t) & & & 0 \\ & \varphi_2(t) & & \\ & & \ddots & \\ 0 & & & \varphi_m(t) \end{bmatrix}. \tag{3.87}$$

Considering

$$[\boldsymbol{F_2}]^T \boldsymbol{C} = \boldsymbol{X_a} = [x_{a1} \quad x_{a2} \cdots x_{ai} \cdots x_{am}]^T,$$

and

$$[\boldsymbol{F_{2-\alpha}}]^T \boldsymbol{C} = \boldsymbol{X_b} = [x_{b1} \quad x_{b2} \cdots x_{bi} \cdots x_{bm}]^T,$$

one can get

$$\boldsymbol{\Phi_m}(t)[\boldsymbol{\Phi_m}(t)]^T [\boldsymbol{F_2}]^T \boldsymbol{C} = \text{diag}\,(\boldsymbol{X_a})\boldsymbol{\Phi_m}(t), \tag{3.88}$$

and

$$\boldsymbol{\Phi_m}(t)[\boldsymbol{\Phi_m}(t)]^T [\boldsymbol{F_{2-\alpha}}]^T \boldsymbol{C} = \text{diag}\,(\boldsymbol{X_b})\boldsymbol{\Phi_m}(t), \tag{3.89}$$

where

$$\text{diag}(\boldsymbol{X_a}) = \begin{bmatrix} x_{a1} & & & 0 \\ & x_{a2} & & \\ & & \ddots & \\ 0 & & & x_{am} \end{bmatrix}, \text{diag}(\boldsymbol{X_b}) = \begin{bmatrix} x_{b1} & & & 0 \\ & x_{b2} & & \\ & & \ddots & \\ 0 & & & x_{bm} \end{bmatrix}. \tag{3.90}$$

Inserting Eqs. (3.88) and (3.89) into Eq. (3.86) results in

$$\boldsymbol{C^T \Phi_m}(t) = \boldsymbol{A^T}\text{diag}\,(\boldsymbol{X_a})\boldsymbol{\Phi_m}(t) + \boldsymbol{B^T}\,\text{diag}(\boldsymbol{X_b})\boldsymbol{\Phi_m}(t) + \boldsymbol{G^T \Phi_m}(t), \tag{3.91}$$

which can be simplified to

$$\boldsymbol{C} = \text{diag}(\boldsymbol{X_a})\boldsymbol{A} + \text{diag}(\boldsymbol{X_b})\boldsymbol{B} + \boldsymbol{G}. \tag{3.92}$$

The vector of coefficients, $\boldsymbol{C^T}$, can be found by solving the above system of algebraic equations. The result of Eq. (3.78) is

$$z(t) = \boldsymbol{C^T F_2 \Phi_m}(t), \tag{3.93}$$

and finally, the response of the Eq. (3.75) is

$$q(t) = q_*(t) + z(t) = q_*(t) + \boldsymbol{C^T F_2 \Phi_m}(t). \tag{3.94}$$

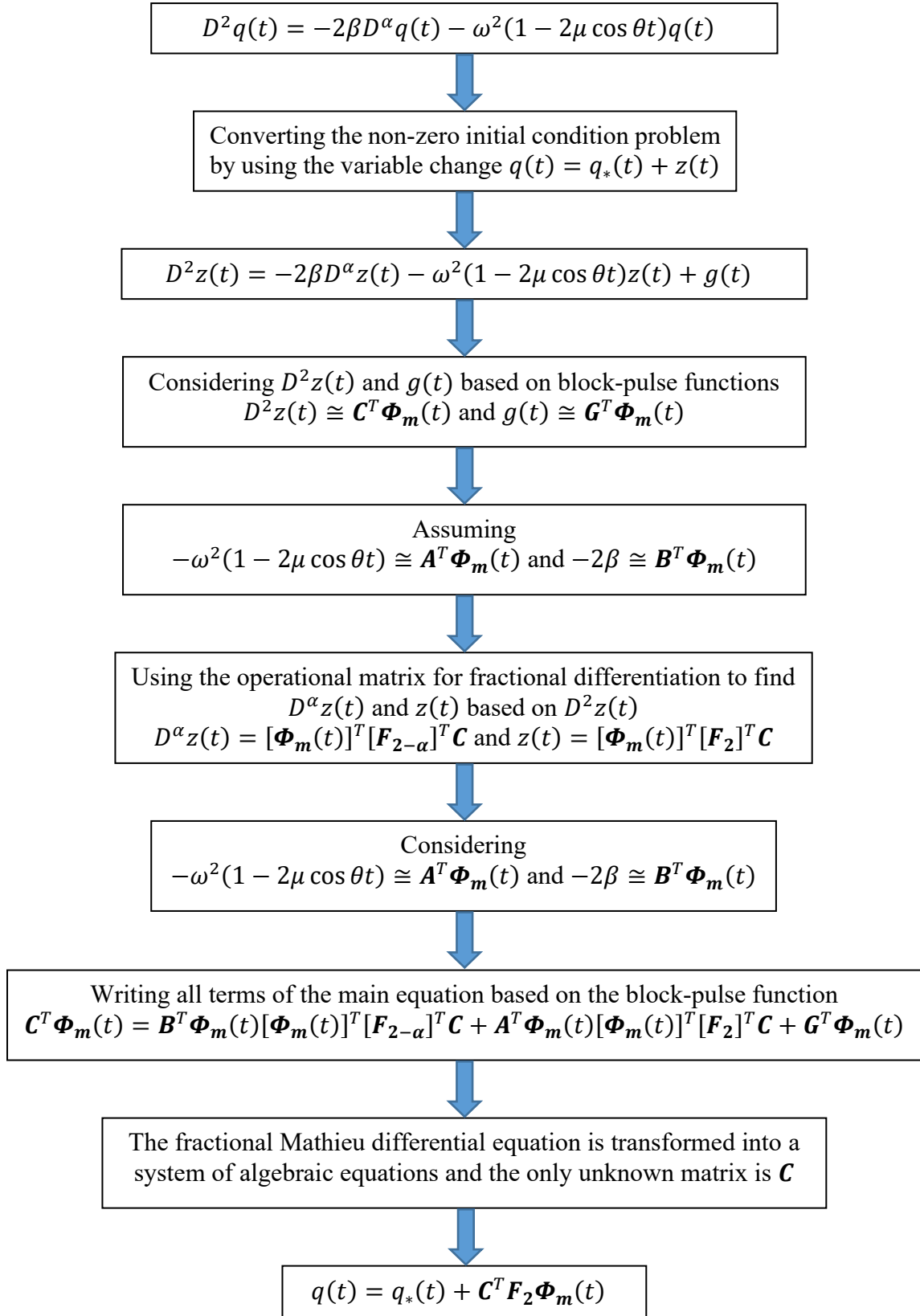The flow chart of the numerical method for solving fractional Mathieu equations is shown in Figure 3.4.

$$D^2 q(t) = -2\beta D^\alpha q(t) - \omega^2(1 - 2\mu \cos \theta t)q(t)$$

Converting the non-zero initial condition problem by using the variable change $q(t) = q_*(t) + z(t)$

$$D^2 z(t) = -2\beta D^\alpha z(t) - \omega^2(1 - 2\mu \cos \theta t)z(t) + g(t)$$

Considering $D^2 z(t)$ and $g(t)$ based on block-pulse functions
$$D^2 z(t) \cong \boldsymbol{C}^T \boldsymbol{\Phi_m}(t) \text{ and } g(t) \cong \boldsymbol{G}^T \boldsymbol{\Phi_m}(t)$$

Assuming
$$-\omega^2(1 - 2\mu \cos \theta t) \cong \boldsymbol{A}^T \boldsymbol{\Phi_m}(t) \text{ and } -2\beta \cong \boldsymbol{B}^T \boldsymbol{\Phi_m}(t)$$

Using the operational matrix for fractional differentiation to find $D^\alpha z(t)$ and $z(t)$ based on $D^2 z(t)$
$$D^\alpha z(t) = [\boldsymbol{\Phi_m}(t)]^T [\boldsymbol{F_{2-\alpha}}]^T \boldsymbol{C} \text{ and } z(t) = [\boldsymbol{\Phi_m}(t)]^T [\boldsymbol{F_2}]^T \boldsymbol{C}$$

Considering
$$-\omega^2(1 - 2\mu \cos \theta t) \cong \boldsymbol{A}^T \boldsymbol{\Phi_m}(t) \text{ and } -2\beta \cong \boldsymbol{B}^T \boldsymbol{\Phi_m}(t)$$

Writing all terms of the main equation based on the block-pulse function
$$\boldsymbol{C}^T \boldsymbol{\Phi_m}(t) = \boldsymbol{B}^T \boldsymbol{\Phi_m}(t)[\boldsymbol{\Phi_m}(t)]^T [\boldsymbol{F_{2-\alpha}}]^T \boldsymbol{C} + \boldsymbol{A}^T \boldsymbol{\Phi_m}(t)[\boldsymbol{\Phi_m}(t)]^T [\boldsymbol{F_2}]^T \boldsymbol{C} + \boldsymbol{G}^T \boldsymbol{\Phi_m}(t)$$

The fractional Mathieu differential equation is transformed into a system of algebraic equations and the only unknown matrix is $\boldsymbol{C}$

$$q(t) = q_*(t) + \boldsymbol{C}^T \boldsymbol{F_2} \boldsymbol{\Phi_m}(t)$$

Figure 3.4 Numerical method for solving fractional Mathieu equations

3.3.4.   **Finding instability regions**

Using the explained numerical method, vibration response of the pile, $q(t)$, can be found based on the specific amounts of dynamic load parameter and frequency. Before finding the instability regions, we should be able to detect unstable responses. For detecting unstable responses, the Lyapunov exponent method is used in this research. Considering vibration response $q(t)$, then for a chosen time interval T the responses are equal to $q(T), q(2T), q(3T), q(4T), \dots$ where T is the period of the periodic axial loading. After NT time intervals $U_1, U_2, \dots, U_N$ can be calculated by

$$U_N = \ln\|q(NT)\|, \tag{3.95}$$

where $N = 1,2,3,4,\dots$ indicates the time intervals and $\|\quad\|$ shows is the Euclidean norm [41]. Also, $\mu_1, \mu_2, \dots, \mu_N$ can be calculated by

$$\mu_N = \sum_{j=1}^{N} \frac{U_j}{NT}. \tag{3.96}$$

It was demonstrated by Goldhirsch [42] that μ_N, when plotted against $1/NT$, tends to a positive number, as $1/NT$ approaches zero, if the system is unstable.

Pile stability behaviour, in addition to pile and soil properties, is a function of dynamic load parameter and frequency ratio. Consider a two-dimensional diagram that consists of the dynamic load parameter and frequency ratio axes. Each point of this space represents a specific value for the dynamic load parameter and frequency ratio. The behaviour of the pile can then be found on each poin using the Lyapunov exponent method and if it is unstable, we mark that point. Thus, by examining all points of the diagram space, instability regions can be found.

3.4. **Summary**

The Bolotin method is explained in the first part of this chapter. This method is traditionally used to obtain instability regions for the conventional form of the Mathieu equation by using even and odd numbered terms of the Fourier series for $2T$ and T period solutions, respectively. It is shown how the coefficients' matrices should be found and how

various instability region approximations should be calculated based on the coefficients' matrices.

Secondly, an approximate method based on the Bolotin method is proposed to solve the fractional Mathieu equation. Caputo's definition expands the fractional derivative related to the fractional damping characteristics of pile surrounding soil. Using the Fourier series, the coefficients' matrices are found based on the fractional order α, shown in Eqs. (3.54) and (3.55), respectively.

Additionally, a numerical solution based on block-pulse functions (BPFs) is introduced to find the vibration response of the fractional Mathieu equation. Using the fractional integration operational matrix for the block-pulse functions, Eq. (3.70) transforms the differential equation into a system of algebraic equations.

Finally, Lyapunov exponent method is explained which helps to detect the pile behaviour (stable or unstable) by using the vibration response. Moreover, it is illustrated that instability regions can be shown by using the vibration responses of nodes in two-dimensional space, consisting of dynamic load coefficient and frequency ratio axes.

In the next chapter, an example of a pile under periodic axial load is solved, instability regions are compared using approximate and numerical methods and the influence on instability regions due to changes in different variables is discussed.

C H A P T E R 4

Dynamic stability of piles under earthquake

This chapter gives an example of dynamic stability of pile foundations based on the fractional damping characteristics of the surrounding soil. Approximate and numerical methods proposed in Chapter 4 are used to generate instability diagrams and the approximate method is validated with the numerical results. The effect of various parameter changes on pile stability under periodic dynamic load is also investigated in this chapter. Moreover, considering an actual dynamic wave recorded during an earthquake, the stability behaviour of a sample pile is studied in the last section.

4.1.   Dynamic instability regions of a pile

Consider a simply supported pile (pin-pin supports) with a tubular cross-section under axial dynamic loadings. The pile has a length (L) of 18 m, an outside diameter equal to 508 mm, and a thickness of 19 mm. As a result, the cross-sectional area (A) is 0.029 m^2. Young's elastic modulus (E) and mass density (ρ) are equal to 2.1×10^{11} N/m^2 and 7.8×10^3 kg/m^3 , respectively. The moment of inertia of the tubular cross-section is

$$I = \pi \times \left(\frac{508-19}{2} \times 10^{-3}\right)^3 \times (19 \times 10^{-3}) = 8.72 \times 10^{-4} \text{ m}^4. \tag{4.1}$$

According to Eq. (2.24), the critical Euler buckling load and the fundamental (natural) frequency of the pile are

$$P_{cr} = \text{EI}\left(\frac{\pi}{L}\right)^2 = 2.1 \times 10^{11} \times 8.72 \times 10^{-4} \times \left(\frac{\pi}{18}\right)^2 = 5.58 \text{ MN}, \tag{4.2}$$

$$\Omega = \left(\frac{\pi}{L}\right)^2 \sqrt{\frac{EI}{\rho A}} = \left(\frac{\pi}{18}\right)^2 \sqrt{\frac{2.1 \times 10^{11} * 8.72 \times 10^{-4}}{7.8 \times 10^3 \times 0.029}} = 27.4079 \frac{rad}{s} = 4.36 \text{ Hz}, \tag{4.3}$$

then the natural period is $T_0 = 2\pi/\Omega = 0.0697s$. By using Eq. (2.23), the dimensionless foundation stiffness parameter is given by

$$\eta = \frac{k_s L^4}{\pi^2 EI} = \frac{k_s \times 18^4}{\pi^2 \times 2.1 \times 10^{11} \times 8.72 \times 10^{-4}} = 0.001321 k_s. \tag{4.4}$$

Based on the above parameters, the equation of motion for a pile surrounded by soil (Winkler's foundation with fractional damping) is shown by

$$\ddot{q} + 2\beta_W D^\alpha q + \omega_W^2 \left(1 - 2\frac{\epsilon}{2(1-\lambda+\eta)}\cos\theta t\right)q = 0, \tag{4.5}$$

where, based on Eq. (2.23),

$$\omega_W^2 = \Omega^2(1 - \lambda + \eta) = 27.4079^2 \times (1 - \lambda + \eta) = 751.2 \times (1 - \lambda + \eta), \tag{4.6}$$

$$\beta_W = \frac{\delta \cdot \omega_W}{2\pi} = 4.36 \times \delta\sqrt{1 - \lambda + \eta} \,, \, 2\mu_W = \frac{\epsilon}{1-\lambda+\eta}\,. \tag{4.7}$$

where λ is the dimensionless static load parameter, ϵ is the dimensionless dynamic load parameter, and δ is the logarithmic decrement of damping. Analyzing the material properties of the pile surrounding soil yields values for the dimensionless foundation parameters, η, and δ. Richart (1970) [22] indicates that the ranges, $0.1 \leq \eta \leq 10,\ 0.05 \leq \delta \leq 0.8$ are realistic for soil foundations. In the current study, we consider $0.5 \leq \eta \leq 4,\ 0.1 \leq \delta \leq 0.4$.

Considering $\eta = 0.5,\ \delta = 0.2$, and $\lambda = 0.5$, Eq. (4.1) may be written as

$$\ddot{q} + 1.7448 D^\alpha q + 751.2(1 - \epsilon\cos\theta t)q = 0. \tag{4.8}$$

Based on Eqs. (3.54) and (3.55), solving the fractional Mathieu in Eq. (4.8) results in the matrices of coefficients, $[C]_{2T}$ and $[C]_T$, which can be used to find the regions of instability. Matrices in Eqs. (4.9) and (4.10) must have zero determinants in order to have a nontrivial solution. Thus, there are two infinite determinants, i.e., Fractional Mathieu infinite determinants (ID).

$$[C]_{2T} = \begin{bmatrix}
\cdots & \cdots & \cdots & \cdots & \cdots & \cdots \\
\cdots & -0.5\epsilon & 0 & 0 & 0 & \cdots \\
\cdots & 1-9r^2+\dfrac{1.745(3r)^\alpha}{(27.4)^{2-\alpha}}\cos\dfrac{\alpha\pi}{2} & -0.5\epsilon & 0 & -\dfrac{1.745(3r)^\alpha}{(27.4)^{2-\alpha}}\sin\dfrac{\alpha\pi}{2} & \cdots \\
\cdots & -0.5\epsilon & 1+0.5\epsilon-r^2+\dfrac{1.745r^\alpha}{(27.4)^{2-\alpha}}\cos\dfrac{\alpha\pi}{2} & -\dfrac{1.745r^\alpha}{(27.4)^{2-\alpha}}\sin\dfrac{\alpha\pi}{2} & 0 & \cdots \\
\cdots & 0 & \dfrac{1.745r^\alpha}{(27.4)^{2-\alpha}}\sin\dfrac{\alpha\pi}{2} & 1-0.5\epsilon-r^2+\dfrac{1.745r^\alpha}{(27.4)^{2-\alpha}}\cos\dfrac{\alpha\pi}{2} & -0.5\epsilon & \cdots \\
\cdots & \dfrac{1.745(3r)^\alpha}{(27.4)^{2-\alpha}}\sin\dfrac{\alpha\pi}{2} & 0 & -0.5\epsilon & 1-9r^2+\dfrac{1.745(3r)^\alpha}{(27.4)^{2-\alpha}}\cos\dfrac{\alpha\pi}{2} & \cdots \\
\cdots & 0 & 0 & 0 & -0.5\epsilon & \cdots \\
\cdots & \cdots & \cdots & \cdots & \cdots & \cdots
\end{bmatrix}$$

(4.9)

$$[C]_T = \begin{bmatrix}
\cdots & \cdots & \cdots & \cdots & \cdots & \cdots & \cdots \\
\cdots & -0.5\epsilon & 0 & 0 & 0 & 0 & \cdots \\
\cdots & 1-16r^2+\dfrac{1.745(4r)^\alpha}{(27.4)^{2-\alpha}}\cos\dfrac{\alpha\pi}{2} & -0.5\epsilon & 0 & 0 & -\dfrac{1.745(4r)^\alpha}{(27.4)^{2-\alpha}}\sin\dfrac{\alpha\pi}{2} & \cdots \\
\cdots & -0.5\epsilon & 1-4r^2+\dfrac{1.745(2r)^\alpha}{(27.4)^{2-\alpha}}\cos\dfrac{\alpha\pi}{2} & 0 & -\dfrac{1.745(2r)^\alpha}{(27.4)^{2-\alpha}}\sin\dfrac{\alpha\pi}{2} & 0 & \cdots \\
\cdots & 0 & 0 & 1 & -0.5\epsilon & 0 & \cdots \\
\cdots & 0 & \dfrac{1.745(2r)^\alpha}{(27.4)^{2-\alpha}}\sin\dfrac{\alpha\pi}{2} & -\epsilon & 1-4r^2+\dfrac{1.745(2r)^\alpha}{(27.4)^{2-\alpha}}\cos\dfrac{\alpha\pi}{2} & -0.5\epsilon & \cdots \\
\cdots & \dfrac{1.745(4r)^\alpha}{(27.4)^{2-\alpha}}\sin\dfrac{\alpha\pi}{2} & 0 & 0 & 0 & 1-16r^2+\dfrac{1.745(4r)^\alpha}{(27.4)^{2-\alpha}}\cos\dfrac{\alpha\pi}{2} & \cdots \\
\cdots & 0 & 0 & 0 & 0 & -0.5\epsilon & \cdots \\
\cdots & \cdots & \cdots & \cdots & \cdots & \cdots & \cdots
\end{bmatrix}$$

(4.10)

Considering a specific amount of the fractional damping order, either Fractional Mathieu IDs represents a functional relationship between ϵ and r, which plots as a set of transition curves in the $\epsilon - r$ plane. Practically, the infinite order of the Fractional Mathieu determinant can't be solved. Based on the results of the first several orders, approximate results can be obtained. By increasing the size of the determinant, instability regions may be calculated more precisely [43].

All the stability diagrams are calculated based on δ, η, λ, and ω where the first two parameters denote soil characteristics and the last two parameters indicate the static load ratio applied to the pile and frequency of the system. Then, knowing the order of the fractional damping and the amount and frequency of dynamic load, the stability of the system can be found.

The effects of the fractional damping order on the pile stability behaviour are shown in Figure 4.1 for the pile's first four instability regions. The minimum dynamic load on each boundary and related frequency ratio are called the critical dynamic load and critical frequency ratio, respectively. The fractional damping order growth results in an increase in critical dynamic load and a slight decrease in the critical frequency ratio in each instability region. In general, if we consider the instability areas as a triangle, the effect of α is more visible near the triangle's apex and not on its sides. For instance, considering the first instability region, by increasing α from 0.5 to 1, the critical dynamic load increases from 0.02 to 0.13. But, at the frequency ratio 1.1, the dynamic load changes from 0.4 to 0.45, and at the frequency ratio 0.9, the dynamic load approximately remains constant at around 0.41.

Figure 4.2 indicates the sensitivity of critical dynamic load changes upon the fractional damping order in different instability regions. The effect of the fractional order, α, is more significant in regions with higher numbers than in regions with lower numbers. For example, by increasing the fractional order from 0.2 to 1, the critical dynamic load grows from around zero to 0.13 in the first instability region, while in the fourth region, it has a significant increase from 0.37 to 0.8.
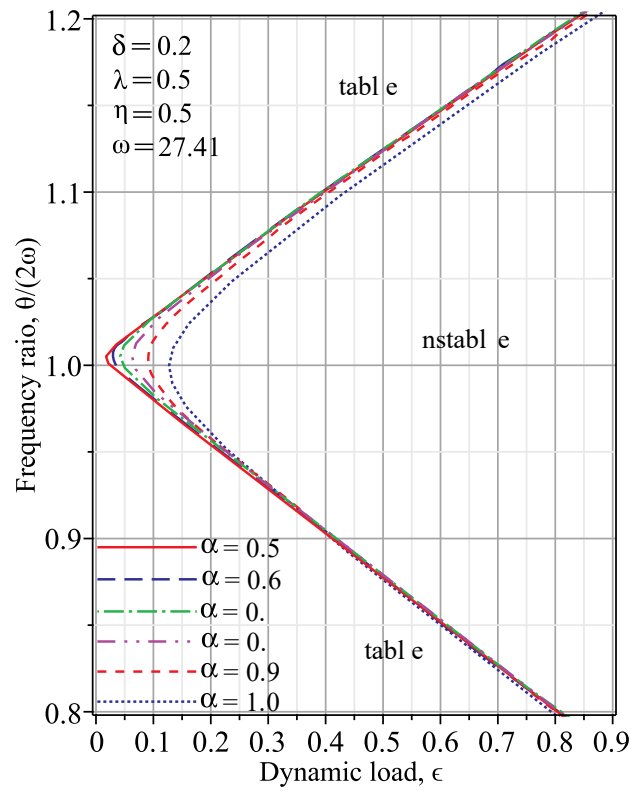
(a) First region of instability
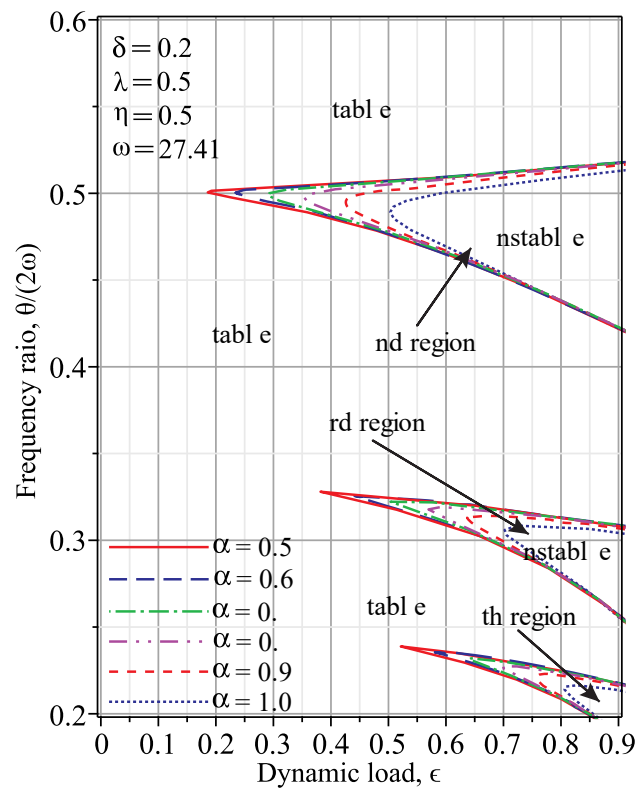
(b) Second, third, and fourth regions of instability

Figure 4.1 Effect of the fractional damping order on the region of instability
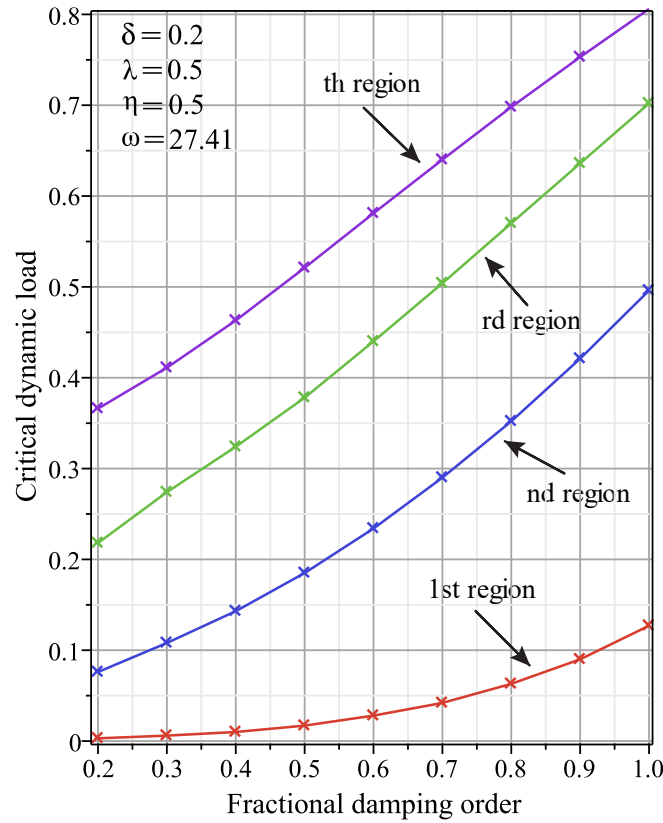
Figure 4.2 Critical dynamic load ratio vs. fractional damping order

4.2. Approximate and numerical solutions

Consider a pile surrounded by soil (Winkler's foundation with fractional damping) with parameters λ=0.5, δ=0. , η=0.5. Eq. (4.8) gives the equation of motion, and the instability regions can be generated, based on the Bolotin method, by using the determinant of matrices in Eqs. (4.9) and (4.10) for the specified order of fractional damping. The instability regions may be calculated by the numerical solution explained in Section 3.3 in detail. For this purpose, the fractional Mathieu differential equation is written in the form of

$$D^2 q = -2\beta D^\alpha q - \omega^2 (1 - 2\mu \cos\theta t)q, \tag{4.11}$$

where the initial conditions are $q(0) = q_0 = 0$ and $D^1 q(0) = q_1 = 0.1$.

Based on the procedure explained in the previous chapter, our numerical solution is helpful for problems with zero initial conditions,

$$q(t) = q_*(t) + z(t), \tag{4.12}$$

where the initial conditions for $z(t)$ are $z(0) = 0$ and $D^1 z(0) = 0$.

Several forms of $q_*(t)$ may be considered to convert the initial conditions into zero, for example,

$$q_*(t) = (5q_0 + q_1)e^{-4t} - (4q_0 + q_1)e^{-5t} = 0.1e^{-4t} - 0.1e^{-5t}, \tag{4.13}$$

which helps to nullify the effects of the initial conditions rapidly.

Considering the variable change in Eq. (4.12), Eq. (4.11) is transformed into

$$D^2 z(t) = -2\beta D^\alpha z(t) - \omega^2(1 - 2\mu \cos \theta t)z(t) + g(t), \tag{4.14}$$

where

$$g(t) = [25 + \omega^2(1 - 2\mu \cos \theta t)] \times (4q_0 + q_1)e^{-5t} - [16 + \omega^2(1 - 2\mu \cos \theta t)] \times (5q_0 +$$

$$q_1)e^{-4t} - \frac{2\beta}{\Gamma(n-\alpha)} \times \left[(5q_0 + q_1) \int_0^t \frac{D^n(e^{-4t})}{(t-x)^{\alpha+1-n}} dx - (4q_0 + q_1) \int_0^t \frac{D^n(e^{-5t})}{(t-x)^{\alpha+1-n}} dx \right].$$

$$\tag{4.15}$$

Inserting q_0 and q_1 into Eq. (4.15) results in

$$g(t) = 0.1e^{-5t} \times [25 + \omega^2(1 - 2\mu \cos \theta t)] - 0.1e^{-4t} \times [16 + \omega^2(1 - 2\mu \cos \theta t)] -$$

$$\frac{0.2\beta}{\Gamma(n-\alpha)} \times \int_0^t \frac{D^n(e^{-4t} - e^{-5t})}{(t-x)^{\alpha+1-n}} dx, \tag{4.16}$$

where $n = 1$ if $0 < \alpha < 1$ or $n = 2$ if $\alpha = 1$.

Using the numerical method, Eq. (4.14) can be solved and $z(t)$ is found,

$$q(t) = q_*(t) + z(t) = 0.1e^{-4t} - 0.1e^{-5t} + z(t). \tag{4.17}$$

In order to find the instability boundary, several sample points are taken from the $\epsilon - r$ plane ($r = \theta/2\omega$), then the behaviour of the pile is investigated for each sample. Finally, the stability or instability of the response is detected. The grid intervals for taking the samples are 0.05 and 0.02 in ϵ and r directions, respectively. Increasing the grid density and number of samples leads to more accurate diagrams and a finer boundary, but it significantly increases computation time. The area indicated by the blue dots in the following stability diagrams shows the instability regions, while the blank areas are related to the stable response of the pile.

Figure 4.3 shows the effect of fractional Mathieu IDs order on the accuracy of the instability boundary. The first-order ID boundary is not accurate for the first instability region

because the lower part of the boundary completely deviates from the numerical boundary. However, the second-order and third-order ID boundaries are acceptable. Figure 4.4 shows that the second-order and third-order ID boundaries are inaccurate for the third instability region, but the fourth-order ID boundary is acceptable. The fourth-order ID boundary remains inaccurate for the fifth instability region. As a result, the desirable ID order indicates the number of required terms of the Fourier series (explained in section 3.3). For example, if the third-order ID boundaries are needed, the odd numbered terms are used for $k = 1,3,5$, while if the fourth-order ID boundary is needed, we should consider $k = 1,3,5,7$ in the Fourier series.

For the second instability region, Figure 4.5 shows that the first-order ID boundary incurs errors; the second-order ID boundary isn't accurate on the lower boundary, but the third-order ID boundary is fine. Figure 4.6 indicates that the generated fourth instability region with neither the second-order nor the third-order ID boundaries is accurate; however, the fourth-order boundary appears acceptable. The instabilities boundary in the sixth region remains unacceptable at the fourth-order boundary. As a result, the desirable ID order indicates the number of required terms of the Fourier series explained in section 3.3. For example, the third-order ID boundaries are needed, the even numbered terms are used for $k = 0,2,4,6$ while the fourth-order ID boundary is needed, we should consider $k = 0,2,4,6,8$ in the Fourier series.
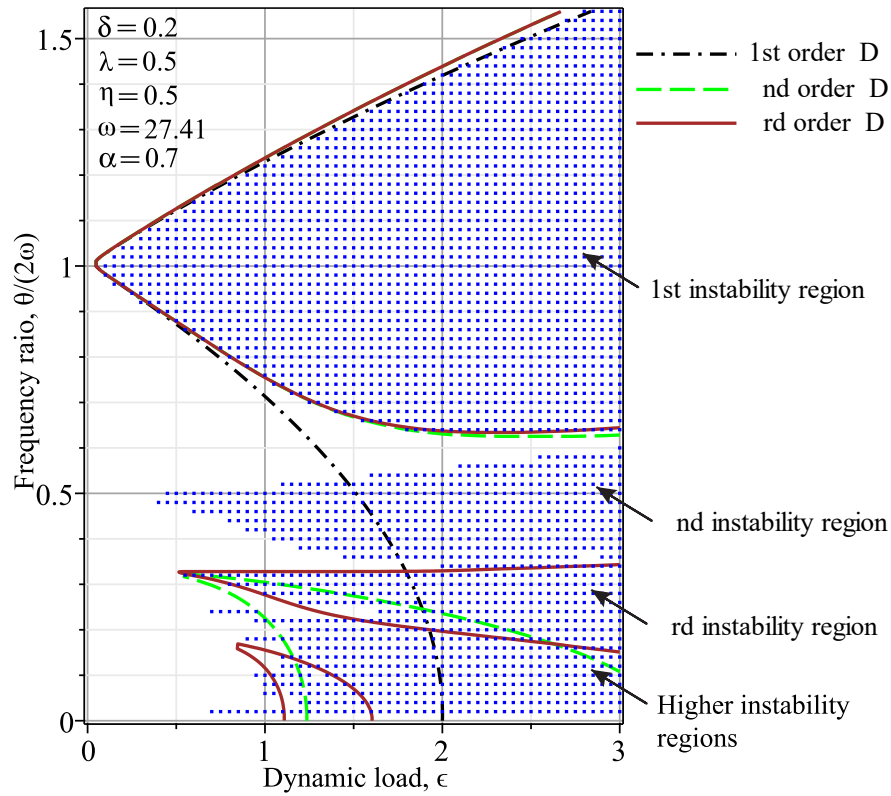
Figure 4.3 Instability regions from numerical simulation and approximate method
(1-3 order ID with period $2T$)
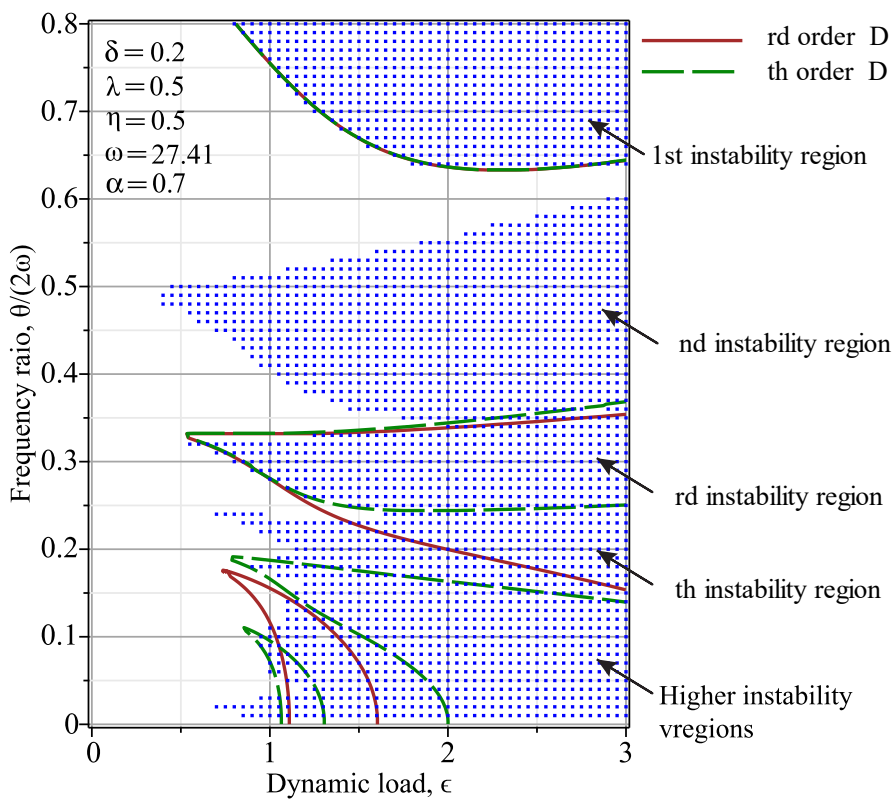
Figure 4.4 Instability regions from numerical simulation and approximate method
(3-4 order ID with period $2T$)
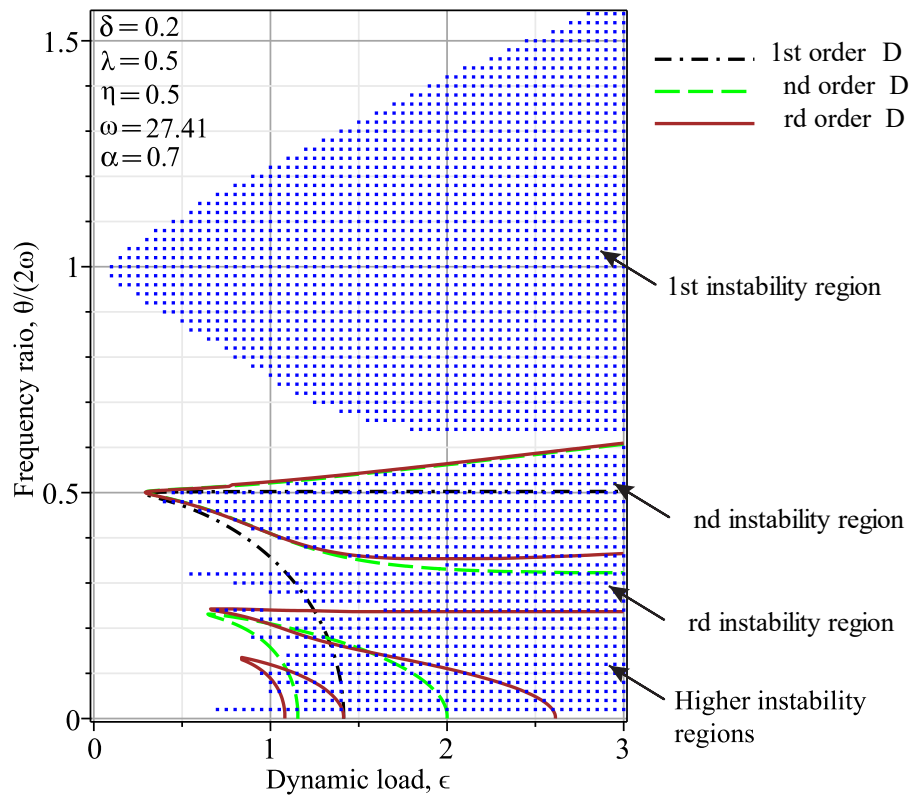
Figure 4.5 Instability regions from numerical simulation and approximate method
(1-3 order ID with period T)
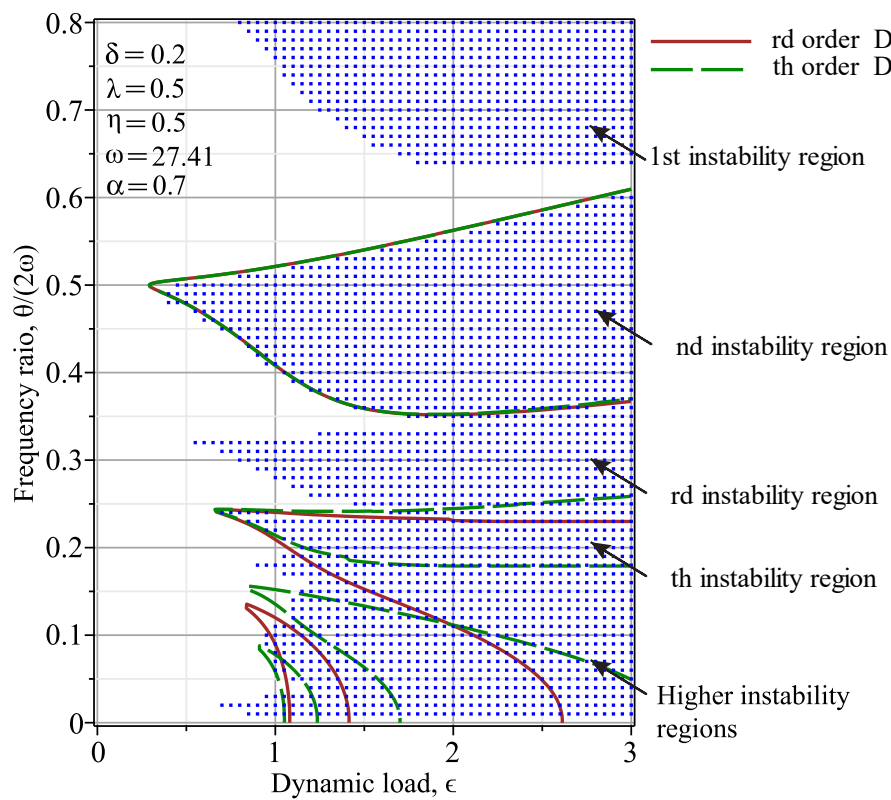
Figure 4.6 Instability regions from numerical simulation and approximate method
(3-4 order ID with period T)
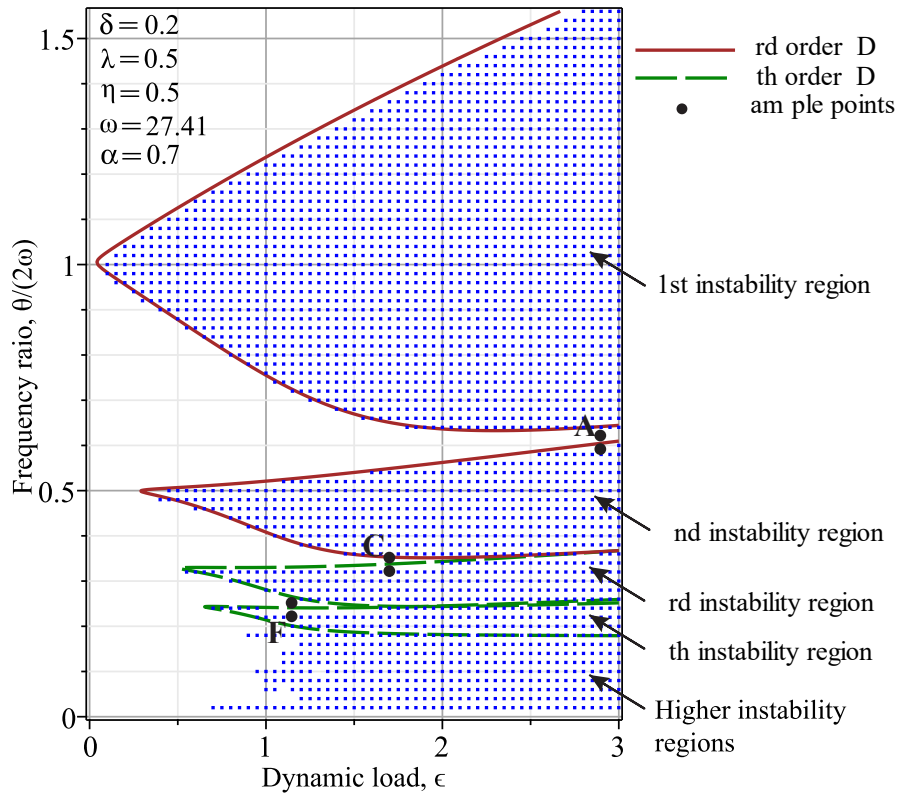
Figure 4.7 Instability regions from numerical simulation and approximate method
(3-4 order ID with period T and $2T$)

Generally, the higher instability regions need higher order Fractional Mathieu IDs. In other words, using the numerical method helps find which order of approximation in the Bolotin method is accurate for each instability region. Figure 4.7 shows the first instability region from the numerical and approximate method based on the third and fourth-order of the Fractional Mathieu ID. Also, some samples (black bullet points) are chosen to better understand the pile response during the axially dynamic loading. Each bullet indicates a set of dynamic load and frequency ratios used to investigate the response behaviour. Figure 4.8 shows Lyapunov exponents stability diagrams for each bullet points (black bullet points in Figure 4.7). At points A, C, and E when $1/NT$ approaches zero, μ_N tends to a negative number, so the pile is stable. On the other hand, at points B, D, and F when $1/NT$ approaches zero, μ_N tends to a positive number, so the pile is unstable. Also, the pile responses due to the different dynamic loads and load frequency ratios indicated in Figure 4.7 are shown in Figure 4.9 to 4.14.
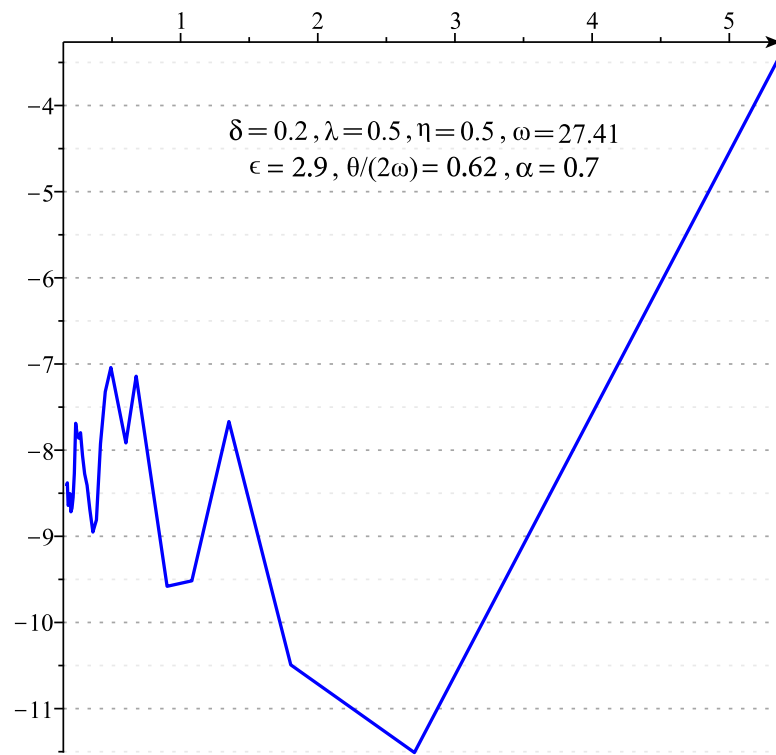
$\delta = 0.2\,,\lambda = 0.5\,,\eta = 0.5\,,\omega = 27.41$
$\epsilon = 2.9\,,\theta/(2\omega) = 0.62\,,\alpha = 0.7$

(a) Point A - Stable

$\delta = 0.2\,,\lambda = 0.5\,,\eta = 0.5\,,\omega = 27.41$
$\epsilon = 2.9\,,\theta/(2\omega) = 0.59\,,\alpha = 0.7$

(b) Point B - Unstable

$$\delta = 0.2\,,\lambda = 0.5\,,\eta = 0.5\,,\omega = 27.41$$
$$\epsilon = 1.7\,,\theta/(2\omega) = 0.35\,,\alpha = 0.7$$

(c) Point C - Stable

$$\delta = 0.2\,,\lambda = 0.5\,,\eta = 0.5\,,\omega = 27.41$$
$$\epsilon = 1.7\,,\theta/(2\omega) = 0.32\,,\alpha = 0.7$$

(d) Point D - Unstable

$$\delta = 0.2, \lambda = 0.5, \eta = 0.5, \omega = 27.41$$
$$\epsilon = 1.15, \theta/(2\omega) = 0.25, \alpha = 0.7$$

(e) Point E - Stable

$$\delta = 0.2, \lambda = 0.5, \eta = 0.5, \omega = 27.41$$
$$\epsilon = 1.15, \theta/(2\omega) = 0.22, \alpha = 0.7$$
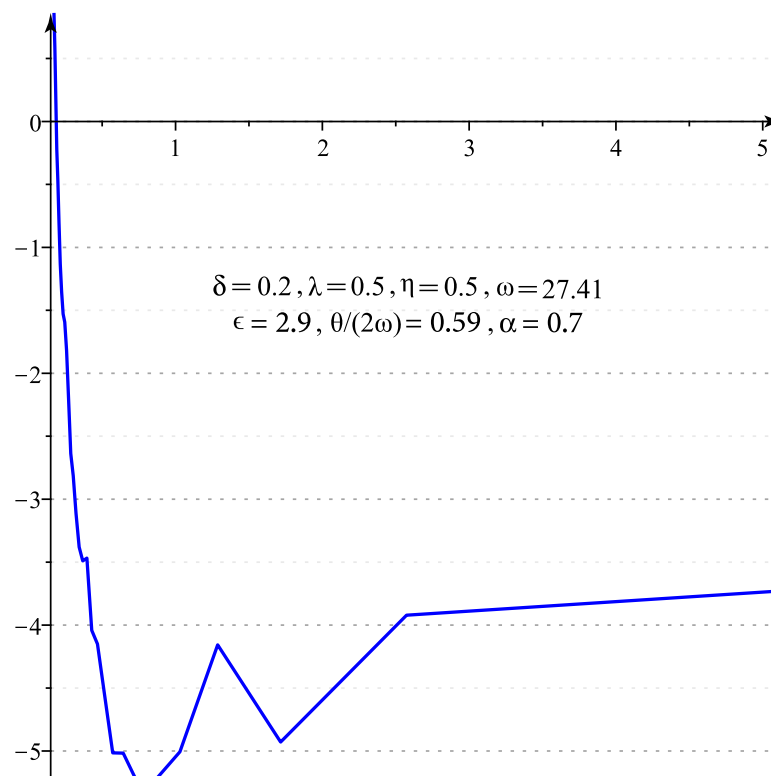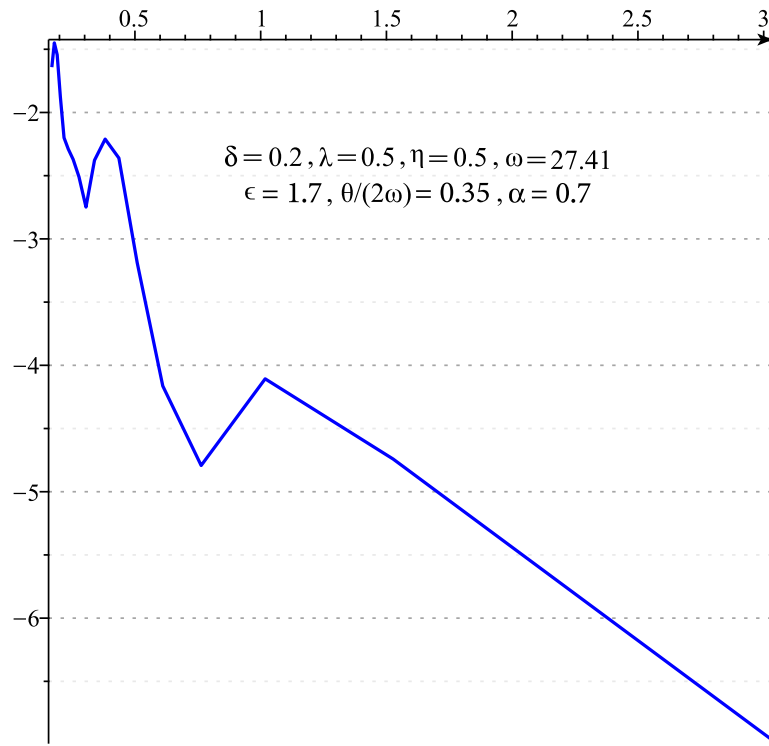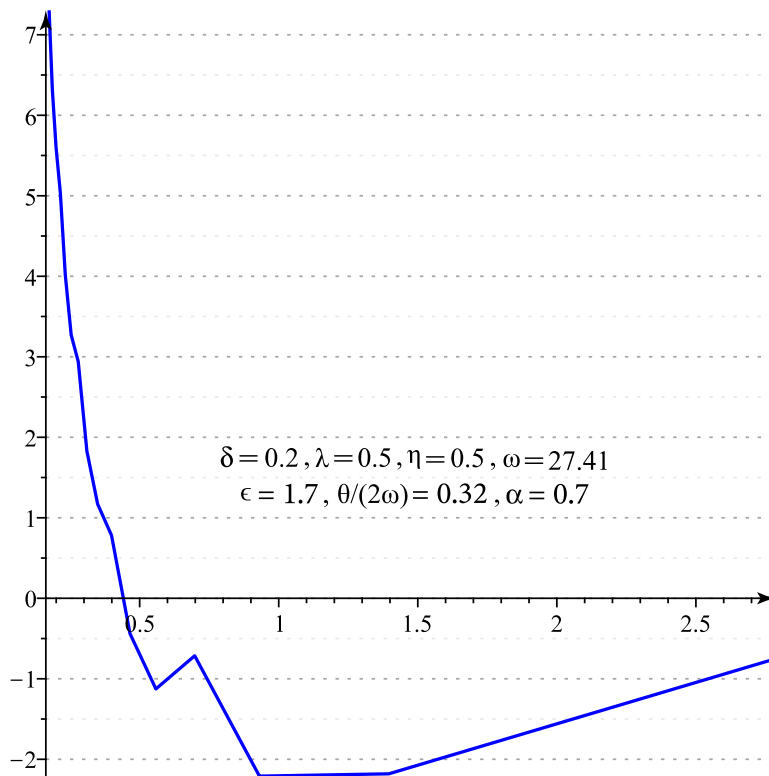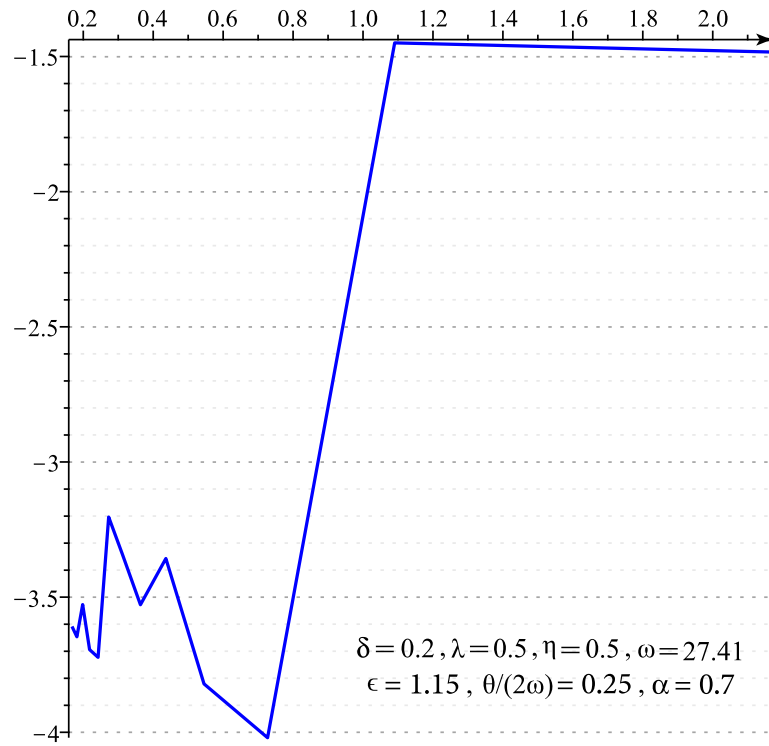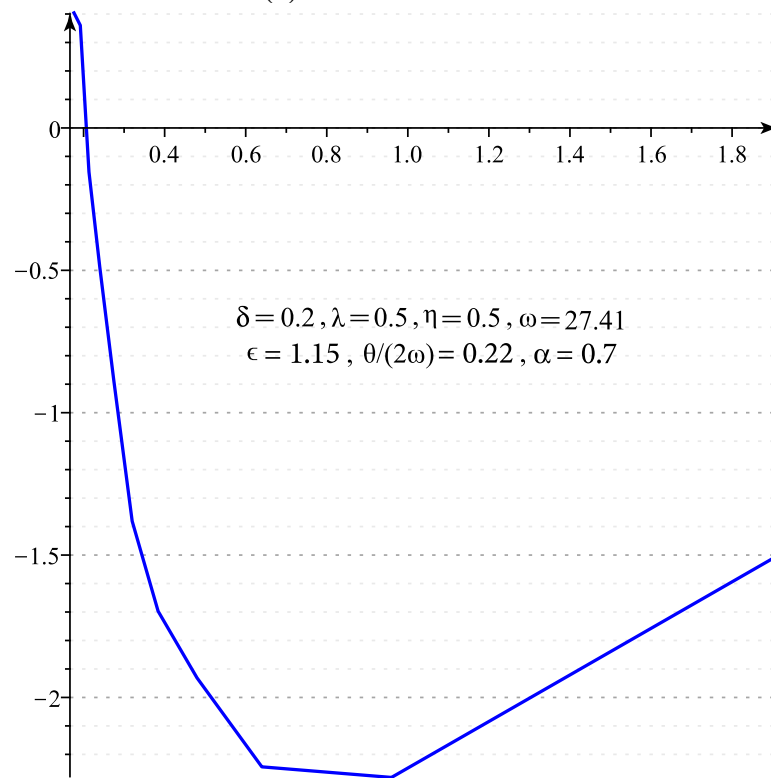
(f) Point F - Unstable

Figure 4.8 Lyapunov exponents stability diagrams

$\delta = 0.2$, $\lambda = 0.5$, $\eta = 0.5$, $\omega = 27.41$
$\epsilon = 2.9$, $\theta/(2\omega) = 0.62$, $\alpha = 0.7$

(a) Damping fractional order $\alpha = 1.0$

$\delta = 0.2$, $\lambda = 0.5$, $\eta = 0.5$, $\omega = 27.41$
$\epsilon = 2.9$, $\theta/(2\omega) = 0.62$, $\alpha = 1.0$
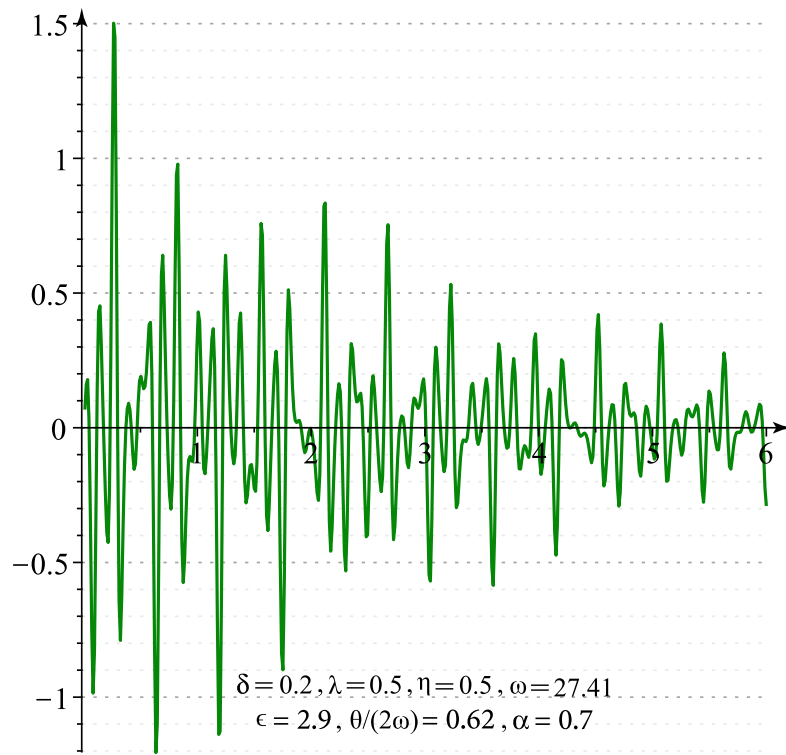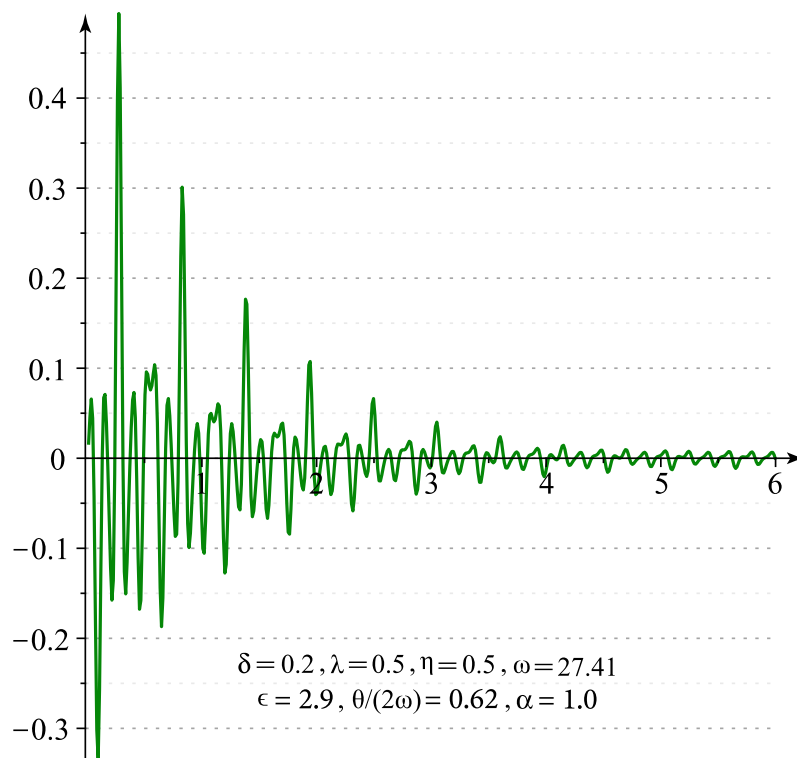
(b) Damping fractional order $\alpha = 1.0$

Figure 4.9 Vibration responses of the pile at point A

$\delta = 0.2$, $\lambda = 0.5$, $\eta = 0.5$, $\omega = 27.41$
$\epsilon = 2.9$, $\theta/(2\omega) = 0.59$, $\alpha = 0.7$

(a) Damping fractional order $\alpha = 0.7$

$\delta = 0.2$, $\lambda = 0.5$, $\eta = 0.5$, $\omega = 27.41$
$\epsilon = 2.9$, $\theta/(2\omega) = 0.59$, $\alpha = 1.0$
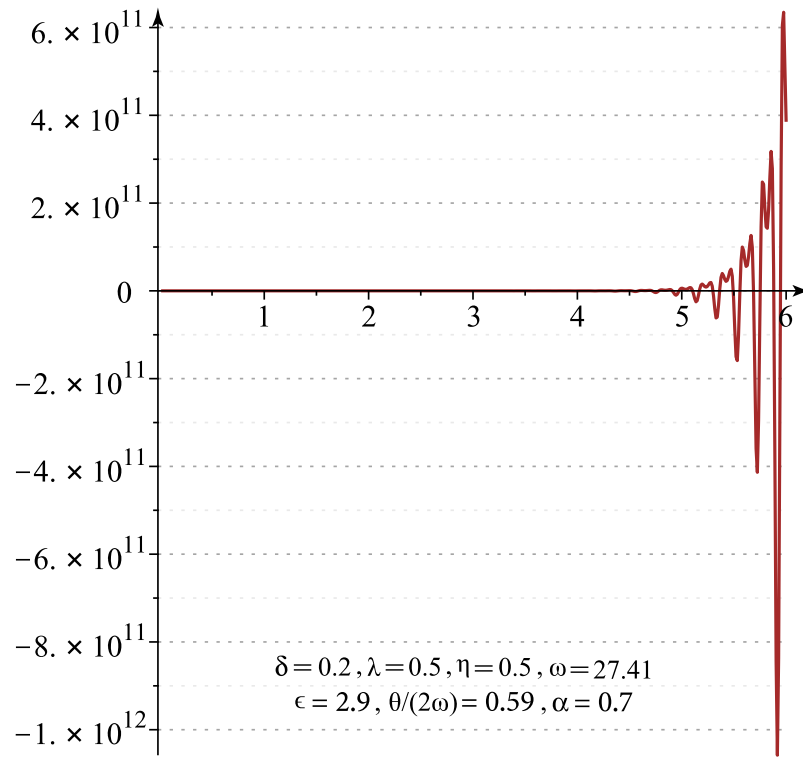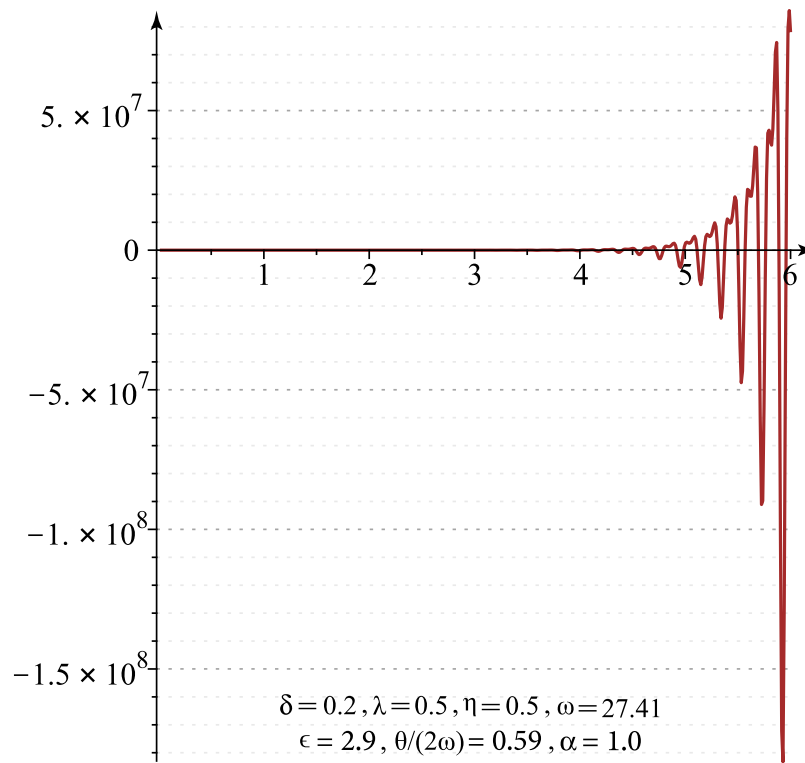
(b) Damping fractional order $\alpha = 1.0$

Figure 4.10 Vibration responses of the pile at point B

$\delta = 0.2$, $\lambda = 0.5$, $\eta = 0.5$, $\omega = 27.41$
$\epsilon = 1.7$, $\theta/(2\omega) = 0.35$, $\alpha = 0.7$

(a) Damping fractional order $\alpha = 0.7$

$\delta = 0.2$, $\lambda = 0.5$, $\eta = 0.5$, $\omega = 27.41$
$\epsilon = 1.7$, $\theta/(2\omega) = 0.35$, $\alpha = 1.0$
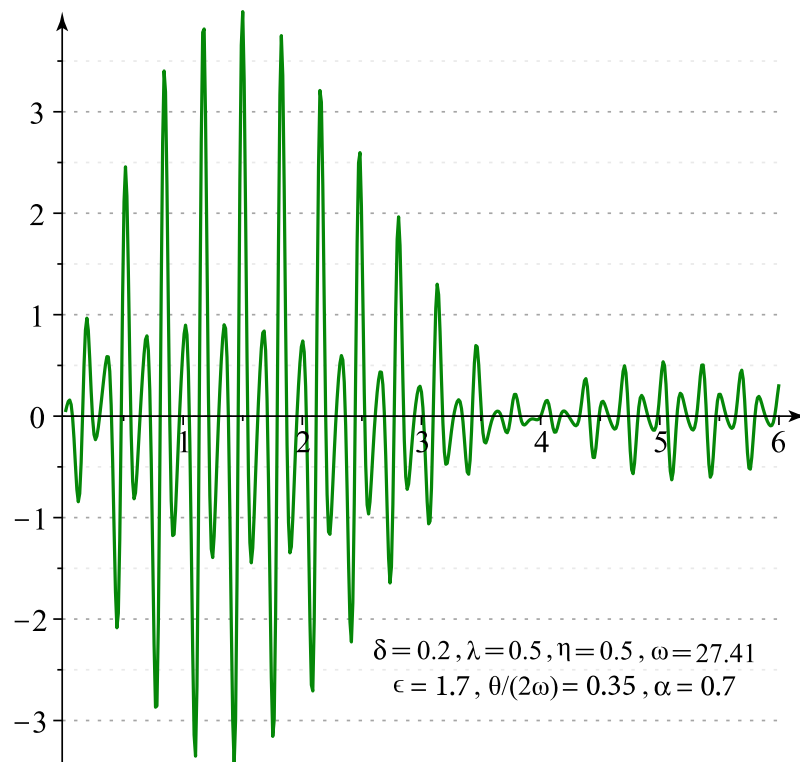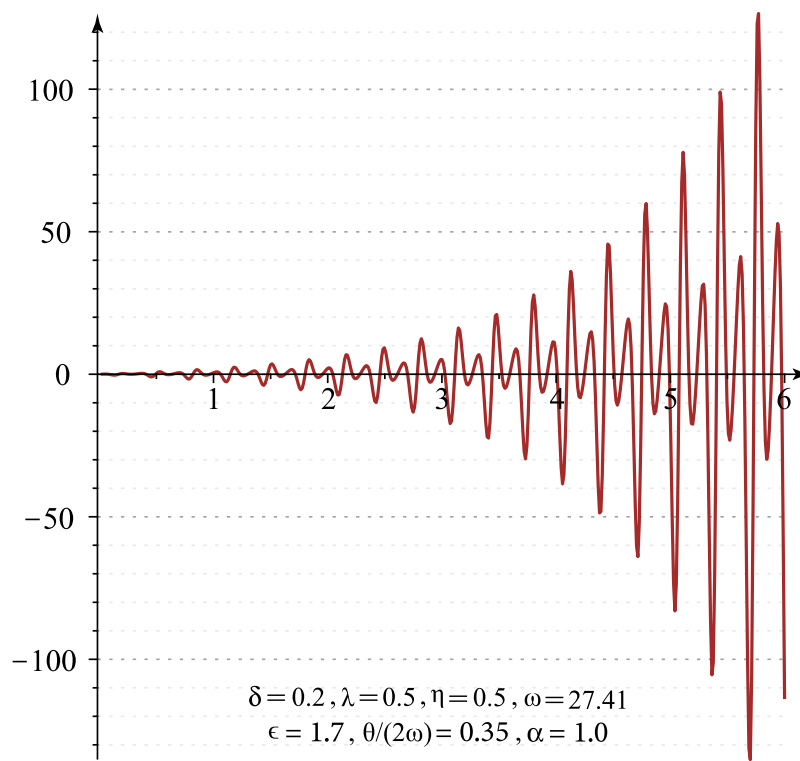
(b) Damping fractional order $\alpha = 1.0$

Figure 4.11 Vibration responses of the pile at point C

$\delta = 0.2 \, , \lambda = 0.5 \, , \eta = 0.5 \, , \omega = 27.41$
$\epsilon = 1.7 \, , \theta/(2\omega) = 0.32 \, , \alpha = 0.7$

(a) Damping fractional order $\alpha = 0.7$

$\delta = 0.2 \, , \lambda = 0.5 \, , \eta = 0.5 \, , \omega = 27.41$
$\epsilon = 1.7 \, , \theta/(2\omega) = 0.32 \, , \alpha = 1.0$
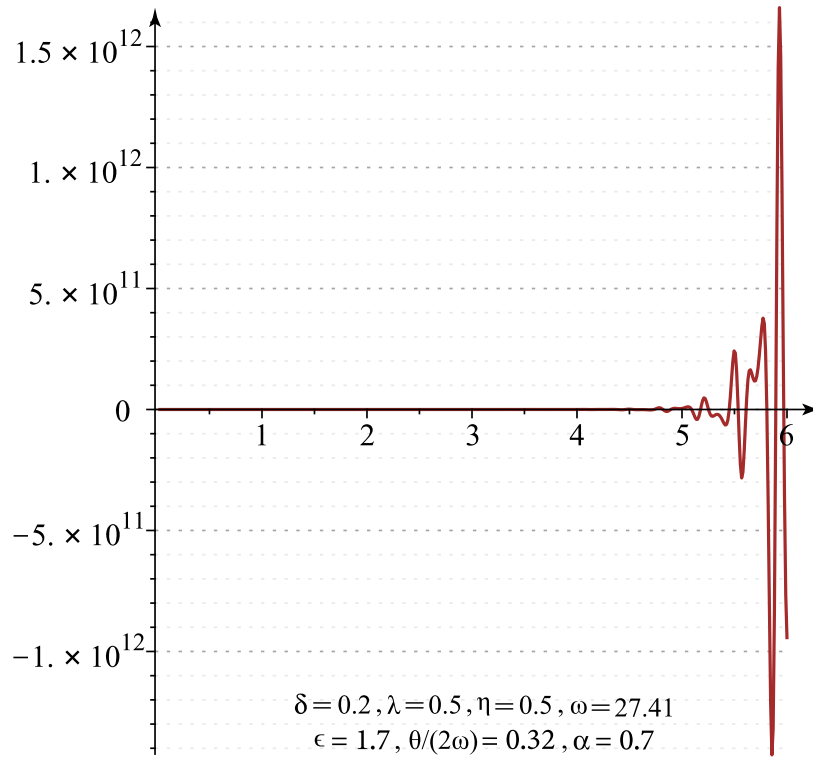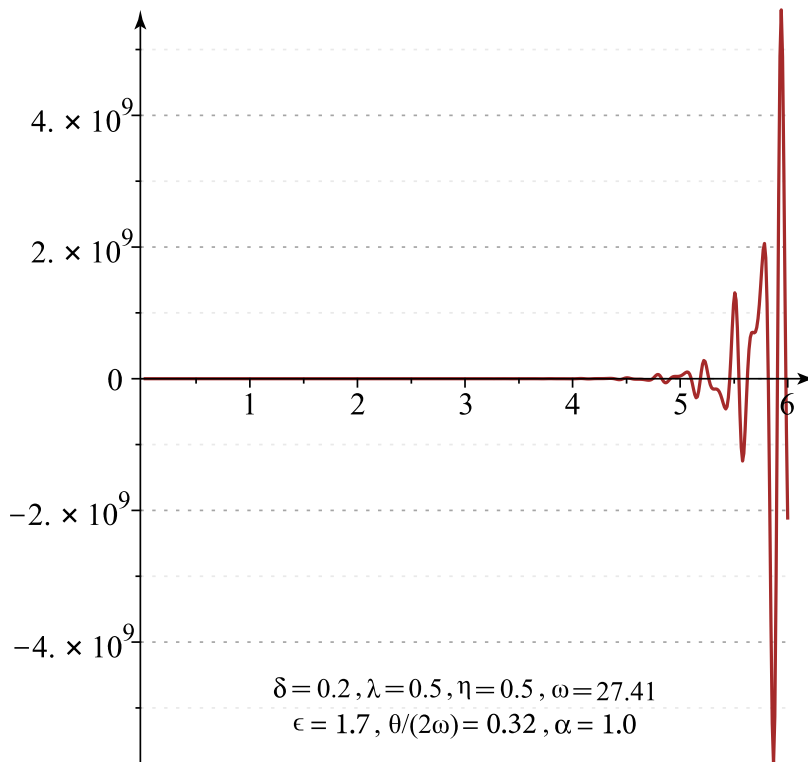
(b) Damping fractional order $\alpha = 1.0$

Figure 4.12 Vibration responses of the pile at point D

$\delta = 0.2$, $\lambda = 0.5$, $\eta = 0.5$, $\omega = 27.41$
$\epsilon = 1.15$, $\theta/(2\omega) = 0.25$, $\alpha = 0.7$

(a) Damping fractional order $\alpha = 0.7$

$\delta = 0.2$, $\lambda = 0.5$, $\eta = 0.5$, $\omega = 27.41$
$\epsilon = 1.15$, $\theta/(2\omega) = 0.25$, $\alpha = 1.0$
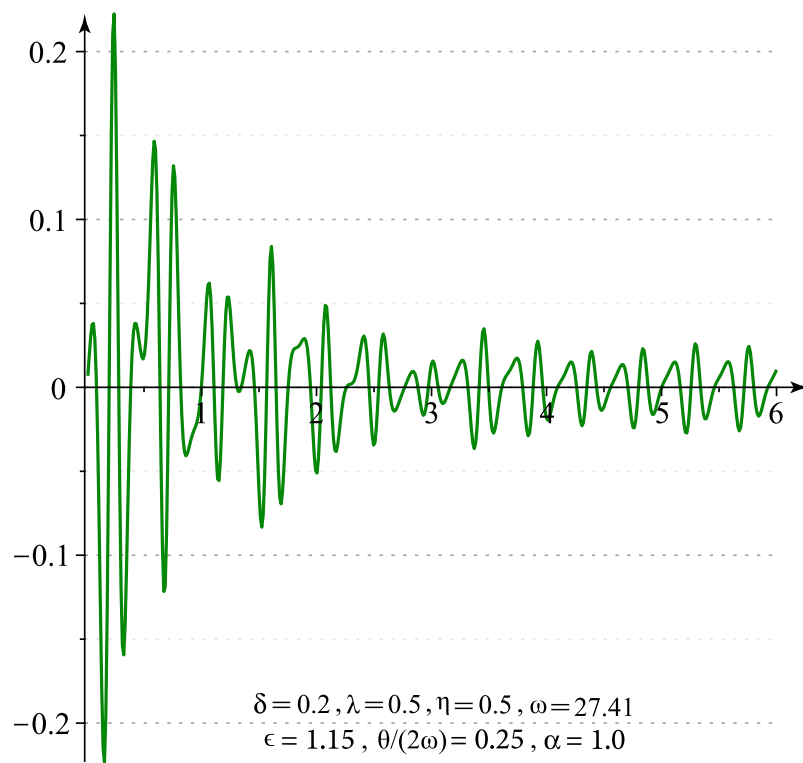
(b) Damping fractional order $\alpha = 1.0$

Figure 4.13 Vibration responses of the pile at point E

$\delta = 0.2$, $\lambda = 0.5$, $\eta = 0.5$, $\omega = 27.41$
$\epsilon = 1.15$, $\theta/(2\omega) = 0.22$, $\alpha = 0.7$

(a) Damping fractional order $\alpha = 0.7$

$\delta = 0.2$, $\lambda = 0.5$, $\eta = 0.5$, $\omega = 27.41$
$\epsilon = 1.15$, $\theta/(2\omega) = 0.22$, $\alpha = 1.0$

(b) Damping fractional order $\alpha = 1.0$
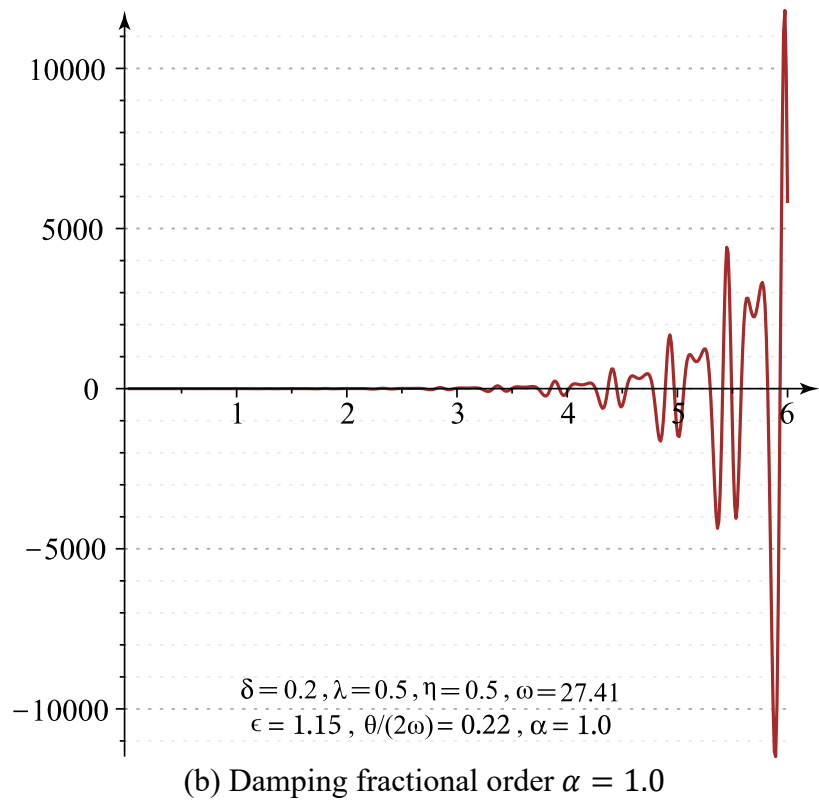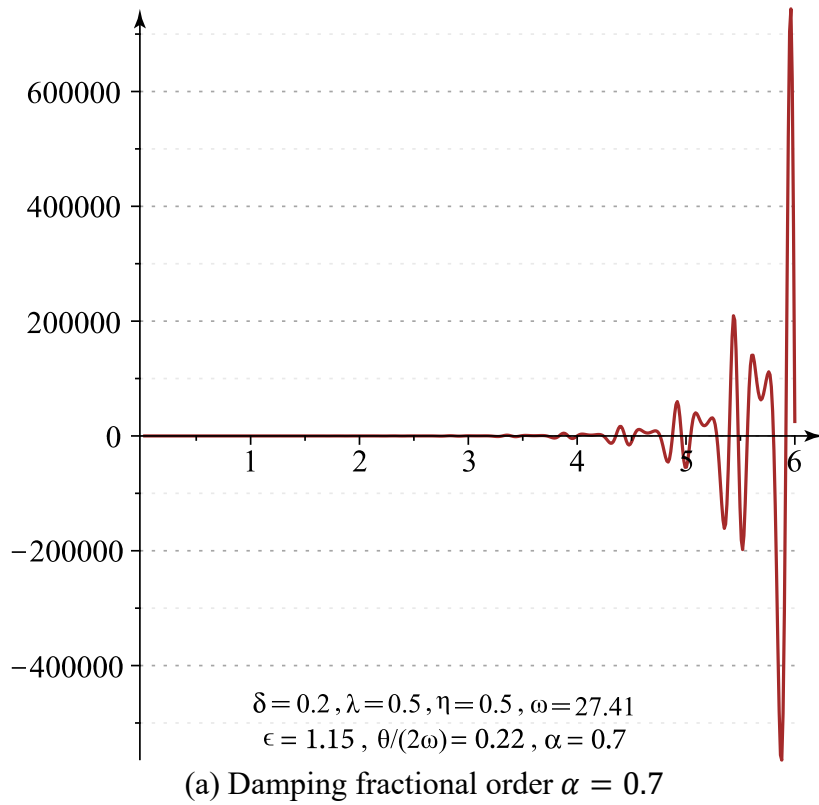
Figure 4.14 Vibration responses of the pile at point F

In the above figures, the response of each sample point is given by the fractional damping orders equal to 0.7 and 1.0 in diagrams (a) and (b), respectively, to better understand the effects of the parameter α on the pile vibration response. Figures 4.9 and 4.13, indicate that the responses for samples at points A and E are stable. However, a more significant fractional damping order helps the pile become stable more rapidly. Figures 4.10, 4.12, and 4.14 illustrate the unstable behavior of the pile for samples at points B, D, and F. Although, practically, no difference occurred to the pile response by increasing α. From a mathematical perspective, the responses shown in diagram (b) are more bounded. In other words, the pile becomes unstable slower. Finally, Figure 4.11 shows the response of the pile at point C, which is too close to the instability region boundary. In this case, by increasing α from 0.7 to 1.0, the behaviour of the pile completely changes from a stable to an unstable condition. It may occur because of the slight changes in the position of the instability boundary.

4.3. Effects of various parameters on pile stability

In this section, we will investigate several parameters' effects on the stability behaviour of the pile during an earthquake as a dynamic load. These parameters include the elastic (η) and damping (δ) parameters of soil, as well as the static component load ratio (λ).

4.3.1.   Elastic parameters of the surrounding soil effect

The effects of soil stiffness on the instability regions are illustrated in Figure 4.15.

(a) $\eta = 0$

(b) $\eta = 0.5$

$$\delta = 0.2$$
$$\omega = 33.57$$
$$\lambda = 0.5$$
$$\alpha = 0.7$$

(c) $\eta = 1$

$$\delta = 0.2$$
$$\omega = 43.34$$
$$\lambda = 0.5$$
$$\alpha = 0.7$$

(d) $\eta = 2$

(e) $\eta = 3$

(f) $\eta = 4$
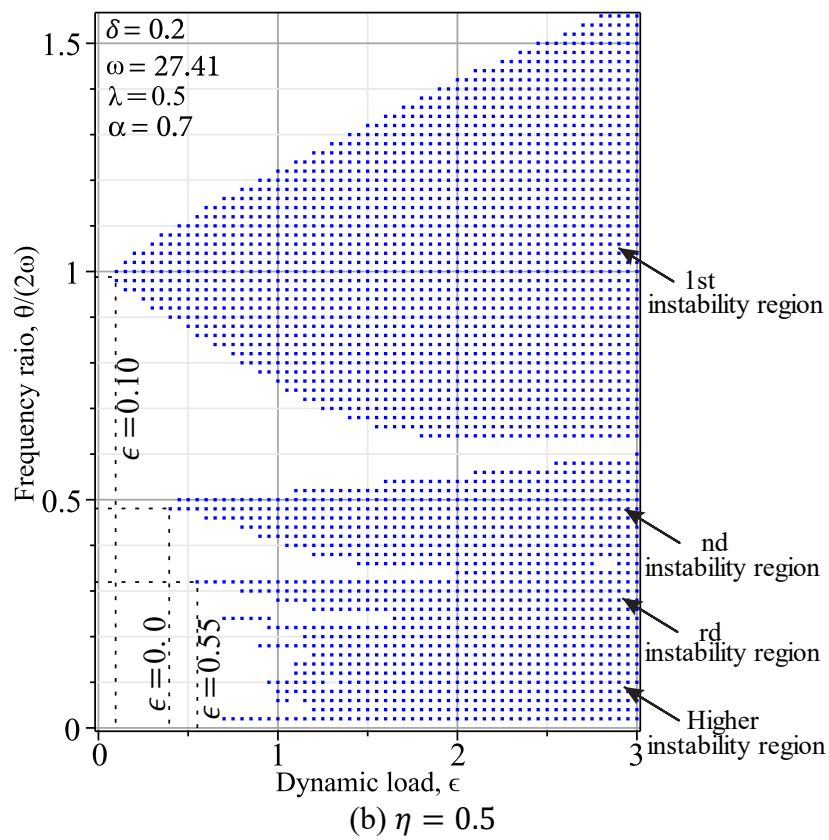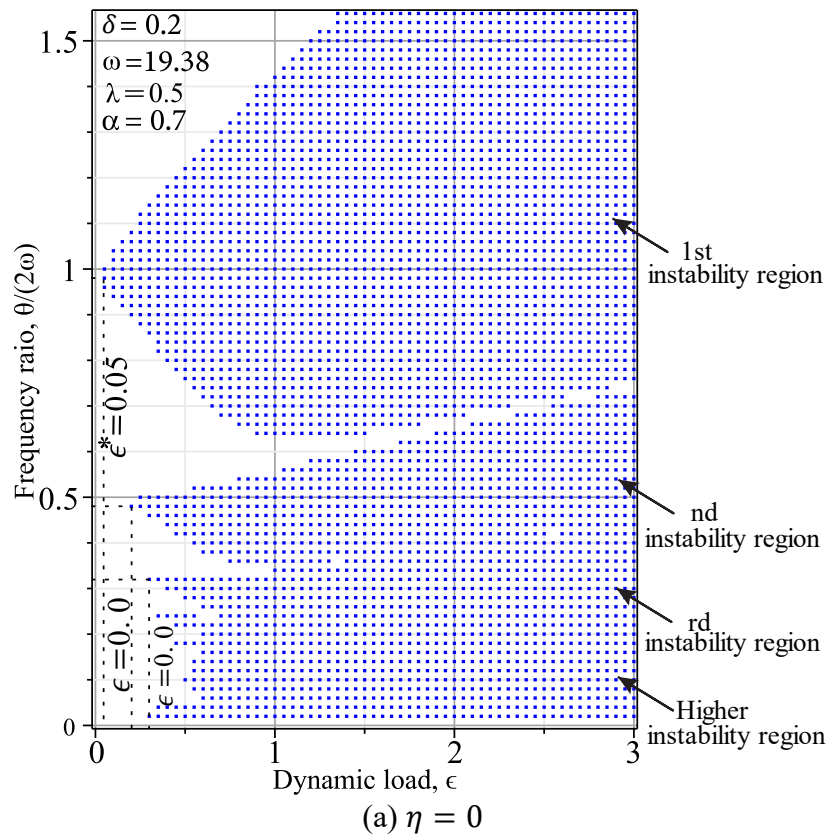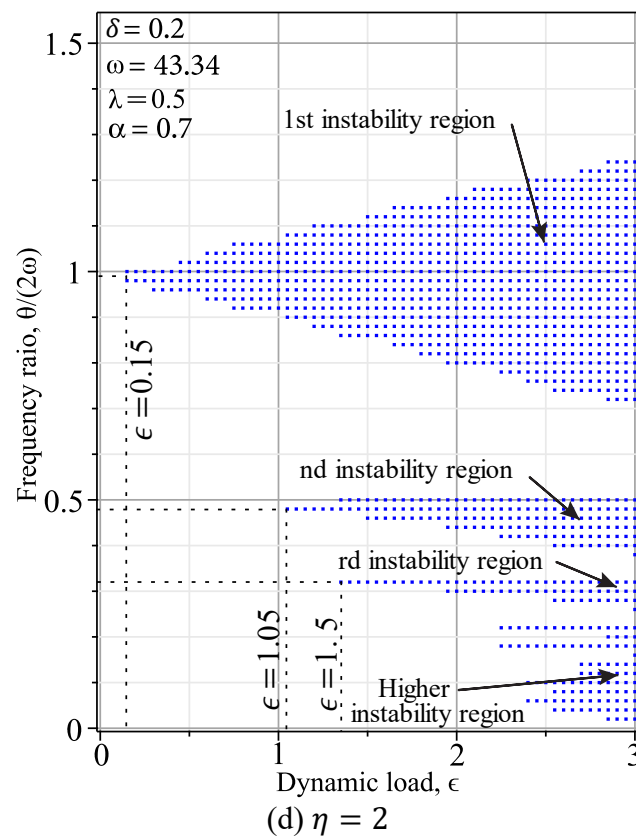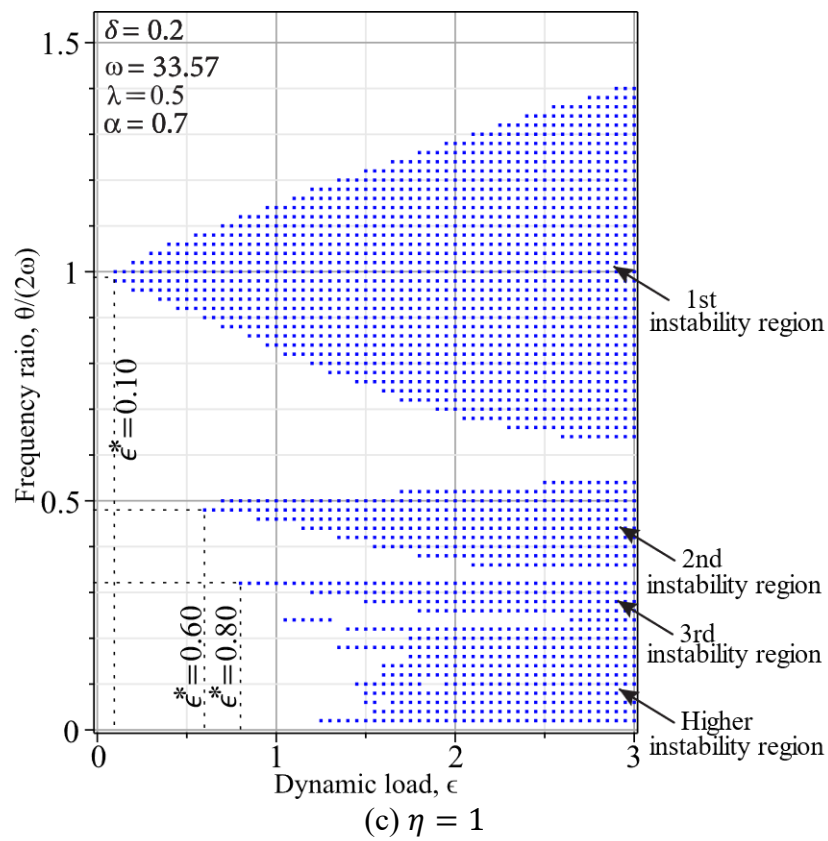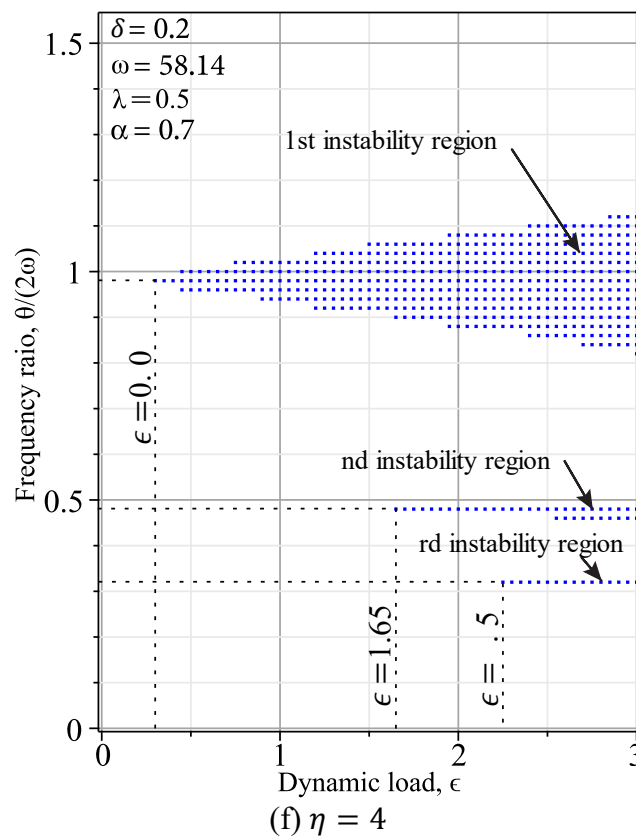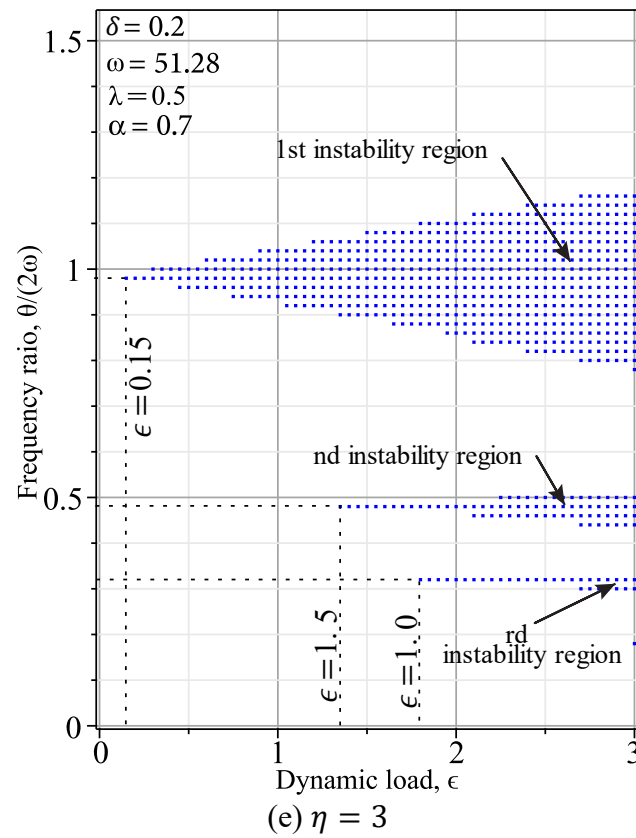
Figure 4.15 Effect of the elastic parameter of surrounding soil (Soil stiffness)

As explained before, the Winkler mechanical model with the fractional damping order is used to model the effect of the pile surrounding soil in the stability calculation. According to Winkler's model, k_s represents the soil stiffness, then based on section 4.2, $\eta = 0.001321k_s$. A critical dynamic load is the minimum value of the dynamic component load for each instability region (ϵ^*), and the corresponding excitation frequency of this point is called critical excitation frequency (θ^*, Hz). Figure 4.15 shows that the critical excitation load and critical dynamic load of the same order of instability region increase with the increasing soil stiffness. Also, the areas of instability shrink by growing the stiffness until higher-order instability regions disappear. The change process of the critical dynamic load and the critical excitation frequency, ϵ^* and θ^*, are indicated in Figure 4.16.

This shows the sensitivity of ϵ^* and θ^* to soil stiffness. By increasing η from 0 to 4, ϵ^* doesn't change much in the first instability region; however, there is a significant growth of ϵ^* in the third instability region. On the other hand, θ^* in the third instability region has little growth in comparison to the first instability region, while the surrounding soil stiffness is increased.

(a)
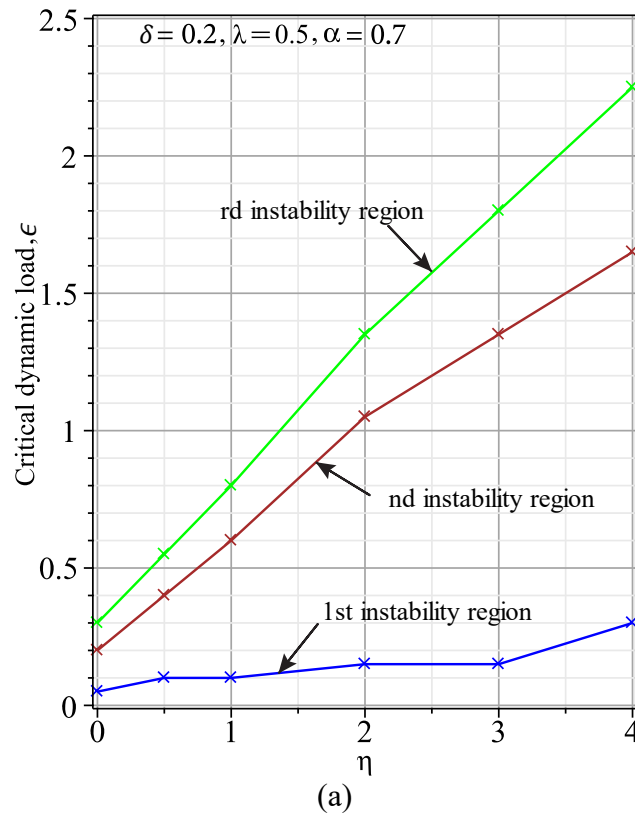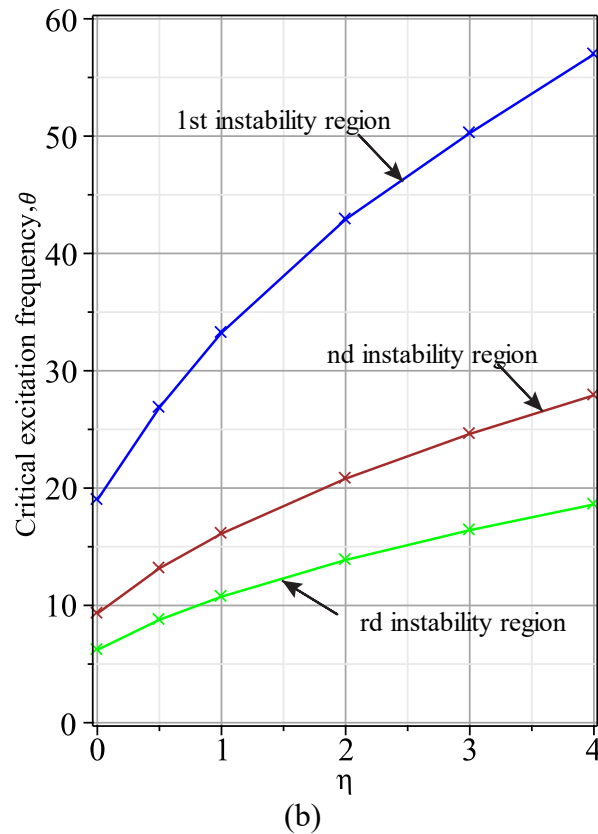
Figure 4.16 Critical dynamic load (a), Critical excitation frequency (b)
changes due to the soil stiffness

4.3.2.   Damping parameter of the surrounding soil effect

Figure 4.17 illustrates that parametric resonances are still possible, even in the presence of damping. When the soil damping parameter is increased, instability's excitation frequency range gradually shrinks until it disappears. Thus, larger soil damping needs a more significant dynamic component load to produce instability. A change in foundation damping from 0.1 to 0.4 increases the critical dynamic component load from 0.1 to 0.3 for the first instability region, from 0.4 to 0.55 for the second instability region, and from 0.6 to 0.95 for the third instability region. Moreover, instability regions shrink noticeably in size.

(a) $\delta = 0.1$

(b) $\delta = 0.2$

(c) $\delta = 0.3$


(d) $\delta = 0.4$
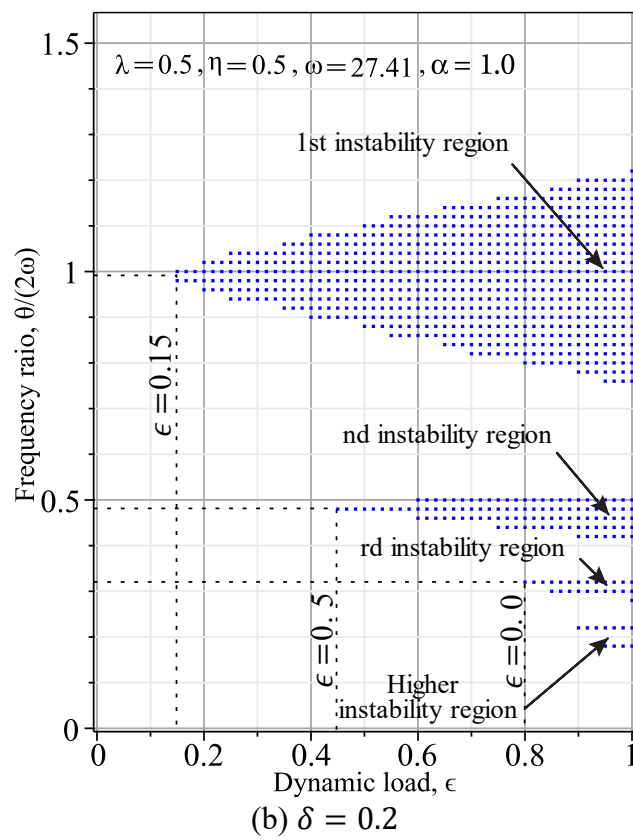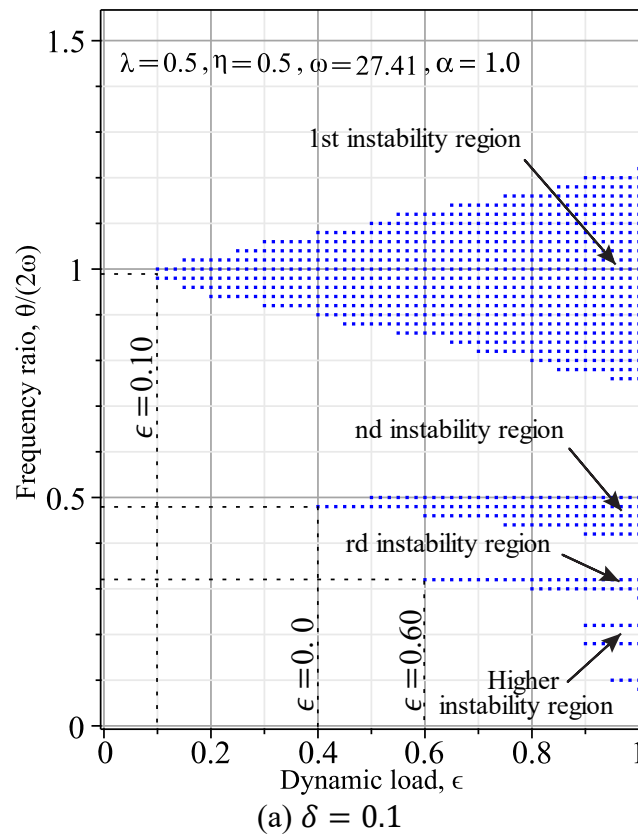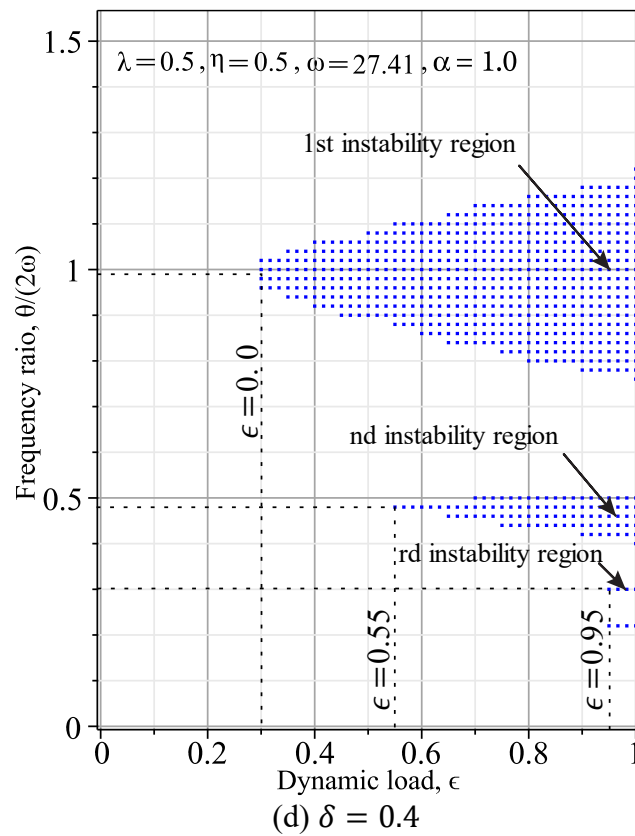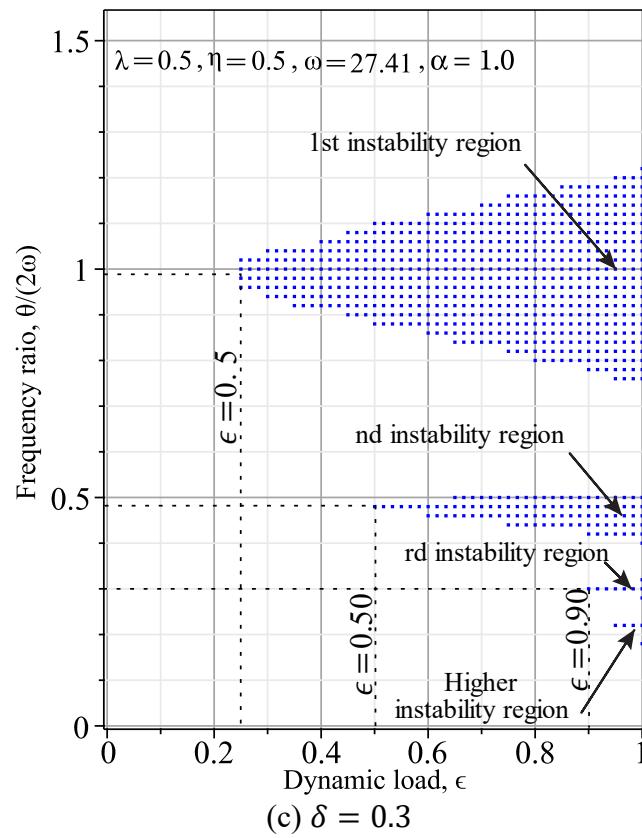
Figure 4.17 Effect of damping parameter of surrounding soil

4.3.3.   Static axial load effect

It is assumed that the dynamic load, which makes the pile unstable, consists of two parameters: the static component and the dynamic component. The static component may come from a superstructure, and the dynamic component may occur due to an earthquake.

Figure 4.18 shows that by increasing the static load parameter, λ, from 0.2 to 0.6, the critical frequency of parametric resonance ($2\omega_W$) is decreased from 31.25 Hz in Figure 4.18 (a) to 26 Hz in Figure 4.18 (e). Also, critical dynamic load parameters are reduced for each instability region and are more sensitive in higher order regions. Higher order regions become visible by increasing parameter λ in the specified range of the dynamic load. Moreover, increasing axial static load on the pile structure may result in a wider range of frequency ratio that causes instability during the dynamic axial loading. In 2022, Deng studied the dynamic stability of beams under a parametric load and obtained similar results. He also generated diagrams which demonstrate instability regions based on frequency ratio and static load parameters for the specified dynamic load parameters [43].
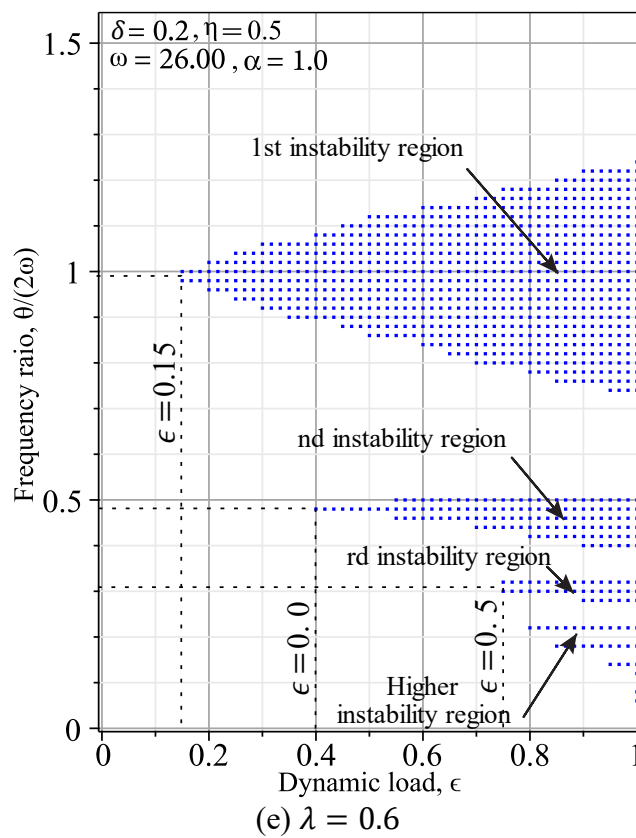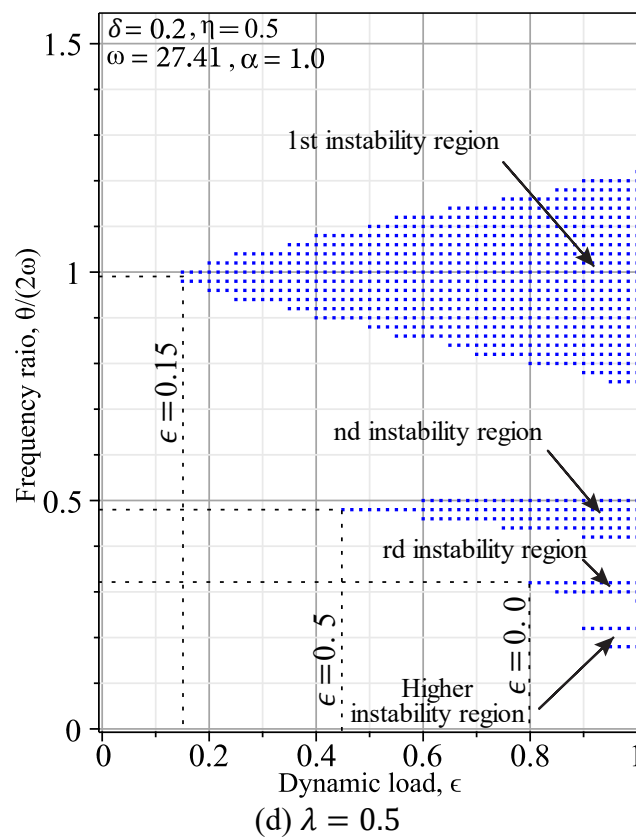

(a) $\lambda = 0.2$

(b) $\lambda = 0.3$

(c) $\lambda = 0.4$

(d) $\lambda = 0.5$

(e) $\lambda = 0.6$
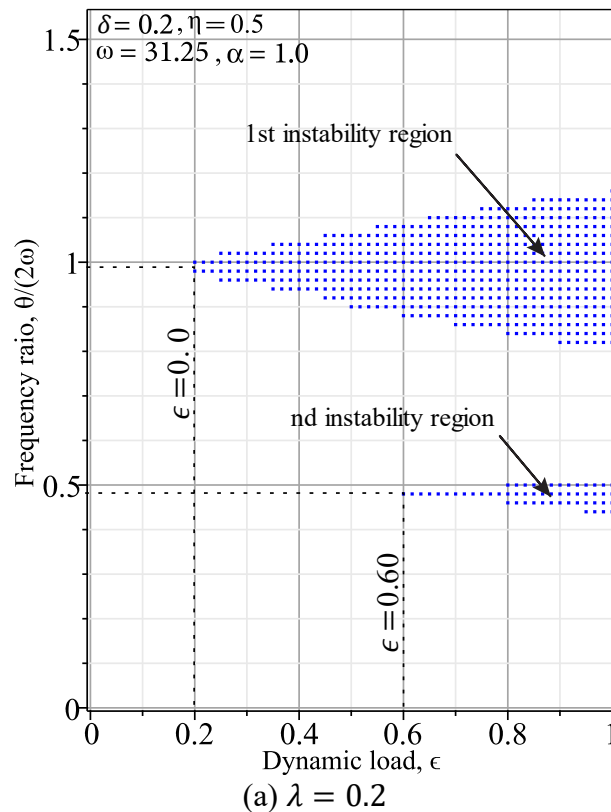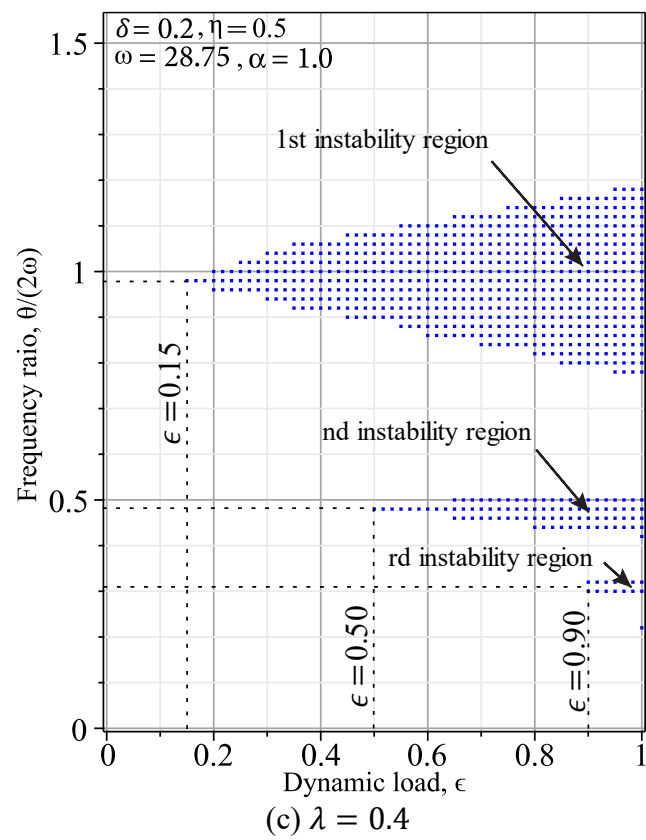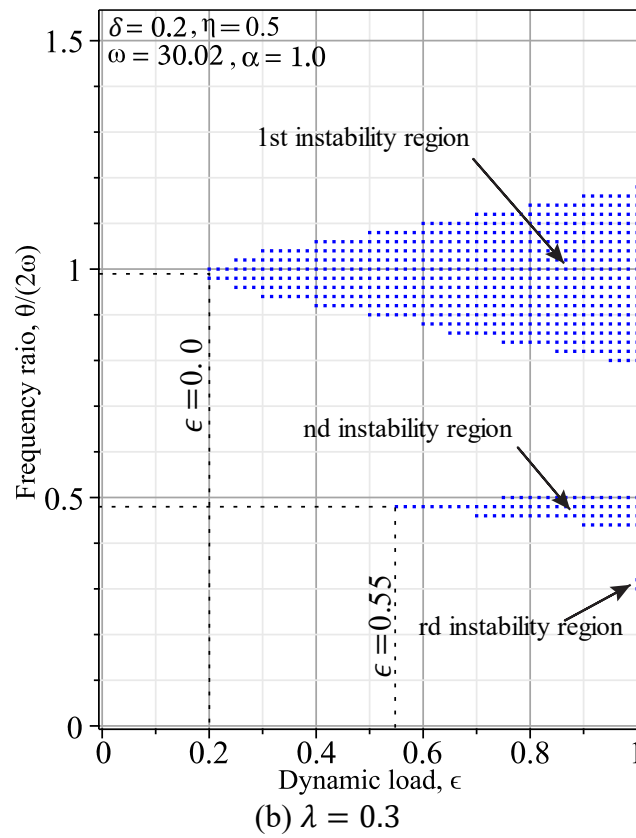
Figure 4.18 Effect of the static load parameter

4.4.   Stability of piles based on a real earthquake

Thus far, the stability of piles under a dynamic axial load has been studied. Consider that the axial load consists of two parts: the static component and the dynamic component, $P(t) = P_s + P_d \cos \theta t$. Also, the effects of various important parameters on instability regions and the critical dynamic load and excitation frequency were investigated to better understand pile behavior. In this section, the stability conditions of a pile under a real earthquake wave are estimated.

Vital ground acceleration records can be gathered from various online sources. In this study, excitation data from the Treasure Island earthquake of September 3, 2000, are used. As illustrated in Figure 4.19, this ground motion record has horizontal and vertical components. Each record is available every 0.01 seconds, which equals a minute long record.
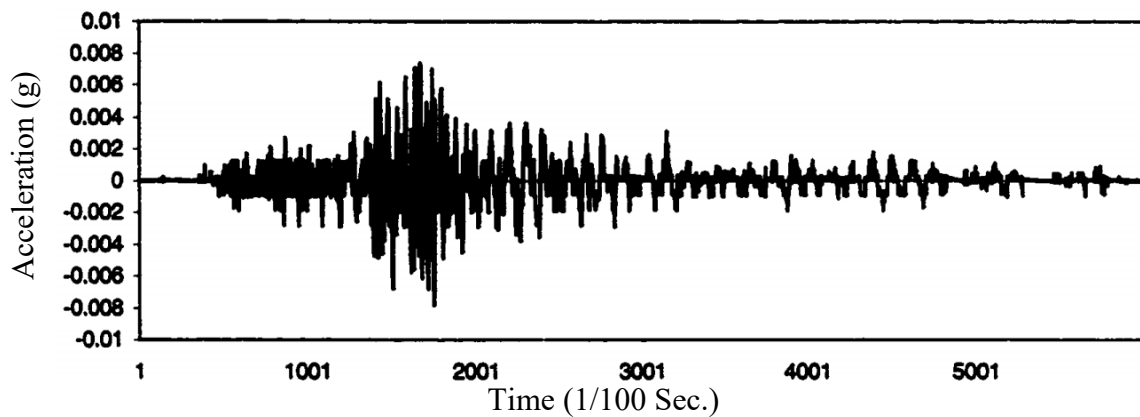
(a) Horizontal component
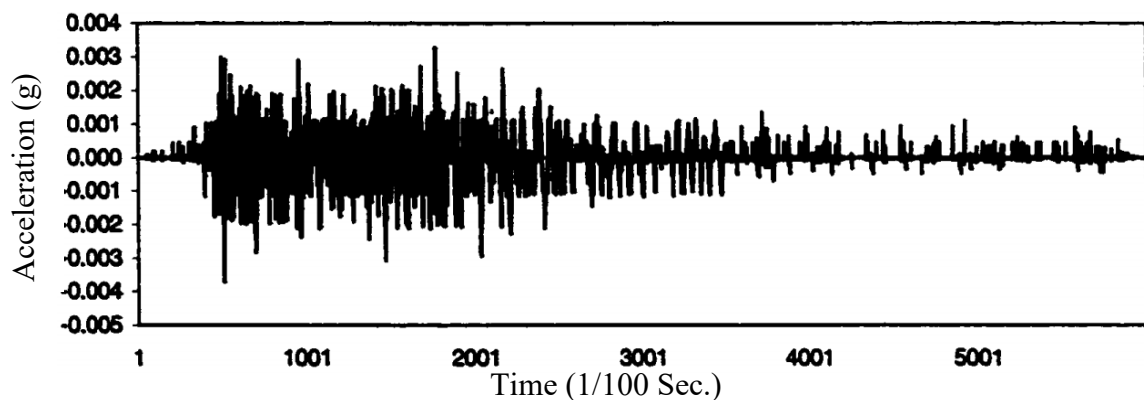
(b) Vertical component

Figure 4.19 Treasure Island earthquake components [44]

We consider the effect of the vertical acceleration of seismic excitation in order to investigate the dynamic stability of a pile. A selection of two short vertical acceleration records of the Treasure Island earthquake is shown in Figure 4.20. The excitation frequency and acceleration of the excitation change over time. Figure 4.20 (a) shows the maximum vertical acceleration $a_v = 0.003$g and the cosine function period $T = 0.13\ s$. Considering the pile, explained in section 4.2, where $\lambda = 0.5, \eta = 0.5, \delta = 0.2$, and $\alpha = 0.7$,

$$P_s = \lambda P_{cr} = 0.5 P_{cr} \xrightarrow{P_s = mg} m = \frac{0.5 P_{cr}}{g}\ , \tag{4.18}$$

where m and g are the total mass carried by the pile and gravity acceleration, respectively and

$$P_d = m a_v = \frac{0.5 P_{cr}}{g} a_v. \tag{4.19}$$

For illustration purposes, because the real vertical acceleration for the specified earthquake is too small, consider two cases, $a_v = 0.5$g and $a_v = $ g, , then, $P_d = 0.25 P_{cr}$ and $P_d = 0.5 P_{cr}$ in the first and second cases, respectively. As a result, based on Eq. (2.23), the dynamic load parameters are

$$\epsilon = \frac{P_d}{P_{cr}} = \frac{0.25 P_{cr}}{P_{cr}} = 0.25 \quad \text{(Case 1)}, \quad \epsilon = \frac{P_d}{P_{cr}} = \frac{0.5 P_{cr}}{P_{cr}} = 0.5 \quad \text{(Case 2)} \tag{4.20}$$
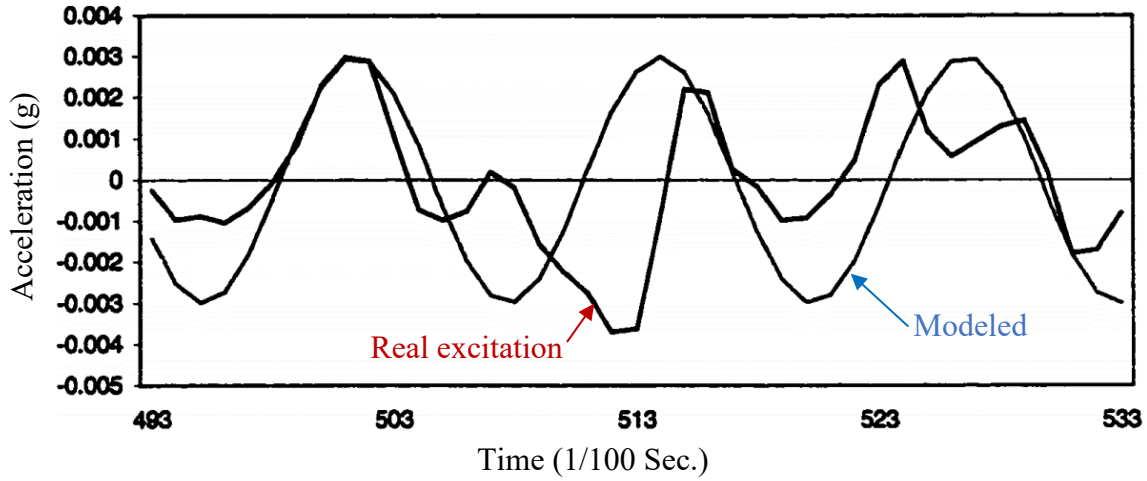
(a) From 4.9 to 5.3 Sec.
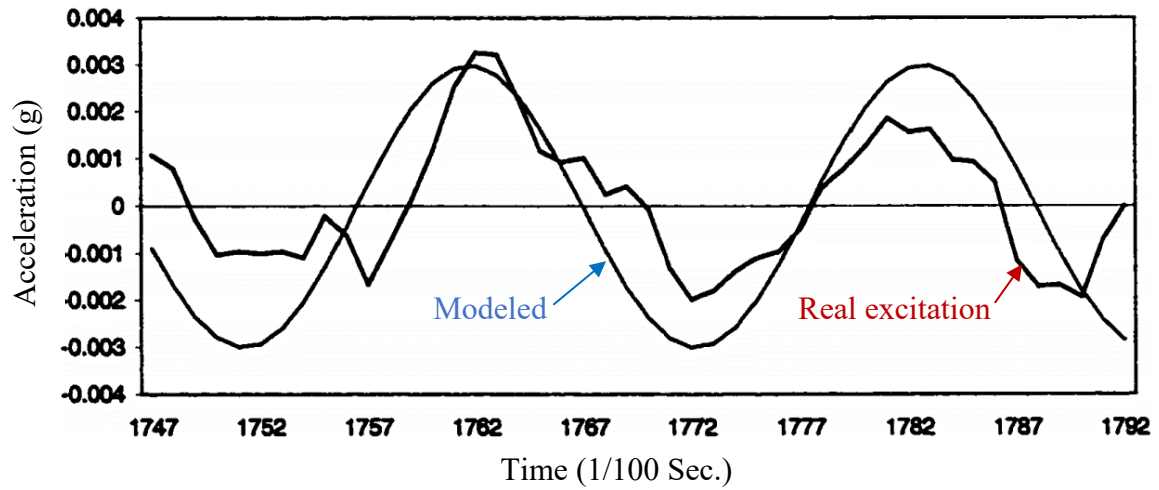
(b) From 17.5 to 17.9 Sec.

Figure 4.20 Actual Vertical Acceleration vs. Assumed Curve
for Treasure Island Earthquake [44]

Also, the earthquake load excitation frequency is

$$\theta = \frac{2\pi}{T} = \frac{2\pi}{0.13} \cong 48.3 \, \frac{rad}{s}, \tag{4.21}$$

and based on Eq. (2.28), $\omega = 27.4 \, \frac{rad}{s}$. As a result, the frequency ratio is

$$r = \frac{\theta}{2\omega} = \frac{48.3}{2 \times 27.4} \cong 0.9 \, . \tag{4.22}$$

Considering the results in Eqs. (4.20) and (4.22), the stability condition of the pile in cases 1 and 2 of the earthquake vertical excitation can be found in Figure 4.21.
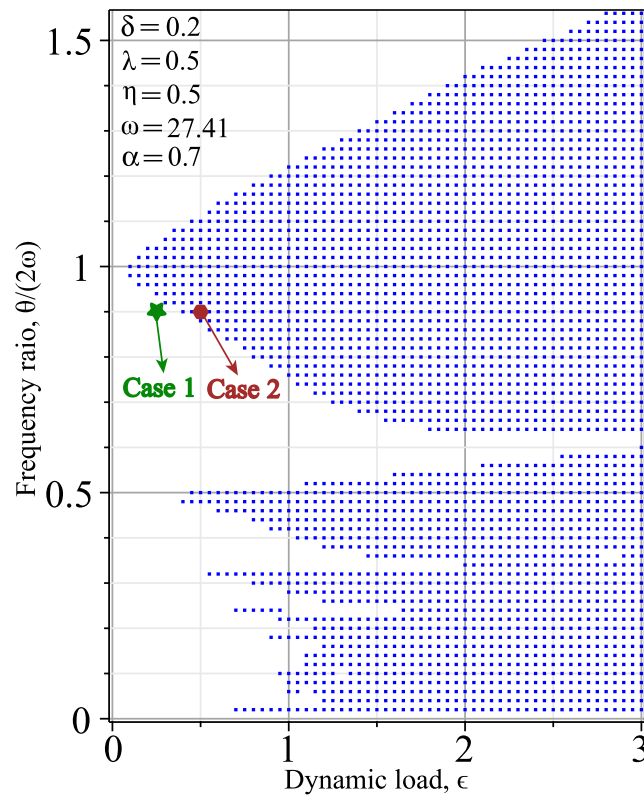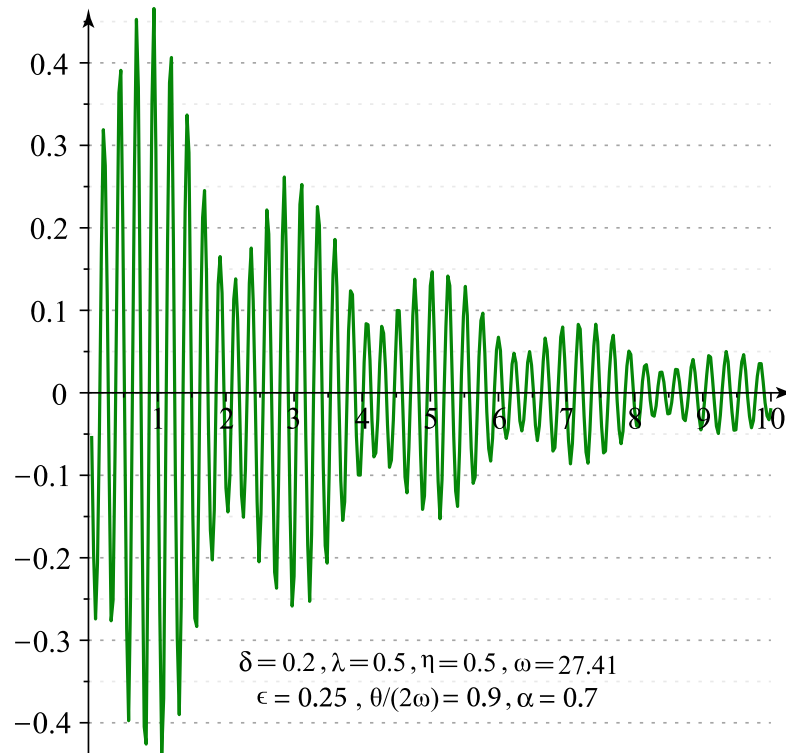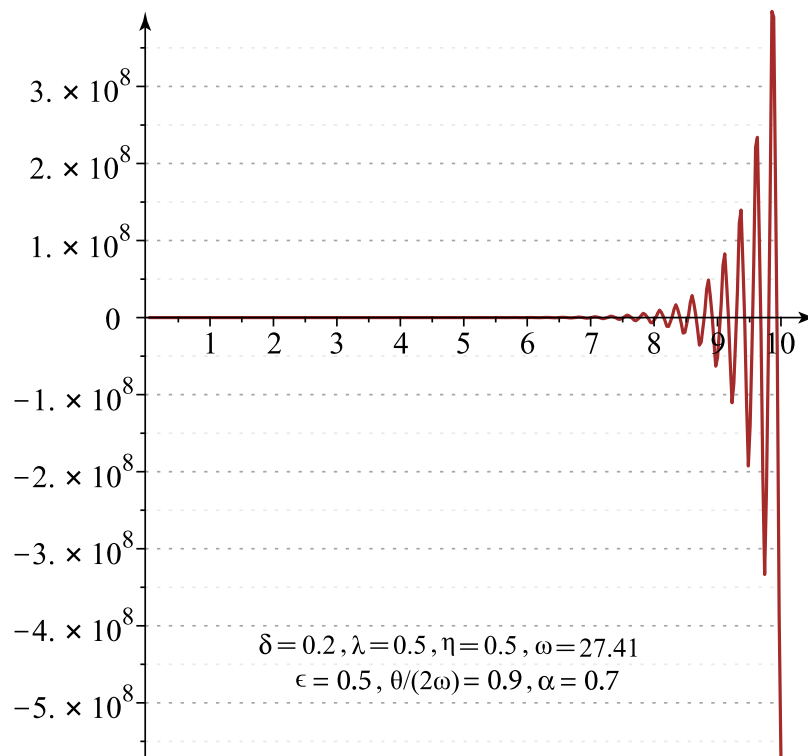
Figure 4.21 Pile stability condition during the earthquake

Figure 4.21 indicates that the pile condition during the earthquake in case 1 ($a_v = 0.5\mathrm{g}$) is stable but in case 2 ($a_v = \mathrm{g}$) is unstable. The vibration responses of the pile in these cases are also illustrated in Figure 4.22.

$$\delta = 0.2 , \lambda = 0.5 , \eta = 0.5 , \omega = 27.41$$
$$\epsilon = 0.25 , \theta/(2\omega) = 0.9 , \alpha = 0.7$$

(a) Case 1

$$\delta = 0.2 , \lambda = 0.5 , \eta = 0.5 , \omega = 27.41$$
$$\epsilon = 0.5 , \theta/(2\omega) = 0.9 , \alpha = 0.7$$

(b) Case 2

Figure 4.22 Pile vibration responses during the earthquakes

4.5. **Summary**

In this chapter, assuming a specific geometry and material for the pile foundation and soil, instability diagrams are investigated under different conditions using two methods. The first method is the approximate method based on the Bolotin solution followed by the numerical method based on block-pulse functions.

It is found that increasing the fractional order of soil damping impacts the top of the instability region diagrams significantly and makes a slight change in other parts of the diagrams. Also, higher instability regions show more sensitivity to fractional order changes of soil damping.

In addition, instability boundaries from the approximate method are validated using the numerical method's results. For the first instability region, second and third-order approximations result in accurate boundaries, while third-order approximation should be used for the second instability region. Also, higher-order approximations are required to get precise results for the higher instability regions.

Moreover, the effects of different parameters like soil stiffness, damping, and static load are illustrated in the instability region. Increasing elastic and damping parameters result in the shrinkage of instability regions and some regions may disappear in a specified dynamic load range. On the other hand, increasing static load parameters applied to piles leads to the expansion of instability regions.

Finally, considering an actual earthquake wave, we explain how the stability condition of a pile should be estimated.

C H A P T E R 5

Conclusions and Future Research

5.1. Conclusions

The goal of this research is to study the dynamic stability behaviour and vibration response of piles surrounded by soil under the action of dynamic axial loads, both theoretically and numerically. The soil media is modeled using the Winkler mechanical model with fractional damping. For this aim, after explaining the literature related to piles' buckling instability and fractional calculus, the below steps are investigated.

1- The equation of motion is derived based on the equilibrium equations of a differential part of the pile length. A subgrade reaction is considered based on the fractional Winkler model. The equation is found in the form of a partial differential equation (PDE).

2- The Bolotin method is explained to understand how the instability regions should be determined. As a first step, this method converts PDE into an ordinary differential equation (ODE) called the Mathieu equation (based on the ordinary Winkler model). Next, the Mathieu equation is solved to find the infinite determinants (ID), which are used to find the instability regions.

3- Considering the Winkler model with fractional damping results in the fractional Mathieu equation. Using the Caputo definition, an approximate method is introduced to solve the fractional Mathieu equation. The method results in the fractional Mathieu ID which can be used to determine the instability regions.

4- The research also includes a numerical method based on the block-pulse function to investigate the stability condition of the fractional Mathieu differential equation. The numerical approach is essentially a solution to the unknown result by using the block-pulse functions and writing other derivative terms employing the block-pulse functions operational matrix of fractional integration. The differential equation is changed into a system of algebraic equations. The result can be found by solving the system, and finally, the stability condition of the result is indicated.

5- After developing the numerical model, considering fractional damping, the accurate stability diagrams are used to calibrate the approximate instability boundaries of fractional Mathieu IDs. In addition, the effects of various parameters are investigated on instability regions' boundary.

6- Finally, it is explained how we should find the instability behaviour of the piles under an actual earthquake wave using an example.

Generally, a fractional Mathieu ID with more orders delineates the boundary more accurately. The first-order fractional Mathieu ID boundary is inaccurate for the first instability region, considering the fractional order equaling 0.7, whereas the second and third-order fractional Mathieu ID boundaries are accurate. There is no accuracy in the second nor third order fractional Mathieu ID boundaries in the third instability region, but there is adequate accuracy in the fourth-order fractional Mathieu ID boundary. However, the fourth order fractional Mathieu ID boundary is inaccurate for the fifth instability region.

Related to the instability diagrams based on the T period solutions, for the second instability region, the first and second-order fractional Mathieu ID boundary is inaccurate, but the third order fractional Mathieu ID boundary is acceptable enough. For the fourth instability region, the fourth-order fractional Mathieu ID boundary should be used to get an accurate result. However, the fourth-order is still unacceptable for the sixth instability region.

Increasing the fractional order of soil damping impacts the top of the instability diagrams significantly and makes a slight change in other sections of the diagrams. In other

words, by increasing the fractional order, the critical dynamic load is increased. Also, higher order instability regions show more sensitivity to the fractional order change.

In the same order of instability region, the critical dynamic load and the critical excitation frequency increase as Winkler's foundation stiffness grows and the areas of instability decrease. Considering this result, we can conclude that the foundation stiffness contributes to the pile's stability in a positive way.

In some cases, parametric resonances still occur despite damping. The instability excitation frequency range gradually shrinks as foundation damping increases until it disappears entirely.

In addition, the effects of the static load component on instability regions are studied. As the static load increases, the parametric resonance frequency decreases, as does the critical dynamic load. The range of the excitation frequency for instability also increases when the static load parameter grows.

5.2.   Future research

The dynamic stability analysis and vibration response analysis presented here could provide insights into how piles can be used in different structures in an efficient and safe manner. There are still some limitations in compiling the numerical solution. The mathematical calculations performed in this numerical model are too large, which means, practically speaking, we cannot use a higher grid density with ordinary computers. Also, as we can see in the stability diagrams, the fourth and higher instability regions are not accurate enough due to grid density. In addition to grid density, this inaccuracy is caused by the time intervals taken in the block-pulse functions. By increasing the number of block pulse functions and decreasing the length of time intervals, the output of the numerical model is obtained more accurately.

Using different types of supports for the pile structure may result in different fractional Mathieu infinite determinants, therefore, this can be considered for future research. Additionally, the numerical method may be extended to the analysis of dynamic stability and vibration under arbitrary parametric conditions.

Different subgrade models like Pasternak and Hetenei may be used in future studies. Also, in the case of using a pile–column system, for example, to construct a highway bridge, the compressive element is partially confined with soil media, so the instability of these systems can be studied by other researchers. Finally, the result of the fractional order damping in soil media should be validated by experimental research to understand the soil behavior better.

References

[1]   Bhattacharya S, Dash S R, Adhikari S. On the mechanics of failure of pile-supported structures in liquefiable deposits during earthquakes. *Current Science,* 2008, 94: 605-611.

[2]   Stringer M. *The Axial Behaviour of Piled Foundations in Liquefiable Soil (Doctoral thesis)*. Cambridge, UK, 2012.

[3]   Wei X, Wang Q, Wang J. Damage patterns and failure mechanisms of bridge pile foundation under earthquake. *14th World Conference on Earthquake Engineering*, Beijing, China, 2008.

[4]   Yang K. *Practical Pile Foundation Engineering*. People's Communications Publishing House, 2008.

[5]   Gabr M A, Wang J J, Zhao M. Buckling of piles with general power distribution of lateral subgrade reaction. *Journal of Geotechnical and Geoenvironmental Engineering,* 1997.

[6]   Hamada M, O'Rourke T D. *Case Studies of Liquefaction and Lifeline Performance During Past Earthquakes*. National Centre for Earthquake Engineering Research, New York, 1992.

[7]   Ishihara K. Liquefaction and flow failure during earthquakes. *Geotechnique, 1993,* 3: 351-415.

[8]   Bhattacharya S. *Pile Instability During Earthquake Liquefaction (Doctoral Thesis).* Cambridge, UK, 2003.

[9]   Hibbeler R C. *Mechanics of Materials*. Pearson Education, 2015.

[10]   Bolotin V V. *The Dynamic Stability Of Elastic Systems*. Holden-Day, 1964.

[11] Burney S Z, Jaege L G. A method of determining the regions of instability of a column by a numerical method approach. *Journal of Sound and Vibration,* 1971*,* 15 (1): 75-91.

[12] Iwatsubo T, Sugiyahla Y, Ishihara K. Stability and non-stationary vibration of columns under periodic loads. *Journal of Sound and Vibration,* 1972, 23 (2): 245-257.

[13] Zhang X, Tang L, Ling X, Chan A. Critical buckling load of pile in liquefied soil. *Soil Dynamics and Earthquake Engineering,* 2020, 135.

[14] Zhang R, Li C, Jin C. Buckling stability analysis for piles in the slope foundation based on cusp catastrophe theory. *Mathematical Problems in Engineering,* 2021.

[15] Deng J, Kanwar N, Pandey M, Xie W C. Dynamic buckling mechanism of pillar rockbursts induced by stress waves. *Journal of Rock Mechanics and Geotechnical Engineering,* 2019, 11: 944-953.

[16] Deng J. Analytical and numerical investigations on pillar rockbursts induced by triangular blasting waves. *International Journal of Rock Mechanics & Mining Sciences,* 2021, 138.

[17] Tanahashi H, Suzuki Y. Review on the mechanical models and formulations of embedment of traditional timber joints in Japan. *Architectural Institute of Japan*, 2020.

[18] Iwatsubot T, Saigo M, Sugiyama Y. Parametric instability of clamped-clamped and clamped-simply supported columns under periodic axial load. *Journal of Sound and Vibration*, 1973, 30(1): 65-77.

[19] Ahuja R, Duffield R C. Parametric instability of variable cross – section beams resting on an elastic foundation. *Journal of Sound and Vibration,* 1975, 39(2): 159-174.

[20] Yokoyam T. Parametric instability of Timoshenko beams resting on an elastic foundation. *Computers & Structures,* 1988, 28(2): 207-216.

[21] Gabr M A, Wang J J, Zhao M. Buckling of piles with general power distribution of lateral subgrade reaction. *Journal of Geotechnical and Geoenvironmental Engineering,* 1997, 123: 123-130.

[22] Engel R S. Dynamic stability of an axially loaded beam on an elastic foundation with damping. *Journal of Sound and Vibration,* 1991, 146(3): 463-477.

[23] Khalila R, Horani M A, Yousef A, Sababheh M, A new definition of fractional derivative. *Journal of Computational and Applied Mathematics,* 2014, 264: 65-70.

[24] Demirci E, Ozalp N. A method for solving differential equations of fractional order. *Journal of Computational and Applied Mathematics,* 2012, 236: 2754-2762.

[25] Machado J T, Jesus I S, Barbosa R, Silva M, Reis C. Application of fractional calculus in engineering (Chapter 38). *Dynamics, Games and Science*, 2011, 1: 619-630.

[26] Adolfsson K, Enelund M, Olsson P. On the fractional order model of viscoelasticity. *Mechanics of Time-Dependent Materials,* 2005, 9: 15–34.

[27] Meng R, Yin D, Zhou C, Wu H. Fractional description of time-dependent mechanical property evolution in materials with strain softening behavior. *Applied Mathematical Modelling,* 2016, 40: 398-406.

[28] Yin D, Wu H, Cheng C, Chen Y. Fractional order constitutive model of geomaterials under the condition of triaxial test. *International Journal for Numerical and Analytical Methods in Geomechanics,* 2013, 37: 961–972.

[29] Wang J, Zhou D, Zhang Y, Cai W. Vertical impedance of a tapered pile in inhomogeneous saturated soil described by fractional viscoelastic model. *Applied Mathematical Modelling,* 2019, 75: 88-100.

[30] Shokooh A, Suarez L. A comparison of numerical methods applied to a fractional model of damping materials. *Journal of Vibration and Control,* 1997, 5: 331-354.

[31] Yan Q, Su Z. Free vibration of elastic Timoshenko beam on fractional derivative Winkler viscoelastic foundation. *Advanced Materials Research,* 2012, 368-373: 1034-1037.

[32] Cai W, Chen W, Xu W. Fractional modeling of Pasternak-type viscoelastic foundation. *Mechanics of Time-Dependent Materials,* 2017, 21: 119–131.

[33] Germoso C, Fraile A, Alarcon E, Aguado J, Chinesta F. From standard to fractional structural visco-elastodynamics Application to seismic site response. *Physics and Chemistry of the Earth,* 2017, 98: 3-15.

[34] Ouzizi A, Abdoun F, Azrar L. Dynamic analysis of beams on fractional viscoelastic foundation subject to a variable speed moving load. In *MATEC Web of Conferences (CMM2019)*, 2019.

[35] Zarraga O, Sarría I, García-Barruetabeña J, Cortés F. An analysis of the dynamical behaviour of systems with fractional damping for mechanical engineering applications. *Symmetry in Mechanical Engineering,* 2019, 11(12): 1499.

[36] Deng J, Kanwar N, Pandey M, Xie W C. Dynamic buckling mechanism of pillar rockbursts induced by stress waves. *Journal of Rock Mechanics and Geotechnical Engineering,* 2019, 11(5): 944-953.

[37] Xie W C. *Dynamic Stability of Structures.* Cambridge University Press, 2006.

[38] Rand R, Sah S, Suchorsky M. Fractional Mathieu equation. *Communications in Nonlinear Science and Numerical Simulation,* 2010, 15: 3254–3262.

[39] Ebadian A, Khajehnasiri A A. Block-pulse functions and their applications to solving systems of higher order nonlinear volterra integro-differential equations. *Electronic Journal of Differential Equations,* 2014, 54: 1-9.

[40] Li Y, Sun N. Numerical solution of fractional differential equations using the generalized block pulse operational matrix. *Computers and Mathematics with Applications,* 2011, 62: 1046-1054.

[41] Aboudi J, Cederbaum G. Dynamic stability analysis of viscoelastic plates by Lyapunov exponents. *Journul of Sound and Vibration*, 1990, 139(3): 459-467.

[42] Goldhirsch I, Sulem P, Stability and Lyapunov stability of dynamical systems: a differential approach and a numerical method. *Physica*, 1987, 27D: 311-337.

[43] Deng J, Shahroudi M, Liu K. Numerical simulation of dynamic stability and responses of beams on elastic foundations under a parametric load. *International Journal of Structural Stability and Dynamics,* 2022.

[44] Liu D. *Dynamic stability analysis of frame systems by application of the finite element method (Doctoral thesis).* University of Louisville, 2001.